
Modeling of the elastic mechanical behavior of thin compliant joints under load for highest-precision applications

submitted by:

B.Sc. Mario André Torres Melgarejo

for the degree of

Master of Science in Mechanical Engineering

Supervising Tutor (TU Ilmenau): M.Sc. Maximilian Darnieder
Dr.-Ing. Sebastian Linß
Responsible Professor (TU Ilmenau): Univ.-Prof. Dr.-Ing. René Theska
Responsible Professor (PUCP): Univ.-Prof. Dr.-Ing. Jorge Rodríguez Hernández

Ilmenau, Germany

Conceptual formulation of Master-Thesis

of Mr. Mario Andre Torres Melgarejo

Topic: Modeling of the elastic mechanical behavior of thin compliant joints under load for highest-precision applications

Description:

In various field of metrology, the demands for precision as well as reproducibility of the measurements are continuously rising. The application of compliant mechanisms as a basis of the mechanical system has given way to an almost frictionless and precise movement. These systems can be found in numerous applications like EMFC-weighing cells, force sensors, etc. A downside of compliant joints is their stiffness towards deflection, which limits the sensitivity of the sensor. Consequently, the flexure hinges are manufactured as thin as possible. The present limit in terms of manufacturing technology is within the range of 50 μm . The modeling of force measuring devices with highest resolutions requires a reliable modeling of thin flexure hinges under different loading conditions.

Objective:

The objective of the present master thesis is a detailed study on the mechanical behavior of a single flexure hinges under different loading conditions and geometrical deviations. The first part focuses on the modeling of the flexure hinge using numerical methods e.g. the finite element method. Additionally, emphasis lies on the elaboration of prerequisites for a precise and trustworthy numerical computation in the required range of accuracy and a careful interpretation of the measurement results. In a further step, the consideration is continued in the context of the flexure hinges in a monolithic weighing cell. The theoretical findings and explanations are experimentally verified by an appropriate measurement setup. The elaboration of an experimental setup, developed by a fellow master student, is supported by finite element models.

Tasks:

- Specification of the tasks, systematic literature research
- Numerical models:
 - Qualification of the models with mathematic background
 - Modeling of the behavior of flexure hinges
- Investigation on flexure hinges for the application in monolithic weighing cells
- Application of the results for a single joint on kinematic structures based on compliant joints

Date of issue:

01.11.2017

Responsible Professor (TU Ilmenau):

Univ.- Prof. Dr.-Ing. René Theska

Responsible Professor (PUCP Lima):

Prof. Jorge Antonio Rodríguez Hernández

Supervisor at TU Ilmenau:

Maximilian Darnieder, Dr. Sebastian Linß

Ilmenau 10.10.2017

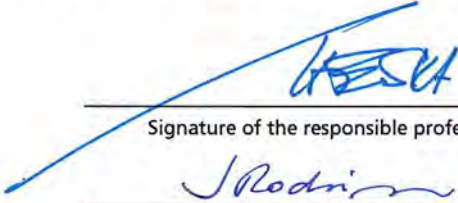
Location, Date

Lima, den 2.10.2017


Location, Date

Ilmenau, 30.10.2017

Location, Date


Signature of the responsible professor TU Ilmenau


Signature of the responsible professor PUCP Lima

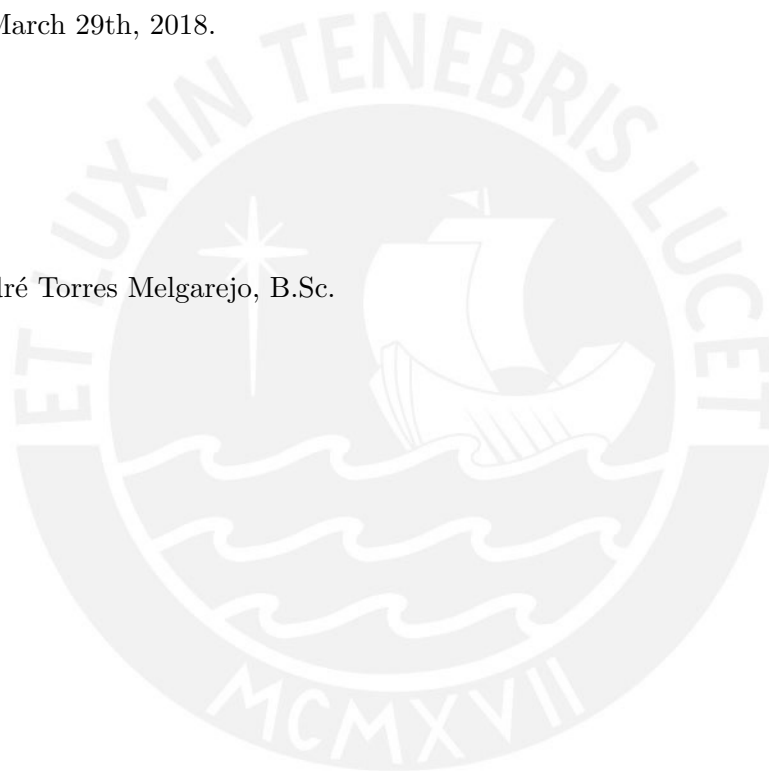

Signature of the student

Statement

I, hereby, declare that the work contained herein is completely my own, except when explicitly stated otherwise in the text, and it has not been submitted for any previous application for a degree.

Ilmenau, March 29th, 2018.

Mario André Torres Melgarejo, B.Sc.



Abstract

For the most demanding measurement tasks in force metrology flexure hinges in compliant mechanisms represent a key component. To enhance the mechanical properties of devices like weighing cells, the ability of precise modeling of flexure hinges is essential. The present scientific work focuses on the modeling of the mechanical behavior of a single flexure hinge subjected to geometric deviations and non-ideal loading conditions as those encountered in weighing cells. The considered hinge has a semi-circular contour and a large width compared to its minimum notch height. This geometry is modeled using the finite element method. Requirements for a trustworthy and efficient computation are elaborated under the consideration of geometric deviations for later parametric studies. Analytical expressions found in the literature are compared to numerical results to prove the validity of their assumptions for thin hinges. The model is used for studying the deviation of the stiffness in non-ideal flexure hinges. Sources of deviation are identified and described by parameters. The range of values for each parameter is chosen on the basis of available manufacturing technology. Influential parameters are identified through a sensitivity analysis. The effect of loading conditions is studied in the context of the application in weighing cells. For the enhancement of the overall sensitivity, the stiffness of the flexure hinges can be reduced. One option, the alteration of the geometry by adding a flexure strip in the center of the semi-circular flexure hinge is studied in comparison to existing analytical equations. The effects of ground tilts for a single loaded flexure hinge are investigated as a foundation for future modeling of a tilt insensitive state of a weighing cell mechanism (autostatic state). By adjusting the vertical position of the center of mass of the lever, the tilt sensitivity can be reduced to zero. An approach to find the position for this state is presented considering the numerical limitations of finite element modeling. Using this approach, the variation of the sought position is evaluated for different values of the design parameters.

Kurzzusammenfassung

Für die anspruchsvollsten Aufgaben in Messgeräten in der Kraftmesstechnik gehören Festkörpergelenke in nachgiebigen Mechanismen zu den leistungsbestimmenden Bestandteilen. Um die mechanischen Eigenschaften von Geräten wie Wägezellen zu verbessern, ist die genaue Modellierung von Festkörpergelenke wesentlich. Die vorliegende wissenschaftliche Arbeit konzentriert sich auf die Modellierung des mechanischen Verhaltens eines einzelnen Festkörpergelenkes, das geometrischen Abweichungen und nicht idealen Lastbedingungen wie sie in Wägezellen auftreten unterliegt. Das betrachtete Gelenk hat eine Halbkreiscontour und eine große Breite im Vergleich zu seiner minimalen Kerbhöhe. Diese Geometrie wird mit der Finite-Elemente-Methode modelliert. Anforderungen für eine vertrauenswürdige und effiziente Berechnung werden unter Berücksichtigung geometrischer Abweichungen für spätere parametrische Untersuchungen erarbeitet. Analytische Gleichungen aus der Literatur werden mit numerischen Ergebnissen verglichen, um die Gültigkeit ihrer Annahmen bezüglich dünner Gelenke zu überprüfen. Das Modell wird verwendet, um die Abweichung der Drehsteifigkeit in nicht idealen Festkörpergelenken zu untersuchen. Quellen der Abweichungen wird identifiziert und durch Parameter beschrieben. Der Wertebereich für jeden Parameter wird aufgrund der zu erwartenden Abweichungen von typischerweise anwendbaren Fertigungsverfahren bestimmt. Einflussreiche Parameter werden durch eine Sensitivitätsanalyse ermittelt. Die Auswirkung der Lasteinleitung wird im Zusammenhang mit der Anwendung in Wägezellen untersucht. Zur Verbesserung der Gesamtempfindlichkeit kann die Steifigkeit der Festkörpergelenke reduziert werden. Eine Option, die Änderung der Geometrie durch Hinzufügen eines Streifens in der Mitte des Festkörpergelenks, wird im Vergleich zu bestehenden analytischen Gleichungen untersucht. Die Auswirkungen von Bodenneigungen für ein einzeln belastetes Festkörpergelenk werden als Grundlage für die zukünftige Modellierung eines neigungunempfindlichen Zustands der Wägezelle untersucht (autostatischer Zustand). Durch das Einstellung der vertikalen Lage des Schwerpunktes des Hebels kann die Neigungsempfindlichkeit theoretisch vollständig beseitigt werden. Ein Ansatz, um die Position für diesen Zustand zu finden, wird unter Berücksichtigung der numerischen Begrenzungen der Finite-Elemente-Modellierung vorgestellt. Mit Hilfe dieses Ansatzes wird die Variation der gesuchten Position für verschiedene Werte der Designparameter ausgewertet.

Table of contents

| | |
|--|------------|
| Statement | i |
| Abstract | ii |
| Kurzzusammenfassung | iii |
| Table of contents | iv |
| List of abbreviations | vi |
| List of symbols | vii |
| 1. Introduction | 1 |
| 2. State of the art | 3 |
| 2.1. Flexures in high-precision applications | 3 |
| 2.2. Modeling | 5 |
| 2.3. Deformation errors in compliant systems | 10 |
| 2.4. Discussion | 14 |
| 3. Finite element modeling of thin flexure hinges | 16 |
| 3.1. Model requirements | 16 |
| 3.2. Geometry and material | 17 |
| 3.3. Loading and boundary conditions | 18 |
| 3.4. Meshing | 19 |
| 3.5. Geometrically nonlinear calculation | 24 |
| 3.6. Mechanical behavior | 26 |
| 3.7. Comparison to analytical models | 28 |
| 3.8. Summary | 35 |
| 4. Investigation of non-ideal flexure hinges | 37 |
| 4.1. Identification of sources of deviation | 37 |
| 4.2. Parametrization of the flexure hinge | 40 |
| 4.3. Model behavior | 43 |
| 4.4. Sensitivity analysis | 45 |
| 4.5. Summary | 52 |
| 5. Application of thin flexures in weighing cells | 53 |
| 5.1. Axially-loaded flexure hinges | 55 |
| 5.2. Ground tilt effect | 60 |
| 5.3. Summary | 68 |
| 6. Conclusions | 70 |

| | |
|--|--------------|
| Appendix | x |
| A. Loading application | x |
| B. Mesh sensitivity analysis | xi |
| C. Circular contour flexure hinge design equations | xiii |
| D. Bending in plane strain | xiv |
| E. Model behavior | xv |
| F. Sensitivity measures | .xviii |
| G. Sampling methods | xx |
| H. Stiffness deviations | .xxii |
| I. Gravity effect in sensitivity measures. | xxvii |
| J. Center of mass position for autostatic state. | xxviii |
| Bibliography | xxxii |



List of abbreviations

- A-LHS : Advanced Latin Hypercube Sampling
- BCM : Beam Constraint Model
- CAD : Computer-Aided Design
- CNC : Computer numerical controlled
- CoP : Coefficient of Optimal Prognosis
- DoF : Degrees of freedom
- FE : Finite element
- FEA : Finite element analysis
- FBMM : Finite Beam based Matrix Modeling
- ICCG : Incomplete Cholesky Conjugate Gradient
- JCG : Jacobi Conjugate Gradient
- LHS : Latin Hypercube Sampling
- MEMS : Microelectromechanical systems
- MoP : Metamodel of Optimal Prognosis
- OAT : One-at-a-time
- PCG : Preconditioned Conjugate Gradient
- PRBM : Pseudo Rigid-Body Model
- WEDM : Wire electrical discharge machining

List of symbols

- a : Number of levels per parameter
 b : Width
 CoP : Coefficient of Optimal Prognosis
 db : Width deviation parameter
 dE : Elastic modulus deviation parameter
 dh : Minimum height deviation parameter
 dR : Radius deviation parameter
 dx : Deviation parameter for hinge position in x -direction
 dx_c : Deviation parameter for hole separation in x -direction
 dy : Deviation parameter for hinge position in y -direction
 $d\beta_{gz}$: Deviation parameter for gravity vector orientation around z -axis
 $d\beta_{gy}$: Deviation parameter for gravity vector orientation around y -axis
 $d\nu$: POISSON's ratio deviation parameter
 $d\theta_x$: Deviation parameter for hole orientation around x -axis
 $d\theta_y$: Deviation parameter for hole orientation around y -axis
 e_{k_φ} : Relative rotational stiffness deviation
 $e_{\sigma_{x,max}}$: Relative deviation of the maximum bending stress
 $e_{\sigma_{z,max}}$: Relative deviation of the maximum out-of-plane stress
 E : Elastic modulus
 E' : Modified elastic modulus
 \mathbf{F} : Load vector
 \mathbf{F}^a : Applied load vector
 \mathbf{F}_i^{nr} : Restoring load vector at the i -th iteration
 F_x, F_y, F_z : Force in the x, y, z -direction
 \vec{g} : Gravity vector
 h : Minimum hinge height

- h' : Hinge height for 10 % of maximum bending stress
 H : Total height
 I_z : Moment of inertia about z -axis
 j : Parameter $j = \sqrt{EI_z/W}$
 \mathbf{K} : Stiffness matrix
 \mathbf{K}_i^T : Tangent stiffness matrix at the i -th iteration
 k : Number of parameters
 k_b : Stress concentration factor for bending
 k_{ij} : ij -th component of the stiffness matrix
 k_φ : Rotational stiffness
 \hat{k}_φ : Normalized rotational stiffness
 l : Hinge length
 L : Total length
 m : Supported mass
 M : Applied bending moment
 M_x, M_y, M_z : Moment in the x, y, z -direction
 n : Order of the polynomial for approximation
 N : Total number of samples
 R : Radius of the circular contour
 R_{Ref} : Reference force value
 \mathbf{R}_i : Residual load vector at the i -th iteration
 s : Flexure strip length
 S_i : Sensitivity index for the i -th parameter
 $SS_E^{Prediction}$: Sum of squared prediction errors
 SS_T : Total variation
 \mathbf{u} : Displacement vector
 \mathbf{u}_i : Solution displacement vector at the i -th iteration
 u_x, u_y, u_z : Displacement in the x, y, z -direction
 W : Supported weight force by the flexure hinge
 W_1, W_2 : Measured and counter weight forces of the weighing cell
 W_B : Weight of the transmission lever of the weighing cell
 W_x, W_y : Component of the weight force in the x, y -direction

- x, y, z : Position in the x, y, z -direction
 x_{CM} : Position of the center of mass
 \bar{x}_{CM} : Position of the center of mass for the autostatic state
 x'_{CM} : Position of the center of mass for the instable state
 \hat{z} : Normalized z -position
 α : Scalar multiplier for the line search method
 β_{gy} : Gravity vector orientation around y -axis
 β_{gz} : Gravity vector orientation around z -axis
 γ : Ground tilt angle
 Δb : Deviation of plate thickness
 Δc : Deviation of hole center position with shift of rotational axis
 ΔR : Deviation of hole radius
 $\Delta x_1, \Delta x_2$: Deviation of hole center position in longitudinal direction
 Δx_{CM} : Step size of x_{CM} for approximation
 Δy : Deviation of hole center position in transversal direction
 $\Delta \theta_x, \Delta \theta_y$: Deviation of hole center perpendicularity to longitudinal and transversal axes
 $\Delta \theta_z$: Deviation of hole center position with rotation of the hinge
 $\varepsilon_{\mathbf{R}}$: Tolerance value of the convergence criteria
 ζ : Dimensionless parameter $\zeta = 1 + \xi$
 λ : Dimensionless parameter $\lambda = R/h$
 ν : POISSON's ratio
 ξ : Dimensionless parameter $\xi = h/2R$
 ρ : Material density
 $\sigma_x, \sigma_y, \sigma_z$: Normal stress in the x, y, z -direction
 $\sigma_{x,max}$: Maximum bending stress at $x = L/2$
 σ_{yield} : Yield strength
 $\sigma_{z,max}$: Maximum out-of-plane normal stress $x = L/2$
 $\hat{\sigma}_z$: Normalized out-of-plane stress
 φ : Angle of rotation of the flexure hinge
 φ_1 : Angle of rotation of the transmission lever.
 $\varphi_x, \varphi_y, \varphi_z$: Rotation around the x, y, z -axis

1. Introduction

With the development of modern science, the need for precision is continuously rising. High-precision systems such as nanopositioners [23, 34, 36], measurement instruments [18, 54, 69], precision machine tools [28, 90] and microelectromechanical systems (MEMS) [43, 92] often require features that are not achievable through conventional design. In measuring technology, for instance, instruments are designed to obtain measurements as precise and repeatable as possible with high resolution. Compliant mechanisms have proven to be suitable for those systems due to their almost frictionless and precise motion. In fact, they are used in many engineering applications, in both macro- and micro/nano-scale, e.g. weighing cells (see Figure 1.1).

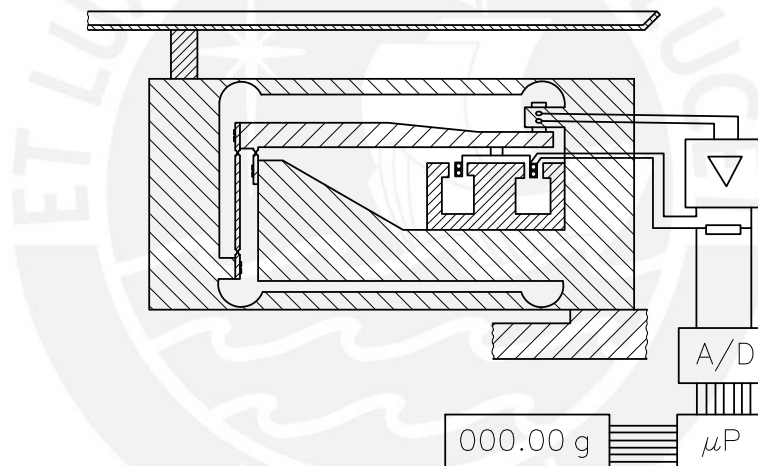


Figure 1.1: Compliant mechanism in a weighing cell. Adapted from [7].

Conventional mechanisms have a number of drawbacks, especially when it comes to precision applications. As a conventional joint is basically an assembly of parts composing the kinematic pair, clearance between elements is necessary to enable relative rotation. Consequently, backlash results in a loss in the precision of motion. Contact between surfaces produces friction, which leads to wear, increased clearance and undesired forces. Lubrication becomes necessary, so they are not suited for vacuum operations or clean environments. The difficulty of manufacturing small parts with good tolerances and their assembly also makes them unsuitable for miniaturization. As a result, compliant joints were developed to replace conventional joints in such applications.

A compliant joint is a connection between two bodies or body segments with at least one relative motion due to deformation [37]. They are usually fabricated monolithically with the rest of the mechanism, meaning that no assembly is needed. Thus, they overcome the aforementioned problems of conventional joints. Mechanisms based on these joints, known as compliant mechanisms, present multiple advantages such as smooth and continuous motion, increased precision, high repeatability, simplified manufacturing, potentially lower costs, compactness, better scalability and ability to work in vacuum

and clean environments. These characteristics make them suitable for high-precision and small-scale applications. However, beside the numerous advantages, compliant joints exhibit certain disadvantages, for example: theoretical modeling can be rather difficult or not always possible, rotational motion is not pure as the center of rotation is not fixed, limited capacity of rotation and performance can be greatly affected by small changes in the parameters of the joint.

The capability of compliant mechanisms to fulfill their expected duties depends mostly on the compliance of the joints. Compliance is defined as a measure of the ability of a body or structure to deform due to the action of external forces [37]. It is the reciprocal of stiffness and it is frequently used for describing the behavior of a compliant mechanism. However, the latter is used for optimization purposes. For quasi-static applications, the stiffness comprises all mechanical properties required for modeling purposes, topology optimization and efficient, reduced models for finite element (FE) calculations [19].

Compliant mechanisms are usually required to be more compliant (or less stiff), especially in force measurement instruments. Flexure hinges of different geometries have been extensively studied through the years. Stiffness in these joints is usually decreased by reducing their thickness down to some micrometers. As dimensions reach the micrometer range, the behavior of a compliant joint becomes more sensitive to small deviations from ideal conditions, e.g. manufacturing and material imperfections. Consequently, the stiffness cannot be accurately determined. Besides, analytical models lose accuracy for very thin compliant joints since they are based on assumptions that lose validity in such ranges.

In systems based on compliant mechanisms, proper modeling and knowledge of the actual performance of their joints are necessary for predicting the overall behavior. For a better understanding of the behavior of compliant joints in highest precision applications, i.e. thin compliant joints, proof of the validity of available expressions and a study on the sources of influence over the stiffness are required. In a first step, a thin compliant joint is modeled using the finite element method to analyze the applicability of analytical and design equations. Then, its response under non-ideal conditions is studied in terms of its rotational stiffness. Sources of deviation are first identified and classified based on a detailed literature research. The identified deviations are described by parameters which must be supported by the model in their respective range of values. Most influential parameters are determined later through a sensitivity analysis. In a further step, the consideration is continued in the context of the compliant joints in a monolithic weighing cell.

The structure of this thesis is organized in six chapters. Chapter 2 reviews the modeling of flexure hinges as well as investigations on the sources of deformation deviation of compliant mechanisms to date. This chapter also discusses the studies yet to be done that will be covered in this work. Chapter 3 focuses on the finite element modeling of a thin flexure hinge and studying the deviation between models. The behavior of the thin flexure hinge under non-ideal conditions is analyzed in Chapter 4. The methodology of study, identification of sources, parametrization of the model, determination of influential parameters and discussion of the results are all included here. Chapter 5 is dedicated to the investigation on flexures for the application in monolithic weighing cells. Finally, conclusions and future work are presented in Chapter 6.

2. State of the art

This chapter provides a review on the literature to date on the modeling of flexure hinges as well as on error sources concerning the behavior of compliant mechanisms. Section 2.1 introduces the fundamentals of this topic for better a understanding of the upcoming sections and chapters. Geometric configuration, material properties and manufacturing are of utmost importance for defining the behavior of a flexure hinge and, thus, are briefly discussed. Models and approximate equations for different types of joints have been widely developed over the years. Most of them are based on basic theories, e.g. EULER-BERNOULLI beam theory. Section 2.2 reviews those expressions and classifies them by the approaches used. Studies on deformation errors of compliant mechanisms are reviewed in Section 2.3, where sources described as parameter deviations are classified and explained. Section 2.4 discusses about the previous sections and the challenges encountered that constitute the basis of this work.

2.1. Flexures in high-precision applications

In literature, numerous types of compliant joints can be found [21], as well as diverse criteria for classifying them [48]. Among all of them, flexure hinges are the most studied type. Flexure hinges, or just flexures, allow relative rotation between two elements through bending [37]. In most applications, especially of high precision, they are used to replace conventional joints in common mechanism configurations, as in Figure 2.1.

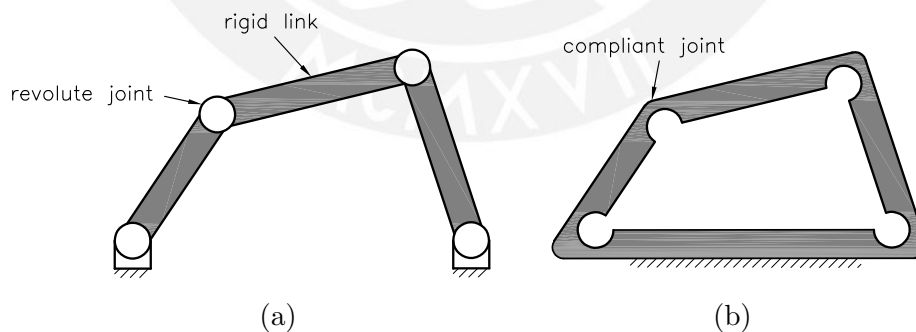


Figure 2.1: (a) Mechanism with conventional revolute joints; (b) Mechanism with compliant joints. Adapted from [10].

Geometry

Flexure hinges are usually subdivided in two big groups: notch type hinges and leaf type hinges (see Figure 2.2). Notch hinges are mostly produced by removing material from a plate leaving a thin neck-like region which serves as the flexible element. The compliant region is limited to the thinnest part of the joint, approximately defining the axis of rotation, which makes them preferred for precision applications. However, due to the high concentration of stress, their capacity of rotation is very limited. In contrast, leaf hinges

consist of a slender member connecting the links, where deformation is distributed over the whole hinge length, i.e. distributed compliance. They are suitable for large displacement applications but are more sensitive to parasitic motions. Among both types, the notch hinge is state of the art [47]. As such, a variety of different notch contours can be found in the literature, e.g. circular, elliptic, parabolic and many more [50].

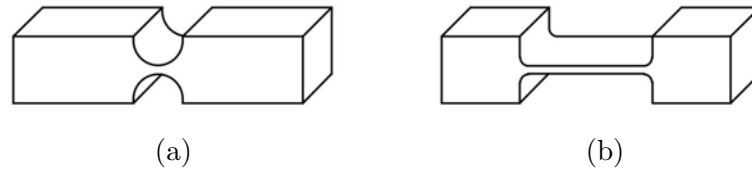


Figure 2.2: (a) Notch flexure hinge with concentrated compliance; (b) Leaf flexure hinge with distributed compliance.

Materials

Depending on the application, compliant mechanisms can be manufactured of different materials, especially metals. Aluminium, steel and titanium are commonly utilized, although other materials and diverse alloys have also been studied, e.g. shape memory alloys [94]. Material selection requirements are often based on the following criteria [19, 23]:

- Stiffness-to-density ratio.
- Admissible elastic strain, based on the yield strength.
- Fatigue strength.

As a result, high strength aluminium alloys, especially the 7075 grade, are widely used in precision engineering applications [23]. Other criteria may also include machinability, resistance against corrosion, low thermal expansion and more [14, 23, 82]. Common materials for compliant mechanisms can be seen in Table 2.1.

Table 2.1: Mechanical properties of common flexure hinge materials [9].

| Material | Elastic modulus (GPa) | Poisson's ratio | Density (g/cm ³) | Yield strength (MPa) |
|-----------------|-----------------------|-----------------|------------------------------|----------------------|
| 2024 Aluminium | 72.4 | 0.33 | 2.77 | 347 |
| 6061 Aluminium | 69 | 0.33 | 2.70 | 276 |
| 7075 Aluminium | 71 | 0.33 | 2.80 | 505 |
| Titanium | 114 | 0.34 | 4.43 | 830 |
| Stainless steel | 193 | 0.30 | 8.00 | 205 |

The values shown above are only referential. Mechanical properties can differ considerably between manufacturers and sources. For example, aluminium alloys 2024 can be found with a specified elastic modulus between 70 and 72.4 GPa [9, 21]. Metals also have different classes or grades for a same composition, e.g. aluminium alloys 2024 can be found with yield strenghts of 75 up to 440 MPa [21]. Those values depend greatly of the manufacturing processes, such as tempering, and also from measurement techniques.

Manufacturing

Most of the advantages of compliant joints already mentioned were based on the fact that they can be manufactured monolithically with the rest of the structure. It is also

possible to assemble them with rigid members using fasteners or through bonding [23]. Assembled joints can be fabricated with standard machining processes, like milling and turning. Yet, the use of fasteners or adhesives in their assembly can affect the performance of the whole mechanism. Monolithic mechanisms offer more predictable and repeatable performance. Common fabrication processes for single- and two-axis flexure hinges include standard milling and drilling. As for multi-axis hinges, turning is usually preferred, although precision casting is also possible [50]. These techniques are best suited for hinges made of metals with dimensions above 1 mm, achieving tolerances of around $\pm 25 \mu\text{m}$ [23]. However, when extremely thin dimensions or complex geometries are required, non-traditional processes such as the wire electrical discharge machining (WEDM) are best suited.

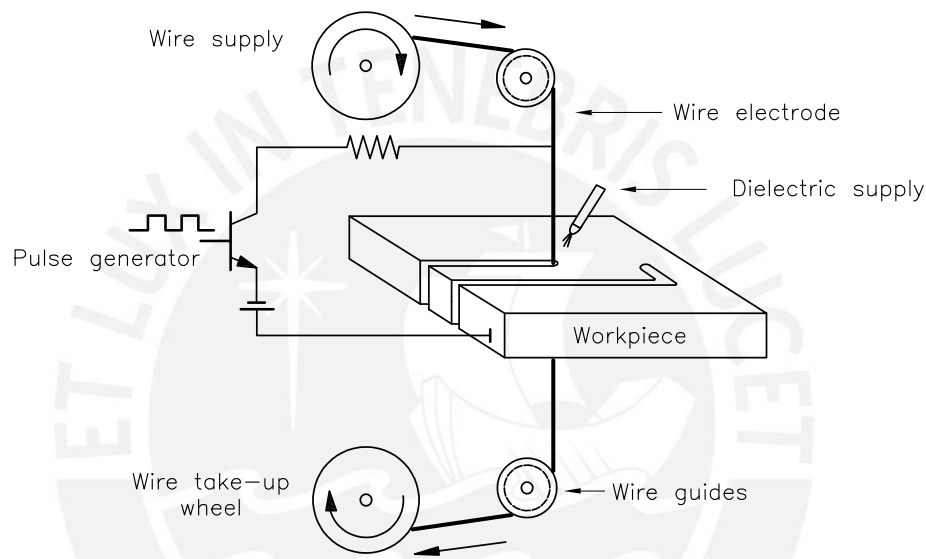


Figure 2.3: Wire electrical discharge machining. Adapted from [29].

In WEDM, the raw material is submerged in a dielectric solution and an electric arc, or spark, is produced by generating a voltage difference between a wire electrode and the workpiece (see Figure 2.3), vaporizing the material locally. The wire is kept in tension by a mechanical device while being continuously fed and travels against the workpiece removing material. The cutting is produced in steps controlled by a pulse generator, which turns the spark on and off. It allows the manufacturing of hinges with minimum thicknesses of around $\pm 50 \mu\text{m}$ [31]. Dimensional accuracy on the order of $\pm 12 \mu\text{m}$ is usually obtained using wires of approximately $\pm 100 \mu\text{m}$ of diameter [23], but tolerances of $\pm 2.5 \mu\text{m}$ can be achieved through this process [63]. Other manufacturing techniques suitable, especially for two dimensional applications, are laser cutting, metal shaping, water jet cutting or photolithographic techniques for MEMS [50].

2.2. Modeling

Unlike conventional joints, flexure hinges exert a restoring force during motion. This force can be either advantageous in systems where an initial position is needed or limiting when high mobility is required. In quasi-static analysis, where no damping or inertial forces are considered, it equals the external loads generating the deformation. Stiffness is usually obtained by applying a certain type of load to the joint and measuring the displacements or rotations of a specific reference point. As all points of a same hinge can displace in

different directions and amounts, it highly depends on the location of the reference point, thus, specifying it can be really complex and involves various parameters [97].

Geometrical configuration, material properties, boundary and loading conditions, and environmental conditions define the mechanical behavior of a compliant joint. Geometry defines the distribution of matter in a body, which plays a major role on its deformation. Thus, location and type of constraints have great influence. Material behavior, whether elastic, viscoelastic or plastic, defines the relationship between the external loading and displacements. Materials possess different values of mechanical properties, which results in different deformations for same geometries and loading conditions. Size-dependency is also present in material behavior as properties are actually average values, resulting from different phenomena occurring in the micro- and nano-scale. External influences, such as temperature and gravity, tend to vary the expected ideal conditions, like dimensions or loading. Nevertheless, stiffness is specified depending on how loads are applied or how deformation occurs, e.g. bending or rotational stiffness. Direction, orientation, type, magnitude and location of loading, in combination with material properties and geometric configuration, determine the direction and magnitude of the displacements of all unconstrained points of a compliant joint. Since there are numerous factors which define the stiffness, modeling approaches are based on various assumptions and considerations.

Mechanical model

An ideal flexure hinge is usually modeled as shown in Figure 2.4. The mechanical model contemplates only the contour region of the joint as a cantilever beam of variable section, where the loading is applied on the free end [50, 62, 91]. Some authors also consider the deformation of the adjacent links [47, 73]. Points of reference of the model commonly specified are the fixed end O, the ideal center of rotation C and the free end P. In fact, all points over the longitudinal axis actually represent the cross section at that position, as flexures are prismatic most of the times. A cartesian coordinate system is located in point O, where two axes are on the plane of motion, one parallel to the longitudinal axis (x -axis) and the other one to the transversal axis (y -axis). Sometimes the origin coincides with point C to match the third axis (z -axis) with the ideal axis of rotation [48, 50].

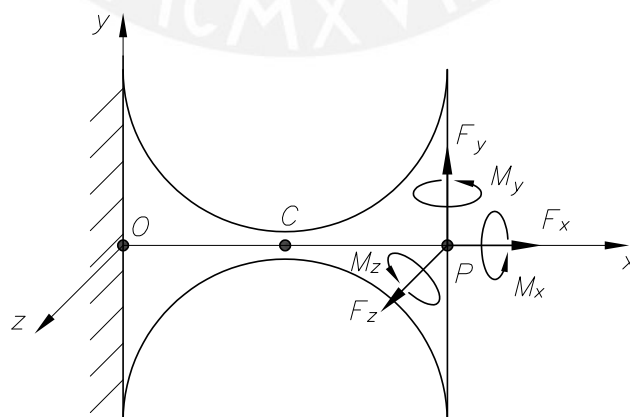


Figure 2.4: Mechanical model of a flexure hinge.

When loads are exerted on the point of reference P, displacements and rotations of its cross section occur, and the elastic behavior of the joint can be formulated as:

$$\mathbf{F} = \mathbf{K}\mathbf{u}$$

where \mathbf{F} is the external load vector acting in point P, \mathbf{u} is the displacement vector of point P and \mathbf{K} is the stiffness matrix. Stiffness is considered a 6×6 matrix, where each ij -th component represent the relationship between the i -th load and the j -th displacement of the load and displacement vectors:

$$F_i = k_{ij}u_j$$

which means that a certain load F_i produces a fraction of the displacement u_j . In perfectly prismatic hinges this is not always possible, as, for example, axial loads do not produce transversal displacements. As a result, some components k_{ij} are zero. The behavior with the complete stiffness matrix should be expressed as [40]:

$$\begin{pmatrix} F_x \\ F_y \\ F_z \\ M_x \\ M_y \\ M_z \end{pmatrix} = \begin{pmatrix} k_{u_x, F_x} & 0 & 0 & 0 & 0 & 0 \\ 0 & k_{u_y, F_y} & 0 & 0 & 0 & k_{\varphi_z, F_y} \\ 0 & 0 & k_{u_z, F_z} & 0 & k_{\varphi_y, F_z} & 0 \\ 0 & 0 & 0 & k_{\varphi_x, M_x} & 0 & 0 \\ 0 & 0 & k_{u_z, M_y} & 0 & k_{\varphi_y, M_y} & 0 \\ 0 & k_{u_y, M_z} & 0 & 0 & 0 & k_{\varphi_z, M_z} \end{pmatrix} \begin{pmatrix} u_x \\ u_y \\ u_z \\ \varphi_x \\ \varphi_y \\ \varphi_z \end{pmatrix}$$

The idealized model contemplates a compliant joint as a pin joint (only rotational motion) with a torsional spring. Then, the behavior of a hinge can be expressed as:

$$M = k_\varphi \varphi \quad (2.1)$$

where M is the external bending moment, φ the angle of rotation and k_φ the rotational stiffness. Ideally, the rotational stiffness is considered to be constant, which means that the rotation angle is directly proportional to the applied moment. As such, the behavior of a hinge represented in a moment-angle graph should be a straight line with k_φ as slope, like in Figure 2.5.

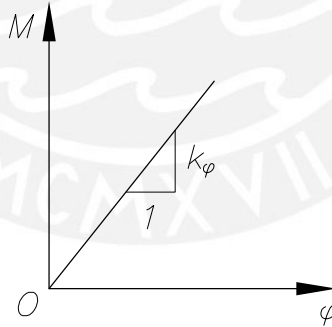


Figure 2.5: Ideal rotational stiffness behavior of a flexure hinge.

Compliance to other rotations exist but flexure hinges are designed as stiff as possible around other axes to avoid possible parasitic motions. However, undesired motions in longitudinal direction cannot be fully eliminated.

Based on this characterization of the hinge, various authors have proposed exact and simplified expressions trying to calculate the value of compliances (or stiffnesses) using many different approaches, especially the rotational compliance. Those values can differ in great manner depending on the assumptions and simplifications made so they are briefly described in the following paragraphs. A summary of the mentioned expressions and corresponding contours studied is presented in Table 2.2.

Analytical modeling

Theoretical description of the mechanical behavior of flexure hinges was first obtained from basic theory, i.e. mechanics of materials. Analytical expressions are often of great complexity so simplified and approximate equations have as well been derived.

- **EULER-BERNOULLI beam theory:**

In 1965, PAROS AND WEISBORD [62] developed, for the first time, an exact compliance equation of the semi-circular flexure hinge by integrating the EULER-BERNOULLI differential bending equation adding dimensionless parameters $\xi = h/2R$, where h is the minimum height of the hinge and R the contour radius, and $\zeta = 1 + \xi$ to reduce its complexity. Furthermore, it was reduced to a simplified design equation for small values of ξ . SMITH ET AL. [76] presented in 1997 closed form equations for the compliance of elliptic flexure hinges based on a modification of the equation by PAROS AND WEISBORD by including the aspect ratio of the ellipse. WU AND ZHOU [91] also derived design equations for calculating the compliances of semi-circular hinges including a dimensionless parameter $\lambda = R/h$ for further simplification. In 2003, MERKEN ET AL. [57] sought to increase the accuracy of the simplified equation by PAROS AND WEISBORD by adding correction factors for the range of dimensions of the hinge and its surface roughness. Later in 2009, CHEN ET AL. [11] introduced a generalized expression for conic curves to obtain a compliance equation depending on three parameters that describe the type and geometry of the contour.

- **CASTIGLIANO's second theorem:**

LOBONTIU ET AL. [52] introduced in 2001 closed form equations for the compliances of corner-filletted flexure hinges derived from CASTIGLIANO's second theorem. In the same way, equations for hinges of different contours were derived later, e.g. circular, parabolic, elliptic and more [50]. In 2010, TIAN ET AL. [84] approximated dimensionless empirical equations by using an eighth-order polynomial to fit compliance results for circular, cycloidal and filleted V-shaped hinges from CASTIGLIANO's second theorem. LIU ET AL. [49] did the same in 2016 for the novel quasi V-shaped hinge using a third-order polynomial.

- **TIMOSHENKO's beam theory:**

In their contribution, DIRKSEN AND LAMMERING [19] derived equations for the rectangular flexure hinge using the TIMOSHENKO beam theory, i.e. shear deformation was considered. The model was used for circular and parabolic contour hinges, however, equations were not presented due to high complexity.

- **Principle of virtual work:**

A new type of flexure hinge, the power-function-shaped, was presented by LI ET AL. [45] in 2013. To obtain its compliances, the principle of virtual work, i.e. the unit load method, was used. According to the unit load method, the virtual rotation is done by a unit load.

The previous approaches have been rather inaccurate for some rather inaccurate for some dimensions, contours and geometries with complex shapes. Consequently, other modeling approaches have been proposed.

- **Pseudo Rigid-Body Model (PRBM):**

An approach for design of compliant mechanisms was presented by HOWELL AND MIDHA [33] in 1994. Compliant joints such as rectangular hinges or flexure beams are replaced by torsional springs of same stiffness connecting rigid links. This approach

is particularly useful for modeling compliant joints based on constant section beams in conventional mechanism configurations, like the cross flexure hinge [39]. However, its main purpose is its use for the synthesis of compliant mechanisms.

- Continuum mechanics:

TSEYTLIN [88] presented formulas for the rotational compliance of hinges of circular and elliptic contours. In his contribution, the contours were approximated by circles of different radius with displaced centers and transformed into rectilinear ones through inverse conformal mapping. Compliance was determined using continuum mechanics theory and tractable equations were derived on the basis of simplified series expansion of trigonometric functions.

- EULER-BERNOULLI beam-column theory:

AWTAR [4] developed in his doctor thesis a model of flexure beams, called the Beam Constraint Model (BCM), based on the EULER-BERNOULLI beam-column theory. By considering equilibrium in deformed state, a possible constraining axial force is allowed to appear in the differential equation, thus, having an influence on the transverse stiffness. Later in 2010, the model was updated for beams of changing section [5].

- Finite Beam based Matrix Modeling (FBMM):

In 2015, ZHU ET AL. [100] presented a novel modeling method called the Finite Beam based Matrix Modeling, where the whole hinge is considered a sequence of n rectangular short beams. Compliance is obtained by a summation of the partial compliances of every short beam.

- Nonlinear theory of large deflections of rods:

Based on numerically calculated results from the nonlinear theory for modeling slender curved rods by ZENTNER [96], LINß ET AL. [47] approximated rotational stiffness equations using a power function expression. Two coefficients were used to consider the different characteristics of each studied contour.

Finite element analysis based empirical equations

The finite element method is the most widely used method for modeling compliant joints. Different complex geometries can be generated in Computer-Aided Design (CAD) softwares for later meshing and computation in commercial FE packages. Finite element analysis (FEA) results are numerical so no general expressions can be obtained. However, some authors offer empirical equations based on those results.

In 1987, SMITH ET AL. [78] obtained a formula similar to that of a simple cantilever beam for semi-circular hinges including a coefficient dependent of the geometric parameters. This coefficient was approximated to fit the finite element analysis results. Later, KOSTER ET AL. [42] presented dimensionless design graphs as a result of finite element calculations for the circular notch hinge. However, no information about the model was provided. In 2005, SCHOTBORGH ET AL. [73] fitted dimensionless polynomial functions of first, second and third order to FEA results of corned-filletted, circular and cross flexure hinges, respectively. MENG ET AL. [56] presented in 2012 a method for calculating the compliances based on CASTIGLIANO's second theorem and FEA nonlinear calculations. Their approach consists in adjusting analytical results to FEA results by means of a contour-dependent correction parameter.

Table 2.2: Review of analytical modeling and empirical equations approaches used for different flexure hinge contours.

| Year | Author | Approach | Contour |
|------|-----------------------|---|-----------------------|
| 1965 | PAROS AND WEISBORD | Integration of EULER-BERNOULLI equation using parameters $\xi = h/2R$ and $\zeta = 1 + \xi$. | C |
| 1987 | SMITH ET AL. | FEA-approximated empirical formula. | C |
| 1992 | KOSTER ET AL. | FEA-based design graph. | C |
| 1994 | HOWELL AND MIDHA | PRBM: replacement with a rigid-body joint with torsional spring. | R, CR |
| 1997 | SMITH ET AL. | Modification of equation by PAROS AND WEISBORD using aspect ratio of ellipse. | C, R, E |
| 2001 | LOBONTIU ET AL. | CASTIGLIANO's second theorem. | C, CF, E, P, H, IP, S |
| 2002 | WU AND ZHOU | Integration of EULER-BERNOULLI equation using parameter $\lambda = R/h$. | C |
| 2002 | TSEYTLIN | Inverse conformal mapping of circular approximating contour. | C, E, P, H |
| 2003 | MERKEN ET AL. | Modification of equation by PAROS AND WEISBORD using correction factors. | C |
| 2004 | AWTAR ET AL. | BCM: model based on EULER-BERNOULLI beam-column theory. | R |
| 2005 | SCHOTBORGH ET AL. | Polynomial function fitting FEA results. | C, CF, CR |
| 2009 | CHEN ET AL. | Integration of EULER-BERNOULLI equation using a generalized conic curve equation. | C, E, P, H |
| 2010 | TIAN ET AL. | 8th-order polynomial approximation for CASTIGLIANO's theorem derived equations. | C, CY, FV |
| 2011 | DIRKSEN AND LAMMERING | TIMOSHENKO's beam theory. | C, R, P |
| 2012 | MENG ET AL. | Correction function for the equations by LOBONTIU by fitting FEA results. | CF |
| 2013 | LI ET AL. | Unit load method. | PF |
| 2015 | ZHU ET AL. | FBMM: Summation of compliance of n rectangular-section partitions. | C, E, ES, PF, FV |
| 2016 | LIU ET AL. | 3rd-order polynomial approximation for CASTIGLIANO's theorem derived equations. | QV |
| 2017 | LINß ET AL. | Power function fitting to results from nonlinear rods model by ZENTNER [96]. | C, CF, E, PL |

C: Circular; R: Rectangular; CF: Corner-filletted; E: Elliptical; P: Parabolic; H: Hyperbolic; PL: Polynomial; IP: Inverse parabolic; S: Secant; CY: Cycloidal; ES: Exponent-sine; PF: Power-function; CR: Cross; QV: Quasi V; FV: Filletted V.

2.3. Deformation errors in compliant systems

As mentioned in Chapter 1, one of the disadvantages of compliant joints is their sensitivity to small changes in their parameters. Compliant mechanisms, as all manufactured products, are not ideally perfect. Manufacturing and material imperfections, especially in the joints, can greatly affect the performance of the whole system. These effects have been discussed by some authors and three groups can be identified:

- Manufacturing deviations.
- Material imperfections.
- External influences.

Manufacturing deviations

Real motion of compliant mechanisms include parasitic errors caused by machining imperfections. Geometric parameters are always manufactured within certain tolerances, as no exact values are achievable. These values are called manufacturing tolerances and are restricted so that they do not significantly affect the intended function of a device. However, they are not only limited by design or function issues, they are limited by manufacturing technologies. Manufacturing of flexure hinges with WEDM is done in multiple steps. Inconsistencies in each step and positioning errors during the process generate imperfections in the resulting compliant mechanism [99]. Some authors have studied their effects. Common approaches consider deviations as variations of individual parameters. Through analytical or finite element (FE) modeling, motion errors in the output of a certain mechanism are quantified. Moreover, all work to date is concentrated on flexure hinges of circular contour, since it is commonly used and easy to manufacture. Parameters considered in the literature are as shown in Table 2.3.

Planar compliant mechanisms are normally cut out of a single metallic plate. Thus, the width of the joints b equals the thickness of the plate, which can be produced by different processes, such as milling or rolling. As the geometric profile is usually generated with WEDM, positioning and cutting errors generate a deviation from the circular contour. For simplification, only deviation of the hole radius R is usually considered. The radius deviation parameter has been defined in two ways: with variation of the minimum hinge height h [74], or with constant minimum hinge height [70]. Both cases would produce different results as the minimum hinge height influences to a greater extent the behavior of a hinge [74]. Aside from shape and dimension deviations of the contour, positioning errors during machining also generate deviation of the position of the holes. Cases considered by RYU AND GWEON [70] are displacements of the holes in the transversal direction, as well as combined cases with the longitudinal case. Opposed displacements in the transversal direction would produce in pure deviation of the minimum height h . Additionally, orientation errors of the wire in WEDM also occur, thus, generating perpendicularity deviation of the holes around the longitudinal and transversal axes.

Among the authors referenced in Table 2.3, only RYU AND GWEON [70] and SHEN [74] have studied the individual influences of the each parameter. In other works, only combined effects on particular mechanisms were studied. From the results of the mentioned authors, a first conclusion can be drawn about circular-contour hinges: the minimum hinge height is the most influential parameter between the geometric deviations. In the work of RYU AND GWEON the hole radius and hole position parameters were most influential. This statement has to be seen against the background of the parameter definition. Their parameter variation leads to a pronounced change of the minimum hinge height of the hinge. The results from SHEN also reveal predominance of the minimum height, especially when its value is reduced.

The results of SHEN indicate a linear deviation caused by the basic parameters (h , R , b) compared to the second-order errors caused by perpendicularity. Perpendicularity deviations generate out-of-plane motions in the joint even when submitted to in-plane

loads. This fact adds a directional component to the point of reference that is not considered by the measurement.

Table 2.3: Review of manufacturing deviation parameters.

| Parameter | Symbol | Representation | References |
|---|--------------------------|----------------|----------------------|
| Hole radius with constant hole center position | ΔR | | [36, 61, 70] |
| Hole radius with constant minimum height h | ΔR | | [74, 99] |
| Hole center position in longitudinal direction | $\Delta x_1, \Delta x_2$ | | [36, 99] |
| Hole center position in transversal direction | Δy | | [36, 61, 64, 70, 74] |
| Hole center position with shift of rotational axis | Δc | | [70] |
| Hole center position with rotation of hinge | $\Delta\theta_z$ | | [36, 61, 70] |
| Perpendicularity of hole centers to longitudinal axis | $\Delta\theta_x$ | | [61, 64, 70, 74] |
| Perpendicularity of hole centers to transversal axis | $\Delta\theta_y$ | | [61, 64, 70, 74] |
| Plate thickness | Δb | | [36, 70, 74, 99] |

Material imperfections

Materials are selected based on the needs of a particular system. Depending on the application, material selection often requires constancy of some properties with predictable variation of others, or even only satisfactorily constant properties. This sometimes leads to the search for unusual special-purpose materials or or purposeful combinations of available materials make use of compensation effect [83]. Moreover, precision applications often confront the designer with situations where unexpected phenomena arise or where assumptions do not apply anymore, e.g. anelasticity in micro-size beams for MEMS [12].

Properties of materials are actually assigned numerical values obtained through experimental procedures in accordance with specialized standards. As such, they are bound to the inherent uncertainty of those experiments. Many values can only be valid for specific conditions of other parameters, like temperature. Sometimes needed properties are not easy to find in the literature, like the degree of mechanical hysteresis, because handbooks include only common properties of widely used materials. More problematic can be the fact that the values of well known materials vary between manufacturers. Heat treatment, cold working and composition can have a great influence over the actual value.

In compliant systems, motion is enabled by the use of the elasticity of a material. Models mentioned in Section 2.2 consider only the elastic modulus to describe the material behavior but it is important to remark some other mechanical properties or parameters encountered in precision design [82]:

- *Elastic drift*: change of strain that occurs after the stress becomes stable.
- *Thermal coefficient of elasticity*: measure of the variation of elastic modulus with variation of temperature.
- *Zero shift*: change of the zero state of the system due to plastic deformations.
- *Mechanical hysteresis*: strain retained during stress cycling.
- *Creep*: slow dimensional change occurring under stress conditions.
- *Ageing properties*: variation of elastic modulus with time.
- *Internal friction*: loss mechanism withing material structure.
- *Fatigue strength*: endurable amplitude of cyclic stress without failure.

These phenomena arise to some degree, usually neglectible in rough design, in all mechanical systems. Such parameters can be fundamental in precision design as they deviate the expected elastic behavior of a material. This encourages sometimes the development of some special purpose materials. For example, nickel-iron alloys can be mixed in different propotions (27 or 42 %) to show virtually zero variation of their elastic modulus with temperature changes. Other alloys can be heat treated to reduce the degree of mechanical hysteresis [83]. Some discussions exist about the ideality of elasticity in flexure hinges [82] but almost no work has been dedicated to study their influence. In fact, the only works that treat this topic are dedicated to the anelasticity of flexure strips at low frequencies and related relaxation effects [67, 79, 80].

External influences

Although manufacturing deviations have been studied intensively by different authors, other influences aside from them are yet to be studied in detail. In their work, NIARITSIRY ET AL. [61] presented the influences of temperature and gravity over the output motion of a compliant mechanism. Temperature effects considered were convection and conduction effects. Convection between the environment and the mechanism proved to be more influent. However, precision systems work in environments with thermal insulation and temperature control. Thus, temperature variations of about $\pm 0,01$ °C can be achievable [61]. In such ranges, temperature does not represent a major problem. In contrast, gravity, especially at nanometer scale, can be a major source of inaccuracy [61]. Gravity produces loading without the presence of input forces so it can change the expected motion of the mechanism, depending on its direction and the mass of the system. Some works have addressed the effect of gravity due to a small deviation of its direction produced by ground tilt [18, 54, 79]. This effect is of particular interest in load measuring systems.

2.4. Discussion

The discovered restrictions and problems of previous investigations and their modeling approaches constitute the challenges to overcome in this work. The following discussion on the current state of the art is treated around two major topics:

- The applicability of previous approaches to model thin flexure hinges under ideal and non-ideal conditions.
- The description of the stiffness of a flexure hinge under non-ideal conditions.

On the one hand, expressions in the literature proved acceptable accuracy only in some ranges of the geometric parameters of a flexure hinge when compared to FEA results, e.g. the minimum height-radius ratio h/R in semi-circular flexure hinges. According to the results of YONG [95], as the value of h/R decreases, the rotational compliance results based on EULER-BERNOULLI beam theory should equal the FEA results. This theory assumes that the dimensions of the cross section are much smaller than the length of the beam. Depending on the contour, this assumption can be invalid but it should correctly apply to thin hinges. However, such conclusion cannot be generalized. Because compliance in other directions is to be avoided, the width of the hinges, especially thin ones, can be actually large. In such case, the mentioned assumption would not apply anymore. Also important is a decrease in dimensions to the micrometer scale as other effects may gain influence. Only two works in the literature have exposed this fact. In the experiments of ZHANG ET AL. [98], polysilicon thin circular micro-hinges of 3 μm of minimum height showed stiffness around 15 times greater than the values calculated with the full equations of PAROS UND WEISBORD [62]. The results of MERKEN ET AL. [57] also show appreciable disagreement between modeling and measurements. In their contribution, flexure hinges of 66 μm of minimum hinge height were compared to three models, being the first one the simplified equation from PAROS AND WEISBORD. The other two models were corrections of the first one considering thick hinges and surface roughness to match the measurements.

On the other hand, most analytical and empirical equations of Section 2.2 consider only the ideal hinge model of Figure 2.4. In the case of circular-contour hinges, for example, the parameters that fully describe the behavior of the joint according to this characterization are the minimum height h , radius R , width b and the elastic modulus E . This means that all possible influences over the stiffness are caused by the deviations of those parameters,

which is an oversimplified approach. A more generalized method, the FBMM [100], was used to model non-ideal geometries, i.e. hinges affected by manufacturing imperfections [99], but modeling of out-of-plane deviations is yet to be done. Also, other effects such as gravity or temperature have no place in these expressions so their study cannot be conducted.

Investigations up to date, related to errors in compliant systems, analyze motion errors caused by manufacturing imperfections and external influences. In most studies, combined effects of manufacturing deviations in the motion of particular compliant mechanisms were considered. As such, their results cannot be applied to study the stiffness of individual joints. Although SHEN [74] analyzed the motion performance of a single flexure hinge, his work was focused on a single-notch circular hinge with a minimum height-radius ratio of 0.4, which can be considered a thick hinge [88]. Another drawback of previous works are the parameters used for modeling non-ideal hinges. Among those investigations, the work of RYU AND GWEON [70] considers the most geometric deviations, but the work of NIARITSIRY ET AL. [61] is the only one that studies the influences of temperature and gravity. Consistency in parameter selection and definition cannot be found among the studies. For example, the hole radius deviation in the study of RYU AND GWEON generates a variation of the minimum height, while SHEN considers it as constant. Such incongruity in parameter definition produces incongruity in the results, distorting the apparent influence of certain parameters between investigations. Extending the previous example, when looking at modeling equations of circular contour hinges, the minimum height and the radius are parameters independent from one another, which means that the definition of the radius parameter in the work of RYU AND GWEON forces a relationship between both dimensions. For a better understanding of the behavior and a correct definition of the sources of error, such studies should aim for independent parametrization, although it is not always possible. Concerning the definition of stiffness discussed in Section 2.2, it can be observed that no actual study on loading conditions as sources of deviation exists in the reviewed literature. Studies of this type have been found for thin flexure hinges.

Based on the problems mentioned, this work will focus on the following studies:

- Analysis of the accuracy of analytical models in determining the rotational stiffness of thin flexure hinges.
- Identification of the parameters that define the stiffness of compliant joints and their sources of deviation.
- Characterization of a flexure hinge under non-ideal conditions.
- Detailed study of the influence of the parameters on the rotational stiffness based on their range of deviation.

A remark should be done to the fact that these studies are conducted to support future design of compliant mechanisms for high-precision applications and some results will be validated through experimentation using a setup developed by a fellow student. Therefore, some limitations will be encountered, e.g. lack of knowledge of anelastic properties.

3. Finite element modeling of thin flexure hinges

It was stated at the end of the previous chapter that the results of this investigation would support future designs of compliant mechanisms. The large number of available geometrical shapes for flexure hinges cannot be covered within the scope of the present study. Therefore, it is necessary to select an appropriate geometry based on its importance in the field of application. In the work of LINß ET AL. [48], a comparison between compliant joint types was presented in which the leaf, notch and cross flexure hinges were rated as the most frequently used. Among them, notch hinges are more suitable for high-precision applications due to their well-defined axis of rotation. Numerous notch contours exist but the majority of investigations are focused on circular-contour flexure hinges, as shown in Table 2.2 and in Section 2.3. Circular contours are suitable for thin hinges as they realize the best accuracy [46] so they are commonly found in highest precision systems, e.g. weighing cells [18]. Therefore, a circular-contour flexure hinge is studied in this work.

It is also necessary to define what characteristics a thin flexure hinge possesses. Although no textbook definition exists, thin hinges are defined by TSEYTLIN [88] as those whose deformation occurs mostly within its boundaries. This means that there exists almost no influence of the adjacent links in the deformation. In his work, circular-contour hinges were categorized based on the ratio between their minimum height h and their radius R in: thick ($0.2 < h/R \leq 1.0$), intermediate ($0.07 < h/R \leq 0.2$) and thin ($h/R \leq 0.07$) hinges. A more general description was later introduced by LINß ET AL. [48] using the relationship between the minimum height h and the total height H for hinges of various contours. For thin hinges $h = 0.03H$ and for intermediate hinges $h = 0.05H$. A thin semi-circular hinge would have a h/R ratio less than 0.062 according to LINß ET AL. Additionally, important is to remark that flexure hinges are designed with high off-axis to on-axis stiffness ratios to reduce parasitic motions. This is accomplished with a large width in comparison to its minimum height. As a result, very thin hinges tend to have high aspect ratios. These considerations are taken into account later for modeling.

3.1. Model requirements

For a proper investigation on the behavior of a flexure hinge, some requirements for the model must be established first. Emphasis is placed on the numerical accuracy of the results but also on the computational efficiency of the calculation due to the later use of the model in studying non-ideal hinges. The requisites are as follows:

- Singularities must be avoided, e.g. sharp corners or point loads.
- Solutions must be mesh independent.
- Low calculation time without compromising solution accuracy.

- Convergence stability, i.e. absence of excessive element distortion.
- Element compatibility, i.e. displacement continuity between elements.
- Shear locking due to bending must be prevented.
- Geometric nonlinearities must be considered.
- The model must support geometric deviations, thus, it needs to be flexible to avoid modeling errors. The type and range of values of these deviations are defined in the next chapter.

These considerations are verified during the modeling steps when they correspond.

3.2. Geometry and material

The consideration of out-of-plane effects requires the development of a 3D model. FE modeling of flexure hinges usually includes not only the notch domain but also a part of the connecting links because deformation not only occurs within the boundaries of the notch [47, 95]. Although this is neglectable for thin hinges according to the definition by TSEYTLIN [88], they are included for later modeling of geometric deviations and to avoid sharp corners due to the end of the contour. The geometry of the flexure hinge is shown in Figure 3.1. The notation used is the same as in [47].

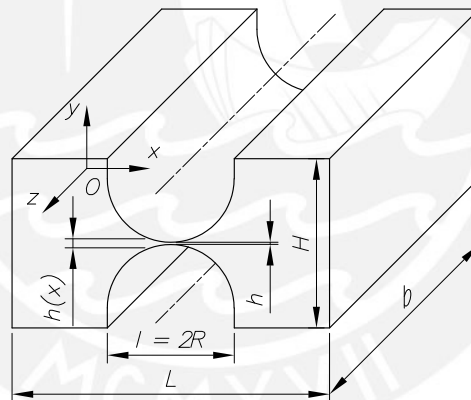


Figure 3.1: Geometry of the investigated right semi-circular flexure hinge.

Following the mechanical model presented in Section 2.2, coordinates origin O is placed at the center of one end face. The x -axis coincides with the longitudinal axis, the y -axis is parallel to the transversal axis and the z -axis parallel to the rotation axis. Ideal dimensions considered for the flexure hinge are presented in Table 3.1. The minimum height h was set at a value of $50 \mu\text{m}$ which lies near the limit achievable with manufacturing technologies without altering the physical characteristics of the material [65, 72]. The h/R ratio for this geometry results 0.0167 , falling in the category of thin hinge according to TSEYTLIN [88]. The width b of the hinge was set at a value of 10 mm , which is sufficient for most planar applications [19]. The aspect ratio b/h amounts to 200 , a typical value for the thinnest flexure hinges [6] although the current limit lies around 375 [32]. The total height H should be greater than the height at the end of the contour $h(x) = h + 2R$ as the geometric deviations later considered could generate singularities at this point. Thus, the total height was set at a value of 9 mm . The height ratio h/H is 0.0055 so it is also classified as thin according to LINß ET AL. [48].

Material properties for the model are assumed perfectly linear elastic. The material is the high strength aluminium alloy grade 7075 with an elastic modulus $E = 71$ GPa, a POISSON's ratio $\nu = 0.33$ and a yield strength $\sigma_{yield} = 505$ MPa, which is widely used for precision engineering applications [47]. The density of the material is $\rho = 2.8$ g/cm³.

Table 3.1: Flexure hinge parameters.

| Parameter | Symbol | Value | Parameter | Symbol | Value |
|----------------|--------|------------|-----------------|------------------|-----------------------|
| Total length | L | 15 mm | Width | b | 10 mm |
| Total height | H | 9 mm | Elastic modulus | E | 71 GPa |
| Hinge length | l | 6 mm | POISSON's ratio | ν | 0.33 |
| Radius | R | 3 mm | Yield strength | σ_{yield} | 505 MPa |
| Minimum height | h | 50 μ m | Density | ρ | 2.8 g/cm ³ |

3.3. Loading and boundary conditions

The rotational stiffness is calculated from an applied bending moment M and the resulting rotation angle φ as in Equation 3.1:

$$k_{\varphi} = \frac{M}{\varphi} \quad (3.1)$$

Another possibility is the application of displacements to obtain the resulting reaction forces. However, since out-of-plane displacements will be present due to deviations later considered, this approach would add unnecessary constraints. As presented in the mechanical model of Figure 2.4, the end of the flexure hinge where the coordinates origin O locates is fixed (no nodal displacements) and loading is applied on the free end. The rotation angle φ is calculated from the displacement components x and y of two reference points of the link on the free end [47] P_1 and P_2 (see Figure 3.2(a)). The edge between the selected points is always parallel to the normal vector of the free end face. Only the in-plane component of the rotation is calculated as non-ideal hinges may rotate around other axes.

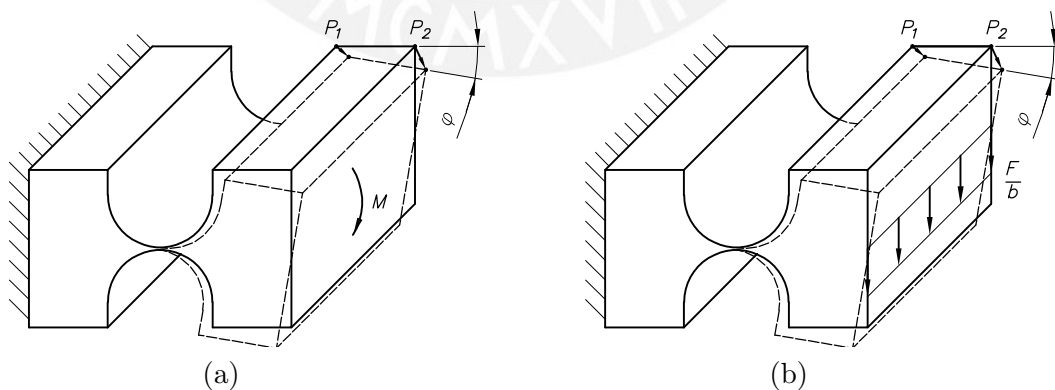


Figure 3.2: Loading and boundary conditions: (a) idealized case; (b) FE model.

Application of the bending moment M should be done through nodal forces as 3D finite elements possess only three degrees of freedom (DoFs) per node. The bending moment M is produced by a shear force F multiplied by the lever arm $L/2$ to the ideal axis of rotation (point C in Figure 2.4). Force F is distributed over the nodes on the edge at position $y = 0$ of the free end to avoid point loads, (see Figure 3.2(b)). This loading condition

ensures that the applied bending moment is always in the same direction (z -axis) and that the reference points are not subjected to any loading, ensuring a rigid-body motion of the edge P_1P_2 . A comparison of results to different loading conditions using the model defined later is presented in Appendix A. In Table A.1, the bending moment M is applied using a distributed shear force, a couple of distributed normal forces and a surface force, and the rotational stiffness k_φ is calculated assuming geometric nonlinearities for different rotation angles φ . Results in Figure A.1 show a strong deviation of the surface force case to the other two, especially for higher rotation angles. Surface loads are always perpendicular to the surface they are applied to, so the nodal forces change their direction with the deformation. In non-ideal flexure hinges, rotations around other axes may exist, making surface forces not suitable for their study. In contrast, shear and normal forces maintain always the same direction. In the case of interest of this work, flexure hinges in weighing cells, the bending moment is generated due to a couple of forces. However, the case in Appendix A would subject reference point P_2 to loading, which is not desired. Since results of the shear force and the couple of forces cases are almost equal for small rotation angles, application through a shear force is an acceptable approach.

3.4. Meshing

Although there is not much information about 3D-FE models in the literature, 2D-FE models of circular contour hinges can be found in various contributions using either free or mapped meshing of triangular or quadrilateral elements. Notch flexure hinges are most suitable for mapped meshing because of their simple prismatic geometries and, thus, it is used in this model. In the case of modeling of thin hinges, emphasis should be placed on the meshing strategy to be used as they present high aspect ratios H/h and b/h . Due to them, the number of elements can be quite high or they can have undesirably high aspect ratios. For example, Figure 3.3 shows two models of a thin semi-circular flexure hinge using two mesh strategies found in the literature. The model from Figure 3.3(a) produces a high number of elements to avoid excessive distortion and the model from Figure 3.3(b) produces highly distorted elements in the zone of interest.

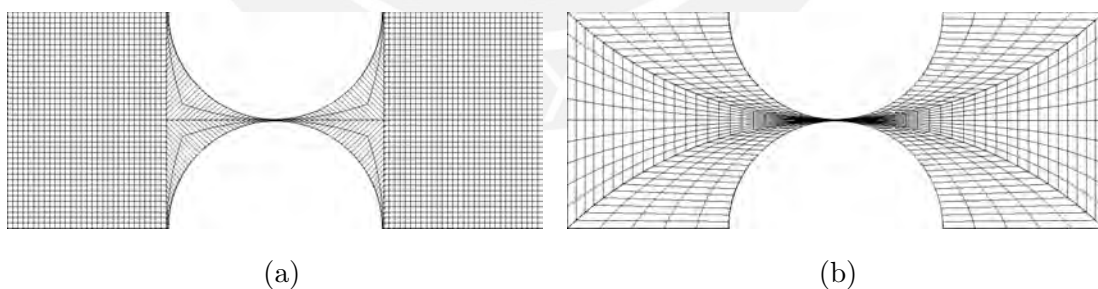


Figure 3.3: Meshing strategy from: (a) YONG [95]; (b) SHEN [74].

Solutions of the model must be independent of the mesh, i.e. numerical convergence. To obtain convergence, mesh must be refined until results do not vary significantly with increasing number of elements. Refinements should be done in zones with high stress gradient to avoid an unnecessarily large number of elements, which results in high computational time. In the case of notch flexure hinges, stresses are concentrated around the thinnest region ($h(x) = h$) where the ideal axis of rotation approximately locates. Transition from rough meshes in zones with low stress gradient to fine meshes should also be taken in consideration. Therefore, the meshing strategy shown in Figure 3.4 is proposed.

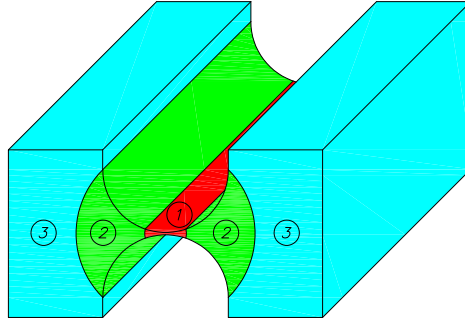


Figure 3.4: Domain partition for meshing.

The domain of the flexure hinge is divided in three zones: a highly refined central zone (1), a transition zone (2) and a rough-meshed outer zone (3). Zone 1 is where most deformation occurs and is limited by the height where the stress is 10% of the maximum normal stress produced by bending considering stress concentration effects [75]. This occurs when $h(x) = h' = \sqrt{10/k_b} h$ where k_b is the stress concentration factor for bending calculated as [75]:

$$k_b = \left(1 + \frac{h}{2R}\right)^{9/20} \quad (3.2)$$

Zone 2 is limited by the end of the circular contour and exists as a transition from the rough mesh in zone 3 to the fine mesh in zone 1. Zones 1 and 2 are limited by cylindrical surfaces to avoid excessive skewness of the elements produced by the circular contour. Element size in the out-of-plane direction in each zone is determined by the minimum element size in the plane of motion and a limiting aspect ratio to reduce the number of elements.

It is important to remark that these meshes may not match at their interfaces and, thus, need to be connected through contact elements. Formulations for contact elements available in ANSYS Mechanical [2] are:

- Pure Penalty: establishes a relationship between the contact surfaces using a spring-like contact. Penetration between surfaces is determined by the defined contact stiffness.
- Augmented Lagrange: utilizes the penalty method but the contact forces are augmented during the equilibrium iterations until the penetration is smaller than a defined tolerance value.
- Normal Lagrange: uses a defined contact force as an extra degree of freedom instead of the contact stiffness and penetration.
- Multi-point Constraints: adds constraint equations to relate displacements between nodes of the contacting surfaces.

To select a suitable formulation, a comparison is presented in Table 3.2 based on the following criteria:

- Convergence behavior: number of equilibrium iterations needed.
- Contact stiffness: need and sensitivity of a normal contact stiffness.
- Penetration: magnitude of the contact penetration.

Table 3.2: Comparison of contact formulations.

| Formulation | Convergence behavior | Contact stiffness | Penetration |
|-------------------------|----------------------|-------------------|-------------|
| Pure Penalty | + | - | - |
| Augmented Lagrange | - | +/- | +/- |
| Normal Lagrange | - | + | + |
| Multi-point Constraints | + | + | + |

Contact needed for a continuous body such as a flexure hinge needs to be always bonded with no penetration. This means that penalty-based methods, where a contact stiffness exists, are not suitable as they would require infinite stiffness, which is not numerically possible. The model must also converge to the solution as fast as possible so methods like Normal Lagrange, where a large number of equilibrium iterations may be needed, do not apply. Therefore, multi-point constraints are used for connecting the zones.

Since 3D solid elements are used, the order of the polynomial used in the interpolation function needs to be defined. Although first-order or linear elements are computationally more efficient due to having less nodes (or DoFs), thin structures modeled with them present shear locking when subjected to bending [8]. This phenomenon increases the stiffness of the structure due to the inability of these elements to capture the kinematics of deformation. This problem can be reduced by increasing the number of elements along the height of the bending beam or by using second-order elements. Increasing the number of elements along the height would also increase them along the out-of-plane direction seeking to avoid high distortion. Second-order elements, on the other hand, avoid shear locking as they can assume a curved shape during deformation due to the midside nodes. In a first step, 20-node quadratic solid elements SOLID186 is used in the model but results are also verified for 8-node linear elements SOLID185.

As previously stated, refinements should be done in zones with high stress gradient but it is also important to analyze how the solution behaves in relationship with the overall mesh. Number and transition of elements along the edges of each zone are studied in Appendix B by assuming different combinations of values for each parameter and observing the resulting value of the maximum bending stress $\sigma_{x,max}$ at $x = L/2$. Stresses are used because they converge slower than displacements since they are derived results. Stress $\sigma_{x,max}$ can also be easily compared with analytical calculations. Solutions like VON MISES stress cannot be compared with analytical values due to the existence of a stress in z -direction in the FE results, which is zero in the analytical approach. This phenomenon is studied later. 200 combinations of parameters were generated using the Advanced Latin Hypercube Sampling (A-LHS) method [35] and simulated assuming geometric linearity. A bending moment $M = 1$ Nmm was applied which results in a stress $\sigma_{x,max} = 240.90$ MPa according to analytical calculations considering stress concentration. The stress concentration factor was calculated from Equation 3.2. Results of these combinations are presented and fitted with a power function in Figure 3.5.

Figure 3.5 shows that $\sigma_{x,max}$ converges to approximately 242 MPa with increasing number of nodes. This means that the numerical solution of $\sigma_{x,max}$ deviates from the analytical result in 0.46%. A sensitivity analysis conducted using the Metamodel of Optimal Prognosis (MoP) [58] shows that results of $\sigma_{x,max}$ depend highly on the number of elements along the length of zone 1 and their transition (see Appendix B). There is not much influence of the number of elements along the height and along the width of this zone

(governed by the aspect ratio parameter) as well as along the length of zone 2 but they influence the overall number of nodes. Other parameters show almost no influence.

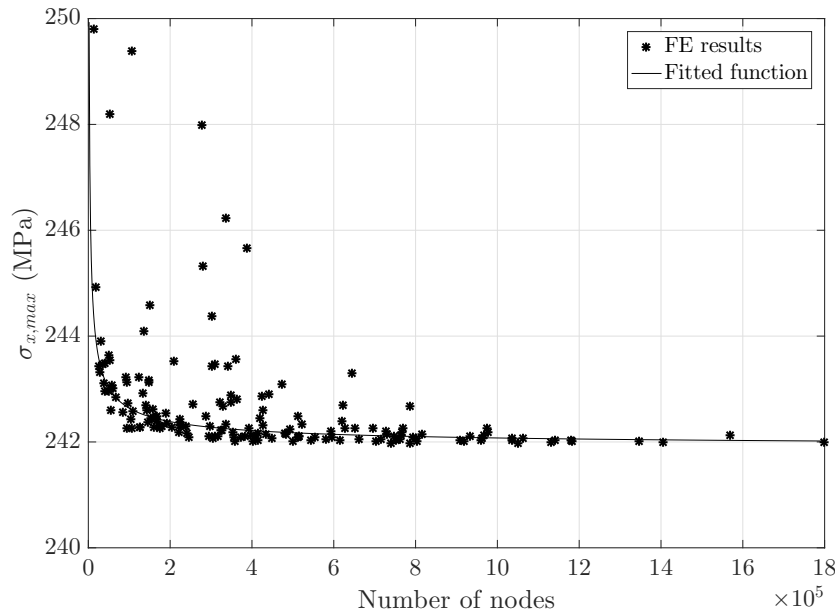


Figure 3.5: Solution convergence of $\sigma_{x,max}$.

Meeting an appropriate mesh would require a suitable combination of parameters for which the solution lies within a certain range of accuracy without excessive computational time. For that reason, the rough meshed model of Figure 3.6(a) is used. Number of elements along the height should be even for the shear force F to be properly applied and was set at 2 in zone 1. Number and transition of elements along the length of zone 1 was selected so that elements have an aspect ratio of approximately 1 in the plane of bending. Maximum aspect ratio of the elements was set at 10. The model is uniformly refined (see Figure 3.6) and convergence of the solution is studied (see Figure 3.7). Additionally, the same meshes are utilized and further refined using linear elements SOLID185 to show their behavior.

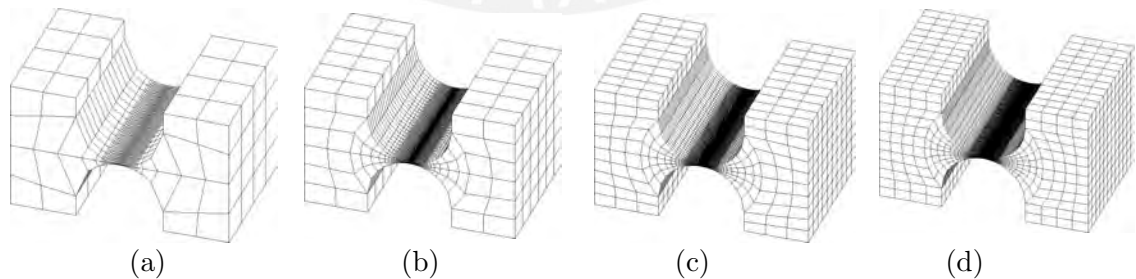


Figure 3.6: Model with different meshes.

Figure 3.7 shows that quadratic elements converge to a solution with lower number of nodes than linear elements. Computational time is less for linear elements for about the same number of nodes but solution converges to approximately 234 MPa, which results in a deviation of -2.86% to the analytical value. This greater negative deviation demonstrates the stiffer behavior of linear elements. Stresses are derived from the displacement results so lower stresses are produced from smaller displacements, i.e. higher stiffness. In contrast, solutions of quadratic elements with meshes (b), (c) and (d) have less than 0.58% of

deviation to the analytical value and a maximum deviation of 0.12% to the converged value from Figure 3.5. Therefore, quadratic elements SOLID186 will be used for the model.

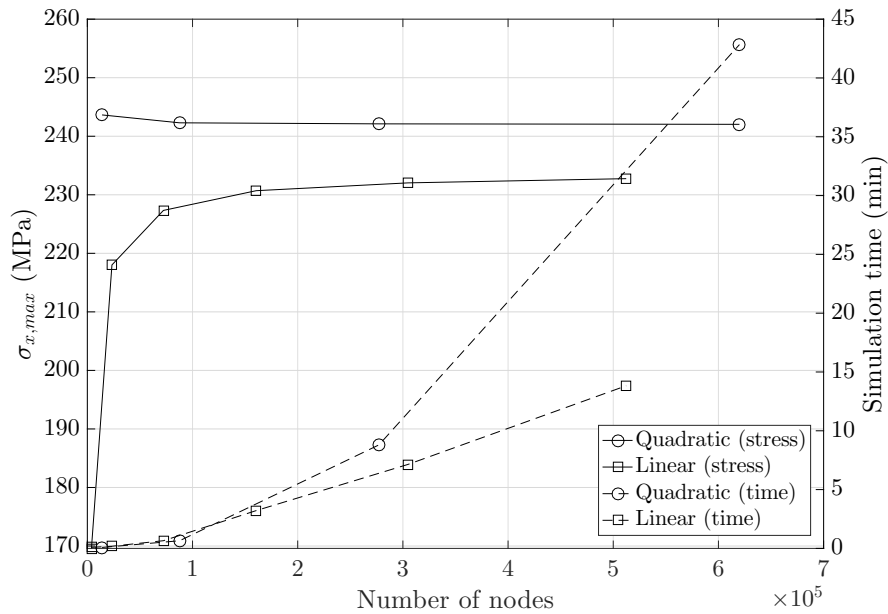


Figure 3.7: Mesh independence.

Simulation time highly increases with the number of nodes (and DoFs), especially for nonlinear calculations. Meshes (b), (c) and (d) required 0.65, 8.8 and 42.8 minutes, respectively, using a processor of 3.4 GHz (4 cores). Taking into account that several simulations are required for this investigation due to the nature of the sensitivity analysis and further studies, mesh (b) will be selected for the model. The number of elements of mesh (b) amounts to 18912, including contact elements, and the resulting maximum bending stress is $\sigma_{x,max} = 242.29$ MPa for linear calculations.

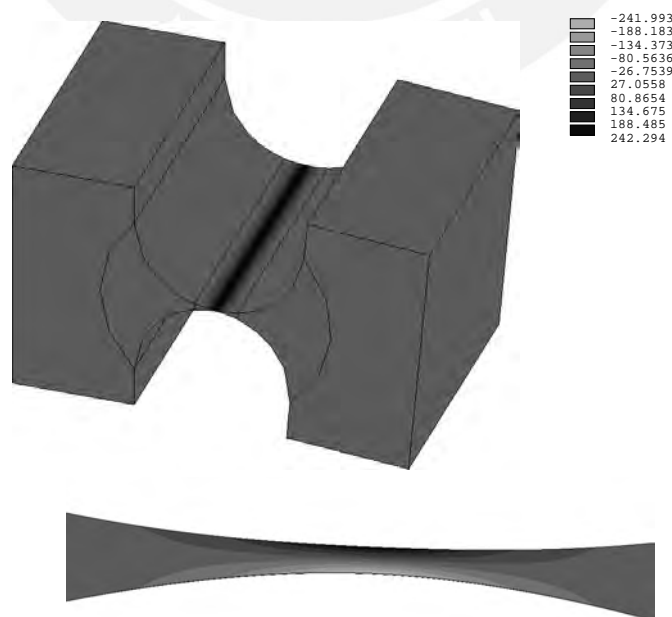


Figure 3.8: Bending stress σ_x in MPa.

3.5. Geometrically nonlinear calculation

Solutions of solid mechanics problems depend also on the deformation itself, resulting in a nonlinear relationship between loading and displacements. This means that the rotational stiffness k_φ is not constant for different rotation angles φ . In nonlinear problems, equilibrium equations are updated during deformation. A common approach for solving such problems is the NEWTON-RAPHSON method [8], used by ANSYS [1]. In this method, an iterative procedure is conducted in which a linear solution is performed for evaluating the out-of-balance or residual load vector \mathbf{R} , which is the difference between the applied loads \mathbf{F}^a and restoring forces \mathbf{F}^{nr} as in:

$$\mathbf{R}_i = \mathbf{K}_i^T \Delta \mathbf{u}_i = \mathbf{F}^a - \mathbf{F}_i^{nr}$$

$$\mathbf{u}_{i+1} = \Delta \mathbf{u}_i + \mathbf{u}_i$$

where \mathbf{K}_i^T is the tangent stiffness matrix. If a specified convergence criteria is not satisfied, \mathbf{K}_i^T and \mathbf{F}_i^{nr} are updated for the resulting \mathbf{u}_{i+1} and the solution repeated until it converges. To obtain better convergence of this method, load is usually applied in a series of increments (time steps), in which this procedure is done for each load increment. For a trustworthy geometrically nonlinear calculation, it is necessary to define information such as number of load increments, convergence criteria and type of equation solver. To optimize convergence, the line search method is used, which is helpful when a stiffening response occurs [1] as is the case of bending of flexure hinges [26]. This method scales the solution vector by a scalar multiplier α , which is automatically determined by ANSYS to minimize the energy of the system [1]:

$$\mathbf{u}_{i+1} = \alpha \Delta \mathbf{u}_i + \mathbf{u}_i$$

Convergence criteria

Convergence criteria is first studied using program-controlled timestepping and the robust direct solver. Force convergence is checked by comparing the vector norm of the force imbalances against the criteria:

$$\|\mathbf{R}\| < \varepsilon_{\mathbf{R}} R_{ref}$$

$\|\mathbf{R}\|$ can be either the L1, L2 or infinite norm of the out-of-balance vector \mathbf{R} and the convergence criteria is the product of tolerance value $\varepsilon_{\mathbf{R}}$ and a reference force value R_{ref} . By default, ANSYS uses the L2 norm for comparison with values of $\varepsilon_{\mathbf{R}}$ and R_{ref} equal to 0.005 (0.5%) and 0.001, respectively [1]. Displacement convergence is also evaluated analogously but serves only as an additional check. Convergence criteria is evaluated by adjusting the value of $\varepsilon_{\mathbf{R}}$ for each norm and observing the variation of the results. The maximum bending stress $\sigma_{x,max}$ and rotation angle φ for $M = 1$ Nmm are calculated for decreasing $\varepsilon_{\mathbf{R}}$ three orders of magnitude and the relative deviations $e_{\sigma_{x,max}}$ and e_φ to the values when $\varepsilon_{\mathbf{R}} = 0.0005\%$ are compared.

Results of nonlinear calculations in Figure 3.9 show that default values of the convergence criteria may be sufficient for this model as their maximum deviations are $1.6 \times 10^{-8} \%$ for $\sigma_{x,max}$ and $5 \times 10^{-9} \%$ for φ when reducing the criteria for all norms. Some slight deviations between norms are appreciated for default values but same results are obtained by all norms when the tolerance is reduced to 0.0005%. Simulation time was not affected by adjusting the convergence criteria so tighter tolerances can be used although default values produce no significant deviation. In this work, the L2 norm will be used and a tolerance of $\varepsilon_{\mathbf{R}} = 0.0005\%$ will be set.

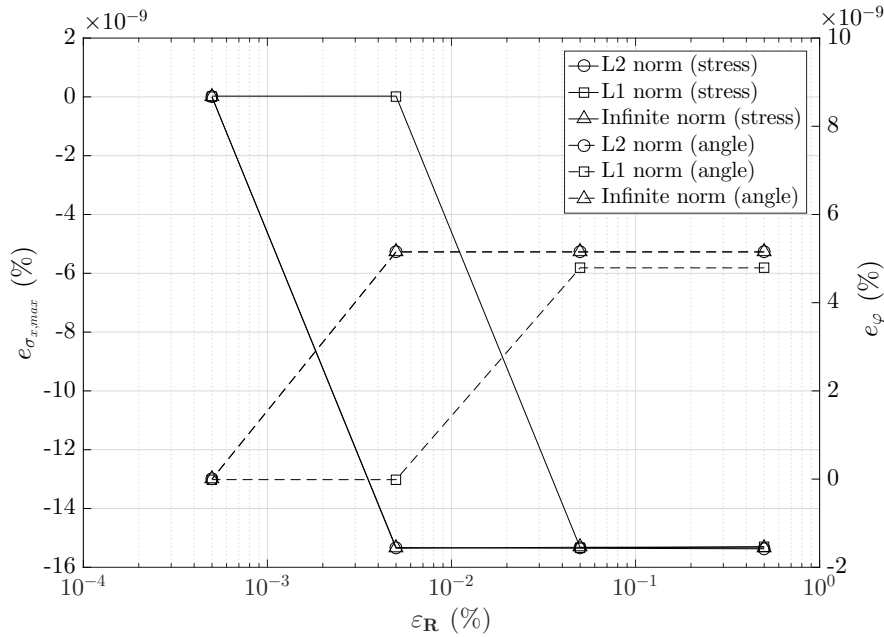


Figure 3.9: Convergence criteria.

Load increments

Using the defined convergence criteria and the direct solver, the number of load increments is evaluated to improve simulation time by increasing them from 1 to 12, which was the number automatically determined by ANSYS in Figure 3.9 for the default convergence criteria and $M = 1$ Nmm. However, automatic increments are not uniformly distributed but are controlled using an a prediction algorithm which calculates a new increment according to the equilibrium iterations needed for convergence of the last step. The number of increments and the number of equilibrium iterations per increment depends on the nonlinearity of the problem. If rotations are large, the number of equilibrium iterations is higher and more increments may be needed. In this case, load is uniformly distributed for each number of time steps and the relative stress deviation $e_{\sigma_{x,max}}$ to the value for 12 load increments is calculated for $M = 1$ Nmm ($\varphi \approx 3.17^\circ$) and $\varphi = 1^\circ$ (see Figure 3.10).

Figure 3.10 shows that with more than two load increments the value of $\sigma_{x,max}$ does not vary anymore but simulation time gets very high (approximately 30 minutes for $M = 1$ Nmm). In contrast, using 1 time step, results deviate in 1.7×10^{-5} % for $M = 1$ Nmm and 4.5×10^{-6} % for $\varphi = 1^\circ$ but simulation time is highly decreased. It is also observed that deviations and simulation time decrease with smaller rotation angles. This is in fact convenient as rotation angles cannot be too large because of the stiffening behavior of the hinge which could lead to false results in later analysis. As such, load will be applied in one increment and rotation angles will be kept small to avoid stiffening and reduce deviations. This is treated later.

Equation solver

There exist two types of solvers for linear equation systems: direct and iterative. The direct solver is based on a direct elimination of equations so they lead to an exact solution. On the other hand, iterative solvers obtain a solution by refining an initial guess until it is within an acceptable tolerance. The need of an iterative solver is based on requirements of time and memory. Defining a suitable solver for this investigation would require a

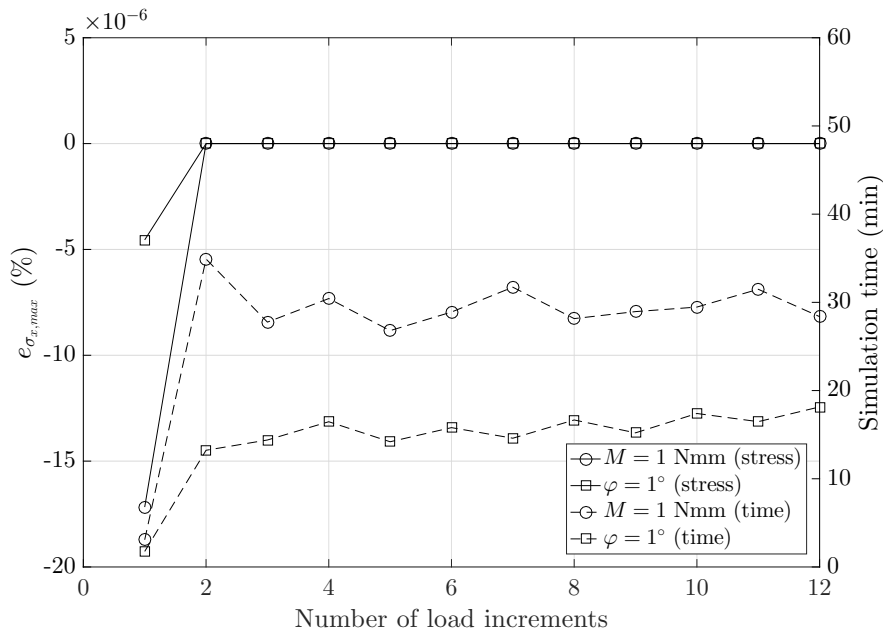


Figure 3.10: Number of load increments.

comparison seeking for improving the computational time. Solvers available in ANSYS are [1]:

- Sparse solver.
- Preconditioned Conjugate Gradient (PCG) solver.
- The Jacobi Conjugate Gradient (JCG) solver.
- The Incomplete Cholesky Conjugate Gradient (ICCG) solver.

They are compared in terms of accuracy of results, simulation time and memory required in Table 3.3, where $\sigma_{x,max}$ is calculated for $M = 1$ Nmm. Tolerance for iterative methods is set at the default value of 1×10^{-8} .

Table 3.3: Comparison of equation solvers.

| Solver | Accuracy $e_{\sigma_{x,max}}$ (%) | Simulation time (min) | Memory (MB) |
|--------|--------------------------------------|--------------------------|----------------|
| Sparse | - | 2.9 | 3415.0 |
| PCG | -2.34×10^{-11} | 3.5 | 614.0 |
| JCG | 2.02×10^{-10} | 46.7 | 483.0 |
| ICCG | 3.73×10^{-10} | 28.0 | 893.0 |

Results from iterative solvers show almost no deviation when compared to the exact solution but simulation time was not improved. In contrast, it increased. The direct solver requires more memory but for this investigation, due to the high number of upcoming calculations, efficiency will be prioritized. As such, the sparse solver will be used.

3.6. Mechanical behavior

The rotational stiffness of the flexure hinge was calculated using the model defined in Section 3.4 while assuming geometric linearity and is presented in Table 3.4. Additionally,

values obtained through analytical and design equations by different authors from the literature are included. These expressions can be found in Appendix C.

Table 3.4: Rotational stiffness k_φ according to different approaches.

| Author | Approach | Value (Nmm/rad) |
|---------------------------------|---|-----------------|
| 3D-FE model (linear) | Finite element method | 18.029 |
| PAROS AND WEISBORD (full) [62] | EULER-BERNOULLI beam theory | 16.243 |
| PAROS AND WEISBORD (simp.) [62] | EULER-BERNOULLI beam theory | 16.209 |
| WU AND ZHOU [91] | EULER-BERNOULLI beam theory | 16.243 |
| TSEYTLIN [88] | Continuum mechanics | 18.542 |
| LOBONTIU [50] | CASTIGLIANO's theorem | 16.243 |
| LINß ET AL. [47] | Design equation based on nonlinear theory for curved rods | 15.887 |

It is to remark that the equations from PAROS AND WEISBORD, WU AND ZHOU and LOBONTIU are exact solutions of the bending differential equation obtained through different methods, so their results are exactly the same. As such, from now on they are treated as a unique approach: the linear beam theory. The simplified equation from PAROS AND WEISBORD is a reduced expression for when the h/R ratio tends to zero. It can be observed in Table 3.4 that there is an appreciable deviation of beam theory results to the 3D-FE model, being the FE model stiffer. This phenomenon is studied in the next section. Stiffness in the nonlinear case was not presented as it is dependent on the rotation angle. Thus, a graphical representation is more suitable.

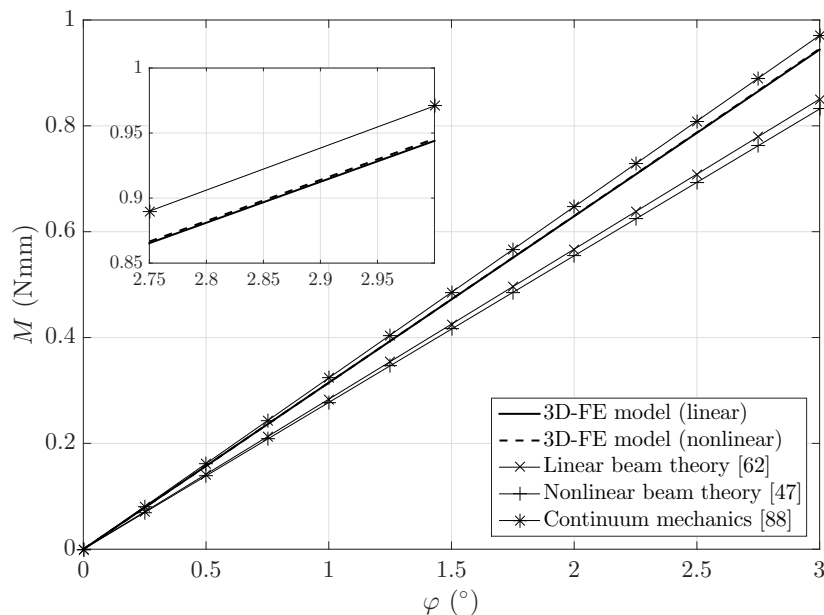


Figure 3.11: Behavior of the flexure hinge according to different modeling approaches.

Figure 3.11 shows the linear and nonlinear behavior of the flexure hinge calculated with the 3D-FE model as well as according to three analytical approaches: linear beam theory, nonlinear beam theory and continuum mechanics. The value of the rotational stiffness k_φ is not constant for nonlinear calculations. In fact, it increases with deformation, as was also observed in the contribution from FRIEDRICH ET AL. [26]. Ideally, $k_\varphi = 18.029$ Nmm/rad

but increases up to almost 0.18% when rotations reach $\varphi = 3^\circ$. This can be appreciated in Figure 3.12, where the relative stiffness deviation e_{k_φ} of nonlinear to linear calculations is presented for different rotation angles. This needs to be taken into account for later steps to avoid false results due to excessive rotations.

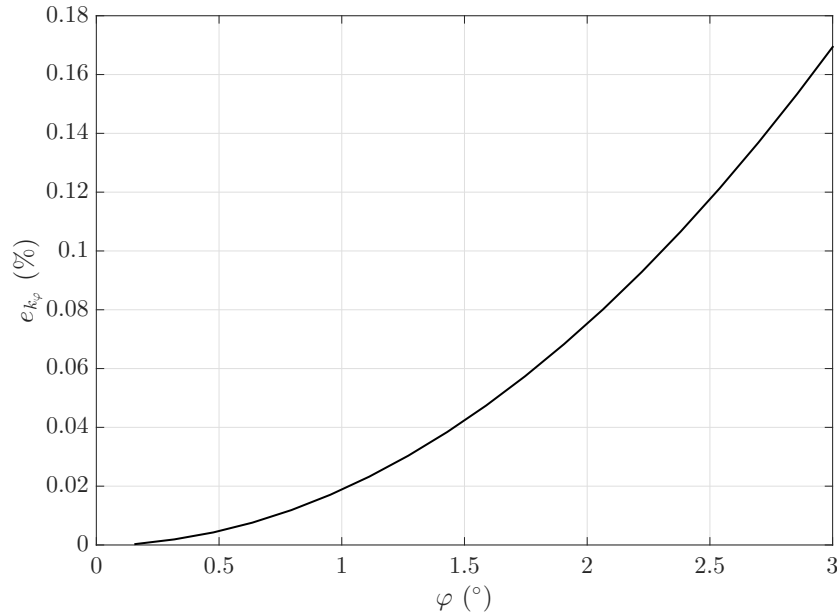


Figure 3.12: Deviation of k_φ in geometrically nonlinear calculations.

3.7. Comparison to analytical models

Disagreement between analytical and numerical results in the modeling of the compliance of a flexure hinge has been evidenced in some works [11, 51, 53, 56, 76, 93, 95], where deviations lie in the range of 3 to 10%. In the contribution of YONG [95], the analytical equations from PAROS AND WEISBORD [62], LOBONTIU [50], WU AND ZHOU [91] and TSEYTLIN [88] as well as FEA-based equations from SMITH ET AL. [78] and SCHOTBORGH ET AL. [73] were compared to a 2D-FE model for semi-circular hinges with ratios h/R in a range from 0.05 to 0.65. Results of this investigation show that relative deviation of analytical equations to their model decreases as the hinge gets thinner. For very thin hinges, analytical and numerical results should coincide. Moreover, their model shows a less stiff behavior than the equations. This is not the case for 3D-FE models, as shown in Figure 3.11.

Modeling deviations

For better depicting the aforementioned phenomenon, the minimum height h of the flexure hinge is increased in a range from 0.05 to 0.1 mm while maintaining every other parameter constant and the relative deviation between results from analytical approaches and the 3D-FE model is evaluated in terms of the rotational stiffness k_φ (see Figure 3.13). Analytical approaches used for the comparison are the exact equation by PAROS AND WEISBORD obtained from linear beam theory [62] and design equations based on nonlinear beam theory by LINß ET AL. [47] and on continuum mechanics by TSEYTLIN [88]. The equations by LINß ET AL. and TSEYTLIN are approximated from exact or numerical results of the theories they are based on. As such, they are only valid in a certain range of values but they are included to see their applicability in the proposed range. FEA-based equations

from other authors are not considered since FE models are already being used. Number of elements is kept constant but, due to the change of geometry, the size of the mesh zones specified in Section 3.4 are accordingly updated to avoid highly distorted elements. Geometric nonlinearity is considered and the applied bending moment M is the same for all cases so that it produces rotations of less than $\varphi = 1^\circ$ in all of them.

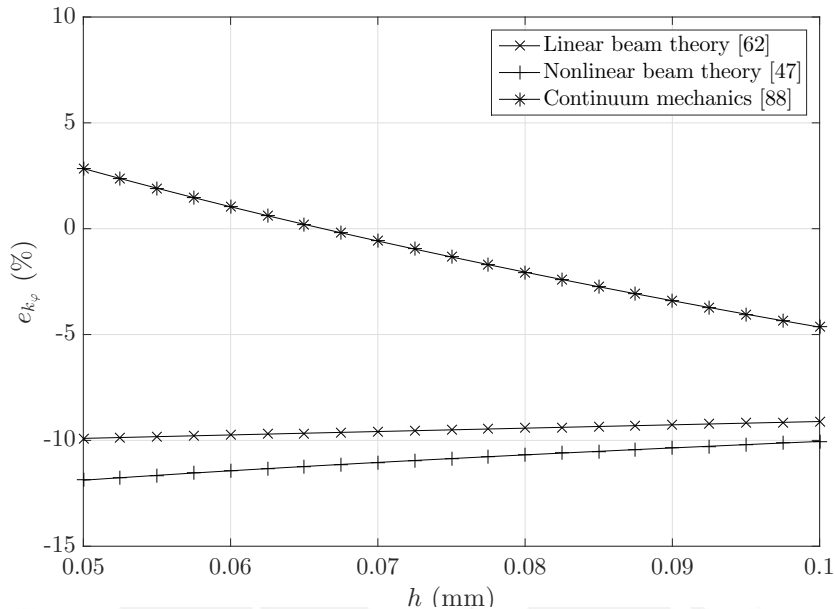


Figure 3.13: Relative deviations of analytical k_φ to 3D-FE model results.

Figure 3.13 shows pronounced relative deviation ($e_{k_\varphi} \approx 9$ to 12%) of the results from EULER-BERNOULLI beam theory and the design equations based on nonlinear beam theory to the 3D-FE model. This deviation increases as the hinge gets thinner (h/R decreases), which contrasts with the work of YONG [95]. This can be explained from two facts. First, EULER-BERNOULLI beam theory assumes that cross sections remain planar after deformation, which is only valid for long slender beams [50]. This was also assumed in the nonlinear beam theory by ZENTNER [96], used to derive the design equations by LINß ET AL. [47]. Second, beam theory assumes a state of plane stress, which considers that stresses out of the plane of deformation are zero [85]. Plane stress is also assumed in 2D-FE models so that as the ratio h/R decreases, the central zone of the hinge tends to a slender beam, which reduces the deviation to the analytical model. However, when the width of the hinge is sufficiently large, a plane stress state can no longer be assumed. In the 3D-FE model, a stress in the out-of-plane direction σ_z exists, as shown in Figure 3.14. This stress reduces the normal strain in x -direction according to HOOKE'S law, producing a stiffer behavior of the hinge.

State of stress

The state of stress of a prismatic body where loading is perpendicularly distributed over its width, e.g. a flexure hinge, lies between two limit cases: plane stress, when the width is very small ($b \rightarrow 0$), and plane strain, when the width is very large ($b \rightarrow \infty$). Plane strain assumes that strains in the out-of-plane direction are zero, which results from the out-of-plane dimension being very large or from its end faces being constrained by two smooth rigid planes [85]. In the case of bending of plates, the cross section is stretched where the bending stress is negative and is compressed where it is positive due to the POISSON'S effect, producing an anticlastic surface [17]. The 3D-FE model deviates in great manner to approaches which assume plane stress. In contrast, the equation from



Figure 3.14: Out-of-plane stress σ_z in MPa for $h = 0.05$ mm.

TSEYTLIN [88] shows deviations of less than 5% in the considered range of h . Although this equation was approximated from the plane differential equation from continuum mechanics, it considers a modified elastic modulus $E' = E/(1 - \nu^2)$ which applies for thin films and plates [87]. The differential equation for a bending plate can be derived in the same way as for bending beams but assuming a plane strain state instead of plane stress, which results in the term $1/(1 - \nu^2)$ differentiating the flexural rigidity of both cases (see Appendix D). This gives rise to the assumption that the 3D-FE model behaves closer to a state of plane strain. In plane strain state, the plate is stressed as if it were also subjected to a bending moment νM [17] producing a distribution of σ_z so that strains are zero along the width, as shown in Figure 3.15. A first proof of the plane strain assumption can be done by the results of stress for $h = 0.05$ mm. The maximum bending stress for $\varphi = 1^\circ$ ($M \approx 0.315$ Nmm) at $x = L/2$ equals $\sigma_{x,max} = 76.21$ MPa and the out-of-plane stress $\sigma_{z,max} = 25.37$ MPa. Since M and σ are proportional, $\sigma_{z,max} = \nu\sigma_{x,max}$ which is the approximately the case here ($e_{\sigma_{z,max}} \approx 0.9\%$).

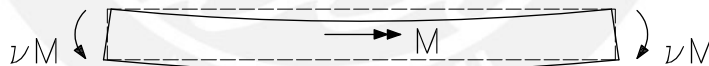


Figure 3.15: Cross section of plate in bending.

To further prove this assumption, two 2D-FE models, one assuming plane stress and one assuming plane strain, were generated using the same mesh strategy as the 3D-FE model. The models are compared to using the previous procedure and are included in Figure 3.13. It is to remark that plane strain models in ANSYS assume a width of 1 (mm), so stiffness results are multiplied by the width of the hinge b and loading is divided by the same factor to avoid false results. Deviations to the 3D-FE model are presented in Figure 3.16. Results show a deviation of less than 1% of the plane strain model and around 10% of the plane stress model to the 3D-FE model, which proves the aforementioned assumption. The behavior concluded in the work of YONG [95] can also be observed in the proximity of results of the beam theories to the plane stress results. This deviation in the 3D model behavior implies a dependency on the width of the hinge.

Width dependency

The analytical equations, as well as the 2D-FE models, consider a linear relationship between the rotational stiffness k_φ and the width b (see Appendix C). If this were true,

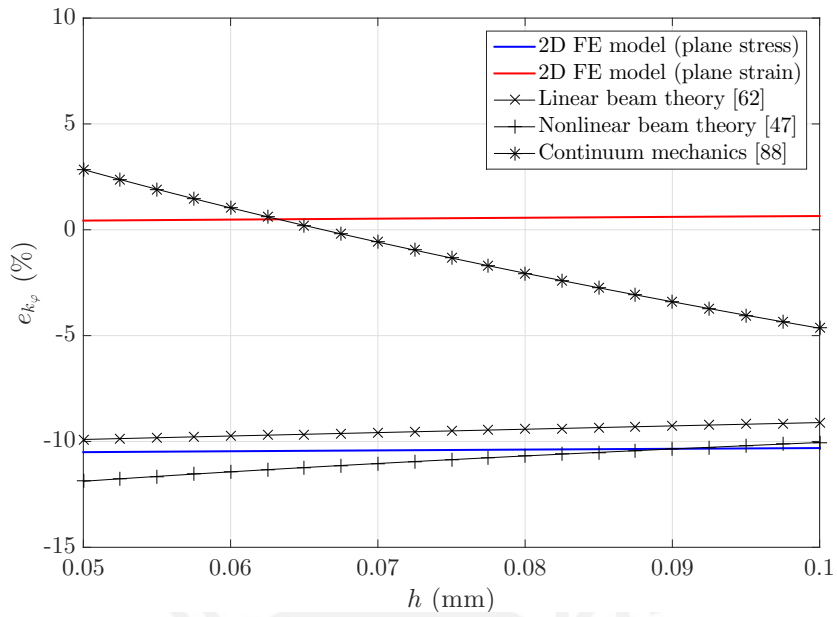


Figure 3.16: Relative deviations of k_φ to 3D-FE model results.

a graph between a normalized stiffness $\tilde{k}_\varphi = k_\varphi/Eb$ and h should not vary for FE calculations using different widths. However, this is not true for the 3D-FE model. To show this behavior, \tilde{k}_φ is calculated for different values of h while maintaining all other parameters constant. This procedure is repeated using different values of b and is presented in Figure 3.17.

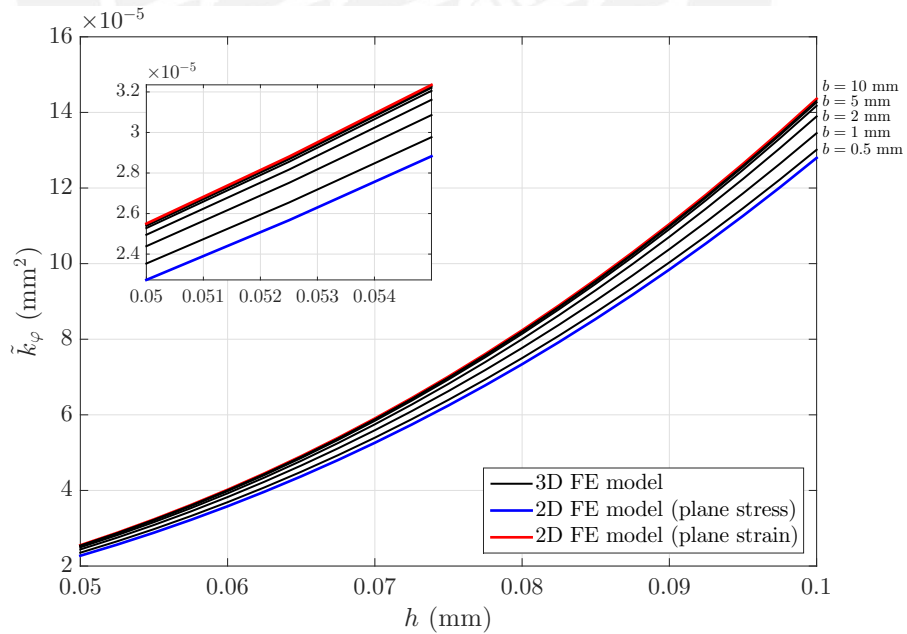


Figure 3.17: Normalized stiffness \tilde{k}_φ for different values of width b .

Figure 3.17 shows that with increasing width b , the behavior of the model changes from a state of plane stress to a state of plane strain. An important observation is that in some value of the width, the results converge into an state of plane strain. This also means that the relationship between the rotational stiffness and the width of a flexure hinge is nonlinear but converges into a linear one (with increased stiffness) when the width is

sufficiently large. This occurs due to the behavior of the out-of-plane stress σ_z . In plane strain, the value of σ_z , which depends on the other two normal stresses σ_x and σ_y , should be constant along the width at a certain position x . Simulations show that σ_z always exists but is concentrated in the middle of the width ($z = 0$) of the hinge when b is small. As b increases, σ_z tends to become uniformly distributed along the width.

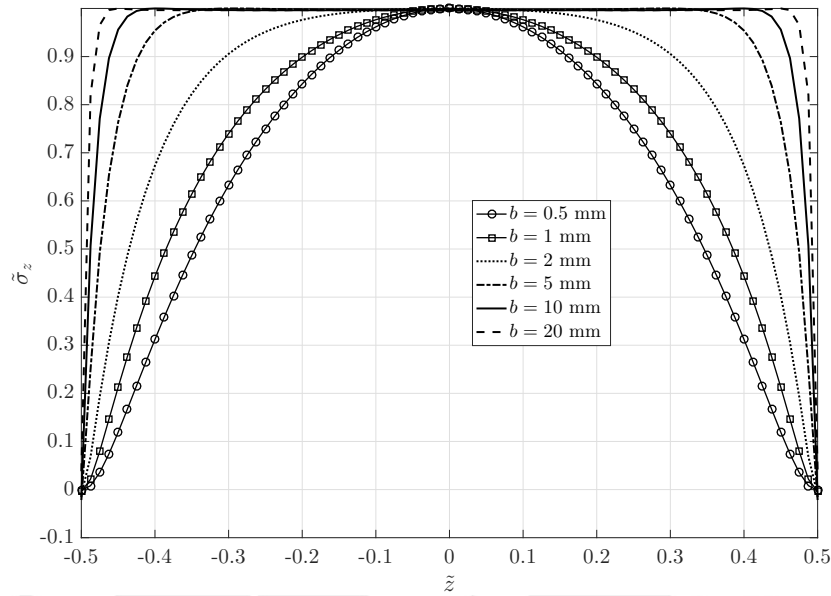


Figure 3.18: Distribution of $\tilde{\sigma}_z$ along the width for $h = 0.05$ mm.

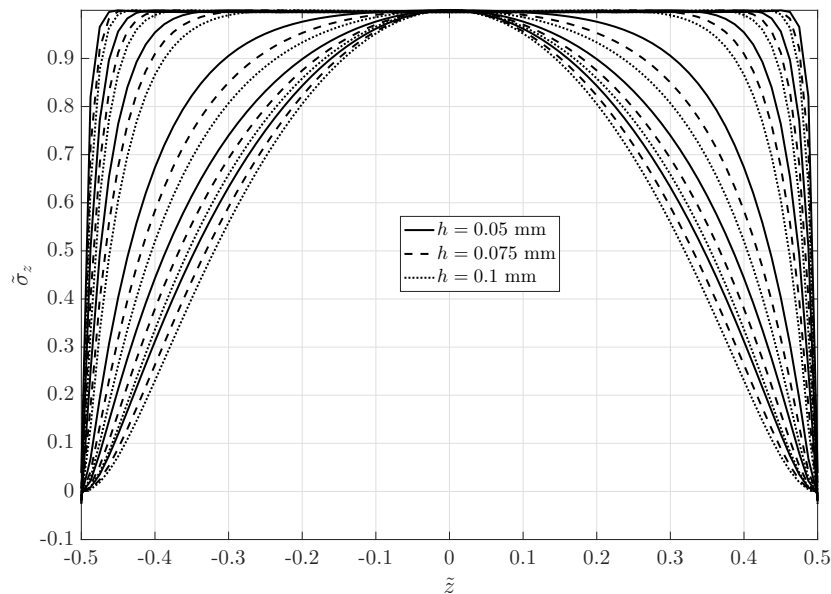


Figure 3.19: Distribution of $\tilde{\sigma}_z$ along the width for different values of h and b .

The behavior of σ_z is depicted in Figure 3.18, which shows the distribution of a normalized out-of-plane stress $\tilde{\sigma}_z = \sigma_z/\sigma_{z,max}$ along the normalized z -position $\tilde{z} = z/b$ calculated at $x = L/2$ for different values of b for the 3D-FE model ($h = 0.05$ mm). Out-of-plane stress σ_z never reaches a uniform distribution since it reduces to zero at the outer boundaries (see Figure 3.14). This explains the small relative deviation of the 3D model to the plane strain model when $b = 10$ mm (see Figure 3.16). Figure 3.19 also shows the distribution of

σ_z for different values of h and b . The values of b presented are the same as in Figure 3.18. It can be observed that the distribution of σ_z converges faster to a state of plane strain as the hinge gets thinner. This is produced by the value of the b/h ratio, which is higher in thinner hinges for a same width.

The b/h aspect ratio

To show the influence of the b/h ratio, the relative deviation of the 3D-FE model to the linear beam theory results is depicted for different values of b/h in Figure 3.20. The equations based on linear beam theory are used for comparison since they are an analytical exact solution and other design approaches are based on their assumptions, e.g. flexure strip equation by EASTMAN [20] used in balance design [69]. Equations by LINß ET AL. [47] and TSEYTLIN [88] are not valid for the geometries considered in this study and will not be further considered. This fact is evidenced in Figure 3.16 as both surpass either the plane stress or plane strain boundaries. The plane stress and plane strain models are also used in the comparison. It is to remark that the radius R is always constant so the ratio h/R varies. To show its relationship to the b/h ratio, the h/R is used for comparison.

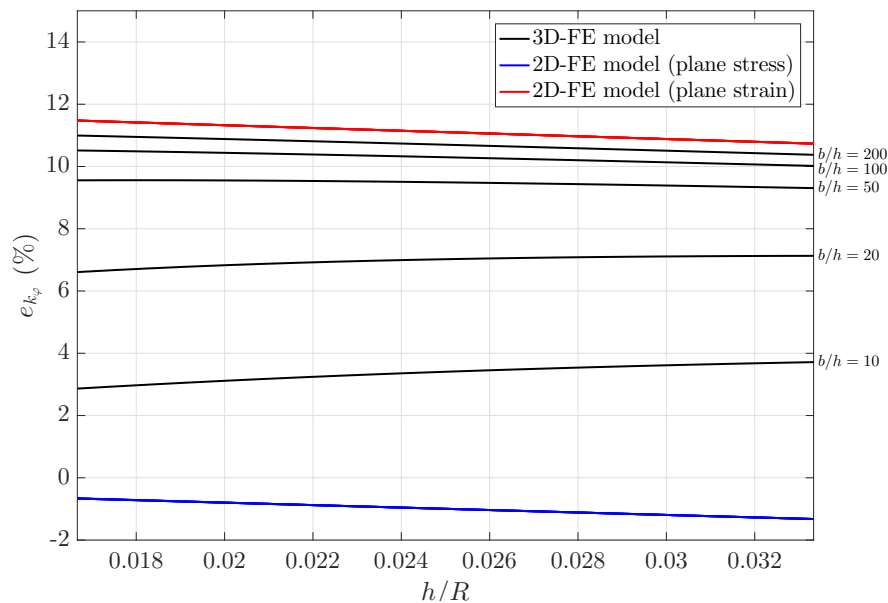


Figure 3.20: Deviations of k_φ to linear beam theory for different h/b ratios when $R = 3$.

The results show that deviation of the plane stress and plane strain models are purely dependent on h/R as no influence of changing the width exists. Results of the plane strain model are $1/(1 - \nu^2)$ times the results of plane stress, as shown in Appendix D. The deviation of the 3D-FE model decreases as the hinge gets thinner for lower b/h ratios. This occurs due to the changing value of $h(x)$ along the length of the hinge which is determined by the contour. For thinner hinges and low values of b/h , the hinge gets closer to a slender beam, for which the EULER-BERNOULLI assumption is valid. Thus, the deviation for a certain b/h ratio depends on the h/R ratio, which describes the contour of thin circular flexure hinges. This is better observed in Figure 3.21, where the deviations are calculated in the same manner, but while maintaining the h/R constant at a value of 0.025. Since h/R is constant, the minimum height h is used for comparison.

Figure 3.21 shows that for a certain h/R ratio, the deviation of each model is constant for each value of b/h . This means that deviation between models of thin flexure hinges of

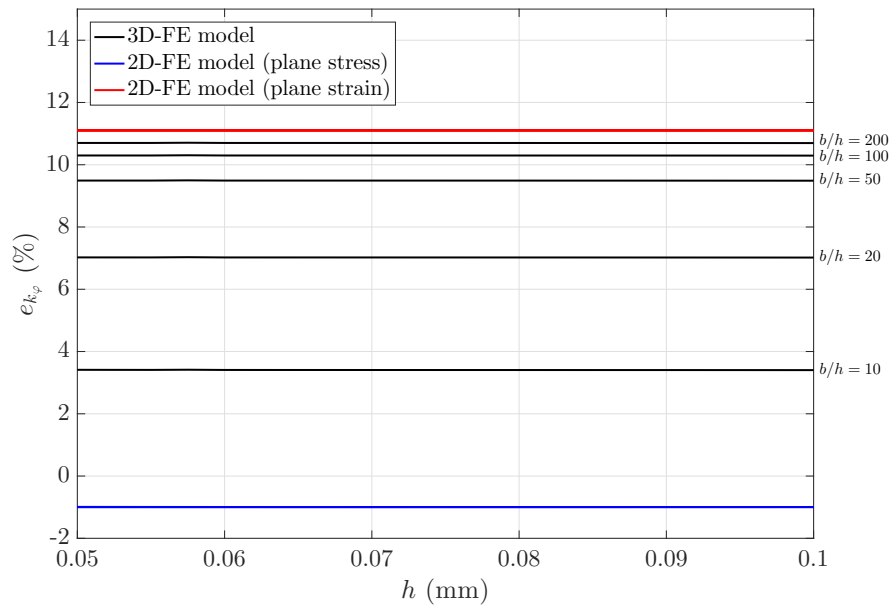


Figure 3.21: Deviations of k_φ to linear beam theory for different h/b ratios when $h/R = 0.025$.

circular contour can be described as a function of only both ratios. Modeling deviations for hinges of other contours cannot be described by only two factors such as b/h and h/R as they are defined by more parameters, e.g. eccentricity for elliptic contours. However, the fact that, besides a contour-dependent deviation, a width dependency exists does not change. In the case of thicker hinges, the total height of the hinge H plays a role in the deformation so it will also appear in the deviations.

Effect of the total hinge height

The effect of H can be demonstrated by using an additional 3D model, such as the one in Figure 3.22. This model was generated in the same manner and with the same settings as the one in Section 3.4 but elements above $h(x) = h + 2R$ were removed. The first model cannot support values of H close to $h + 2R$ due to high distortion of those elements.

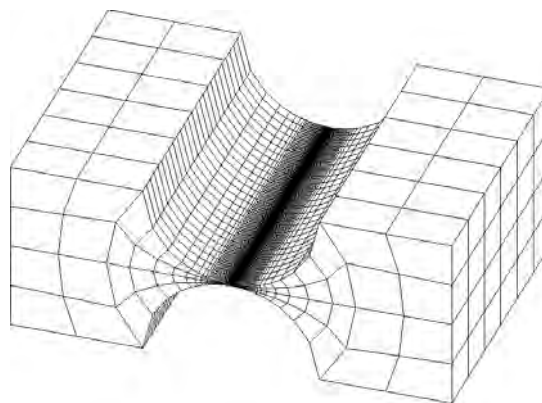


Figure 3.22: 3D-FE model for flexure hinges with $H < h + 2R$.

Relative deviation of the rotational stiffness is calculated by changing the value of H for the hinge with $h = 0.05$ mm and maintaining all other parameters constant. Results are

compared to the value of k_φ for $H = 12$ mm. Values up to $H = 6.05$ mm ($h/H \geq 0.0083$) are calculated using the model from Figure 3.22 and above $H = 6.75$ mm ($h/H \leq 0.0074$) using the model defined in Section 3.4. Values of H between 6.05 and 6.75 cannot be modeled with the first proposed model due to element quality and are depicted with dashed line in Figure 3.23. Results show that, when $H < h + 2R$, the rotational stiffness rapidly decreases. Also the results of the second model seem to converge to a stiffness value lower than the value for $H = 12$ mm. This occurs due to the model having less elements than the first one, i.e. less stiff.

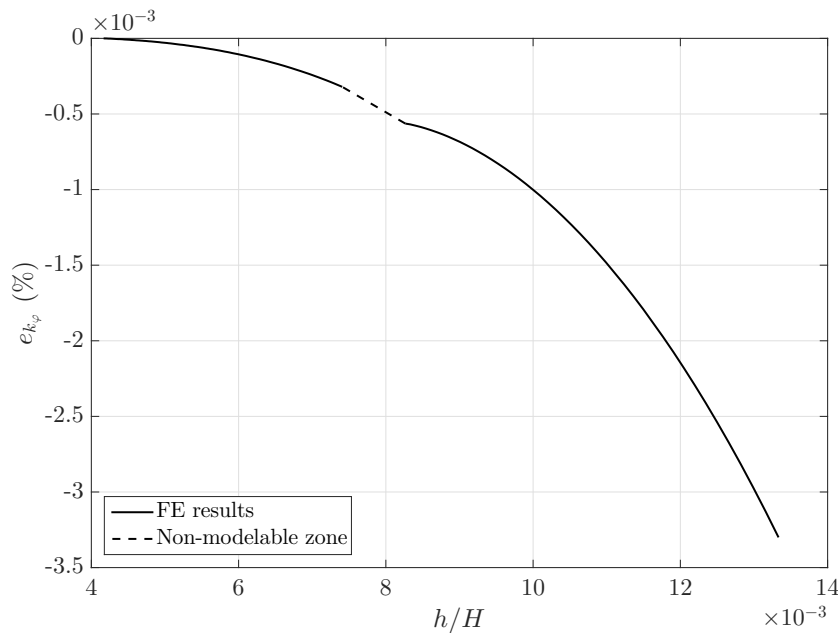


Figure 3.23: Deviations of k_φ due for different values of h/H .

3.8. Summary

Analytical expressions found in the literature are mostly based on the assumptions of the EULER-BERNOULLI beam theory, which apply only to slender beams. Thin flexure hinges, although slender in the plane of bending, are usually wide in the out-of-plane direction. To prove the validity of these assumptions for modeling flexure hinges with such characteristics, a 3D-FE model was developed. Due to the high aspect ratios of these hinges, element quality can be compromised. Meshing was done by dividing the domain in zones, each with its own mesh and connected with the others through multipoint constraints. Settings were defined to ensure the accuracy and efficiency of geometrically nonlinear calculations. The rotational stiffness of the flexure hinge was calculated using different approaches and compared to FE results. The 3D-FE model was found to be around 10% stiffer than most analytical expressions, except the one from TSEYTLIN [88], which considers a modified elastic modulus that applies for thin plates. Using 2D-FE models for comparison, one assuming a plane stress state and other assuming plane strain, the 3D-FE model was found to be closer to a plane strain state for minimum heights between 0.05 to 0.1 mm and a width of 10 mm. The existence of an out-of-plane normal stress along the width suggests a nonlinear width dependency. A normalized rotational stiffness, which only depends on the contour parameters h and R , was used to prove this assumption. A nonlinear relationship between the rotational stiffness and the width was found to be related to the distribution of the out-of-plane stress along the width.

FE results show that depending on the aspect ratio b/h , thin flexure hinges can have a behavior closer to a plane strain state, like plates. Even for low ratios, for example: $b/h = 10$, deviations to the analytical results can be around 3% for the thinnest hinges. The relationship between the rotational stiffness k_φ and the width b is nonlinear when b/h is small, but is almost linear when it is sufficiently large. When assuming a plane stress state, a deviation still exists between analytical and 2D-FE results. This deviation depends only on the h/R ratio in circular contour flexure hinges. In fact, deviation to analytical models depends only on the ratios b/h and h/R for thin circular flexure hinges. The total height H , expressed by the h/H ratio, has an almost neglectible influence on the rotational stiffness of thin hinges when compared to the other parameters. As h/H increases, its effect rapidly increases, especially when $H < h + 2R$. This may be of interest for thicker hinges, but is only considered in the expression by LINß ET AL. [47].



4. Investigation of non-ideal flexure hinges

Studying the mechanical behavior of a flexure hinge requires analysis of its response under different conditions in terms of stiffness. This response is measured as the deviation from an ideal state generated by the variation of different parameters. Knowledge of most influential parameters is of great importance for predicting their behavior. This work proposes the following approach for identifying these parameters on a circular-contour thin flexure hinge (see Figure 4.1).

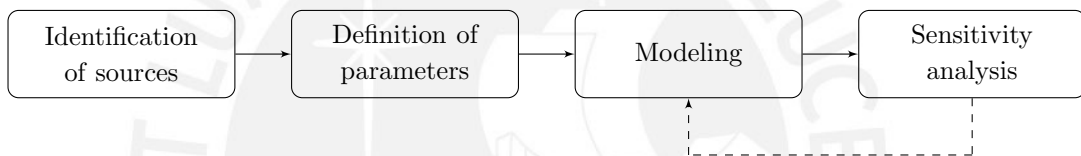


Figure 4.1: Workflow.

First, possible sources of deviation are identified based on the definition of the stiffness. Suitable parameters for these sources are defined considering modeling limitations. A proper selection of parameters is necessary for reducing the dimensionality of the model and to obtain significant results. It is also important to establish their range of values to avoid modeling errors and for a trustworthy analysis of their influences. With this characterization of the joint, a model needs to be generated for evaluating the stiffness. The model presented in Chapter 3 is used for this matter. As discussed in Section 2.4, analytical models and approximate equations in the literature are not suitable for this study because of their assumptions and limited parameter inputs. In contrast, FE calculations can be easily conducted using CAD generated models. It is also important to analyze how the model behaves under new geometric conditions. Most influential parameters are obtained later through a sensitivity analysis. Due to its integration with ANSYS and functionalities, OptiSlang inside ANSYS is used in this step. For this analysis, calculations of the stiffness are conducted using various combinations of values of the input parameters. Thus, it also helps to identify errors in the model (see Figure 4.1). These combinations, or samples, are generated based on an experimental design and influence of parameters are represented numerically by sensitivity measures. To determine a suitable sampling method and sensitivity measure, comparisons are presented.

4.1. Identification of sources of deviation

Stiffness of a system is defined by its geometrical configuration, material properties, loading and other conditions, as stated in Section 2.2. As such, the sources of deviation can be classified in four groups:

- Geometric deviations.

- Material behavior.
- Loading conditions.
- Other influences.

Variation of these characteristics of the hinge produces a deviation to some degree on its stiffness. However, non-bounded parameter ranges may lead to undesirable results which distort the sensitivity values. Some limitations must be placed for a significant study. In this investigation, geometric deviations are those produced by the manufacturing process, which are limited by its tolerances. Deviation sources related to material behavior consist of deviations in the value of its properties produced by the inaccuracy of its determination. This is better explained in the next paragraphs.

Geometric deviations

There exist many processes for manufacturing flexure hinges. When it comes to thin hinges and complex geometries, WEDM is mostly preferred, thus, it is used for defining the deviation parameters. WEDM is considered extremely accurate when compared to standard manufacturing techniques. The reason lies on three facts [38]:

- No contact exists between the cutting tool and the workpiece, eliminating adverse effects such as mechanical stresses, chatter and vibration.
- The wire used as cutting tool possesses small diameters and high mechanical properties which should produce very fine and clean cuts.
- The movements of the workpiece are governed by a computer numerical controlled (CNC) system significantly reducing positioning errors.

Yet, errors inherent to the manufacturing process are always present. The tension of the wire influences a phenomenon known as wire-lag, in which various forces generated by the occurrence of sparks during machining produce a static deflection opposing the cutting direction [66]. This effect produces erosion in the corners of the workpiece resulting in dimensional and flatness errors [38]. In the case of circular contours, when the radius are small ($R < 3$ mm), the wire-lag produces a significant effect on the dimensional accuracy [15]. Depending on the electrostatic and electromagnetic forces occurring during cutting, a concavity effect may also appear (see Figure 4.2).

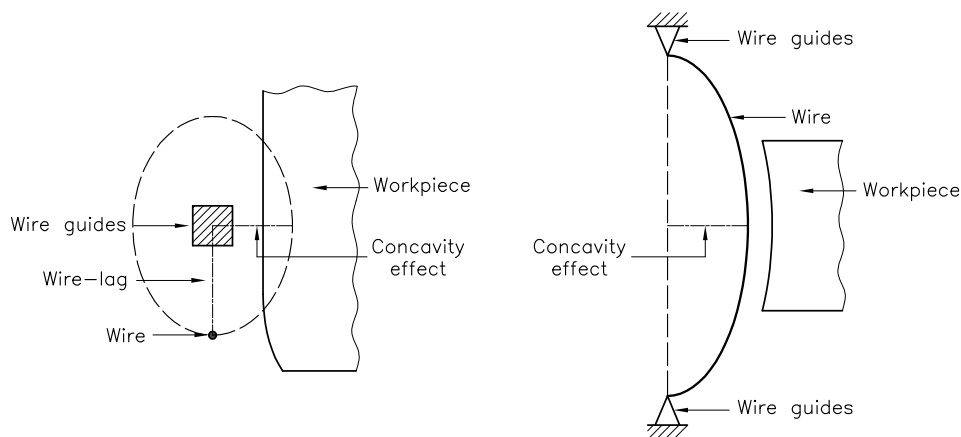


Figure 4.2: Wire-lag and concavity effects. Adapted from [15].

Parameters of the pulse, such as intensity, duration and frequency are mainly responsible for overcutting (see Figure 4.3). Overcutting occurs because the size of the cavity in the workpiece is larger than the diameter of the wire. Its exact size is difficult to predict but it is proportional to the discharge current. Normally, WEDM machines are incorporated with measures for compensating overcutting but it cannot be fully eliminated [38].

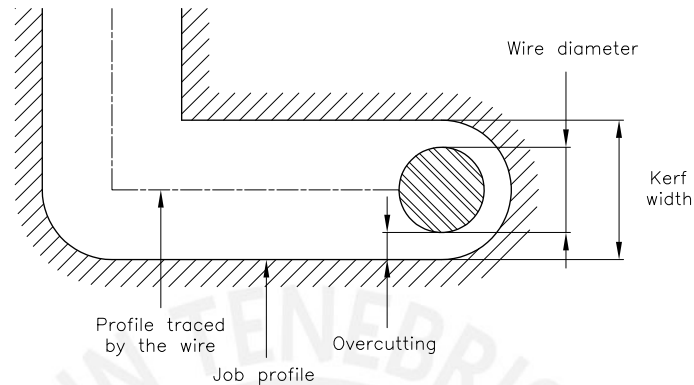


Figure 4.3: Overcutting effect. Adapted from [44].

Excessive pulse duration and discharge current, as well as low pulse off-time generate high levels of heat, which results in a high number of sparks leading to wire vibration and wear. When combined with high cutting speeds, the removal of material is not uniform, producing circularity errors of the contour [81]. Surfaces machined by WEDM are affected by metallurgic transformations and recast layer growth due to the heat input, compromising its structural integrity, thus, leading to reduce fatigue life [15]. Surface roughness is highly influenced by the duration of the pulse, the discharge current and wire speed. Higher discharge energy produces melting explosion, eroding larger material (craters) and surface layers, which, when combined with high wire speeds, produces an increased surface roughness [29]. It is important to remark that positioning and orientation errors are also present due to the accuracy of the CNC guiding systems of the WEDM machines [99].

Material behavior

Flexure hinges are purposefully considered perfectly elastic bodies where elastic modulus fully defines its material behavior. This means that a perfectly linear relationship between stresses and strains is assumed. This is not always the case, but linearity can be assumed when stresses are really low, about 1/10 of the elastic limit [82]. On the other hand, materials do have a certain degree of mechanical hysteresis and other anelastic behaviors, e.g. creep (see Section 2.3). Anelasticity has been reported in highest precision systems such as the flexure-based balance by QUINN ET AL. [69]. This balance uses flexure strips of a copper beryllium alloy, which show a relaxation after-effect following a small angular displacement (about 0.003°) at low frequencies. It was concluded that this anelastic behavior is a bulk property of the material and is not produced by the surface damage due to the manufacturing [68]. The damping component of this behavior was found to be dependent on the stress levels in high strength materials, which are commonly used in flexure hinges.

In addition to the absence of information on the values of anelastic properties, lack of consistency in the values of elastic constants also suppose an important problem. Elastic constants of a material consist on the elastic modulus, the *Poisson's* ratio and

the shear modulus, which are experimentally determined and, hence, are subjected to its inherent uncertainty. Multiple parameters influence the results of tensile tests, which can be summarized in four categories: test specimen, test system, environment and test procedure [27]. As a result, available values found in the literature or in data sheets vary among them and may differ to real values. For example, the value of the elastic modulus can be difficultly accurate to better than 1% [77].

Loading conditions

The rotational stiffness of a flexure hinge assumes that it is subjected to a pure bending moment which produces a certain rotation. In real applications, they are subjected to more complex loading conditions. For example, the central flexure strip in mass comparators is subjected to a bending moment produced by the difference of weights and a tensile force equal to their sum [69]. EASTMAN [20] determined that the stiffness of a flexure in such conditions varies with the value of the tensile force. Consideration of this phenomenon in the upcoming sensitivity analysis would result in a loss of generality of the measures, as the value of this force depends on the overall system. Application of out-of-plane loads are not considered either due to the same reason. Nevertheless, further investigation is necessary for describing the behavior of notch hinges under non-ideal load conditions and is conducted in a later chapter in the context of weighing cells.

External influences

Geometry, material properties and loading conditions can be affected by external factors, e.g. environment. Dimensions of the joint can change in presence of thermal effects, such as conduction or convection, or due to corrosion. Material properties are also temperature-dependent. Flexure-based high precision systems are often operated under vacuum or highly controlled conditions, to exclude environmental influences to a large extent. Loading conditions change in presence of gravity. The weight of the hinge exists as an additional load, whose effect varies with the direction of the weight force relative to the hinge. Flexure hinges may have any orientation in space due to design [30] or have small changes of orientation due to ground tilt.

4.2. Parametrization of the flexure hinge

Parametrization of the model for a sensitivity analysis ideally requires selected parameters to be independent from one another. This is not always possible, especially for geometric deviations, but it is taken into account for the selection of parameters. Machining processes of flexure hinges produce the following types of deviation: dimensional, flatness, perpendicularity, circularity and positioning, and parameters to describe them are considered as follows (see Table 4.1):

- Dimensional errors are treated as the variation of value of the basic parameters: minimum height dh , radius dR and width db . Deviation of the total height H due to manufacturing would have almost no effect on the behavior of a thin flexure hinge since changing H in the order of millimeters only produces deviations in the stiffness in the order of 10^{-4} % and manufacturing deviations lie in the order of micrometers.
- Flatness errors occur in the flat faces of the hinge, which consist mainly on faces of the adjacent links. Flatness of the lateral faces alters the width of the notch section in a non-uniform way and its contemplation would require various parameters which

impose a correlation with db and increase the complexity of the model. As such, these effects are not considered.

- Perpendicularity errors in the faces of the adjacent links are not considered. Inclination of the holes is described by their orientation around the longitudinal x -axis $d\theta_x$ and transversal y -axis $d\theta_y$. Both holes are considered always parallel, otherwise, the height of the hinge would not be constant along its width.
- The circularity error is not considered as it cannot be described without increasing the complexity of the model, e.g. generating a certain irregular profile. Another approach could be changing the hinge contour, but it can increase the number of parameters depending on the contour selected and dR would not apply anymore. Modeling of surface roughness also would require the modeling of an irregular profile, so it is not considered.
- Positioning errors of the machine are considered as deviation of the position of the holes in longitudinal and transversal directions. These deviations are treated as hole separation in x -direction dx_c and hinge positions in x -direction dx and in y -direction dy . Hole separation in y -direction would be equal as dh so this parameter is already considered.

Based on this characterization, the non-ideal flexure hinge shown in Figure 4.4 is studied.

Table 4.1: Geometric deviations representation

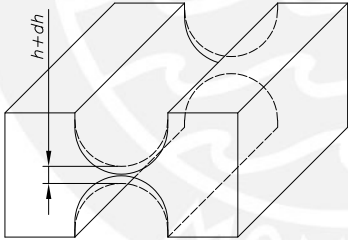
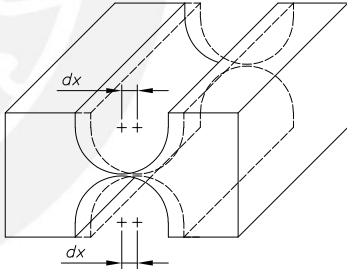
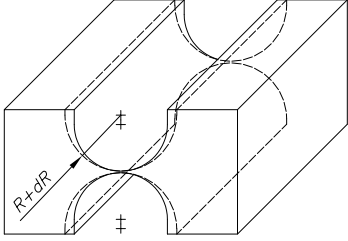
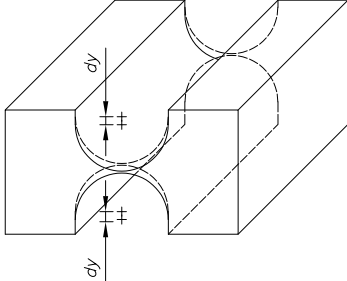
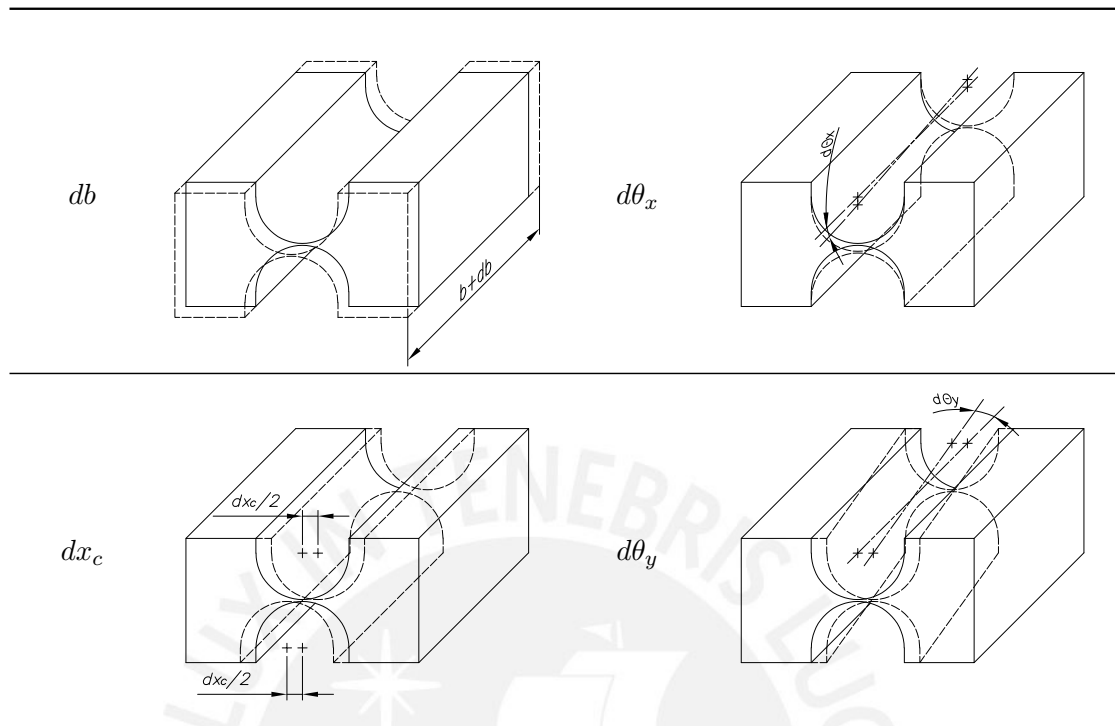
| Symbol | Representation | Symbol | Representation |
|--------|---|--------|---|
| dh |  | dx |  |
| dR |  | dy |  |

Table 4.1 (Cont.): Geometric deviations representation



Anelastic behavior of the material is not considered in this work as it introduces the time variable, highly increasing the complexity of the model. Material behavior is assumed perfectly elastic and parameters to be considered are the deviation of the elastic modulus dE and the POISSON'S ratio $d\nu$. The elastic modulus E is a basic parameter for defining the behavior of a flexure hinge so the lack of consistency in its value is considered as a deviation parameter. It was shown in Section 3.7 that thin hinges follow a behavior according to a plane strain state, in which the POISSON'S ratio ν plays a role. As such, the lack of consistency of values of this parameter is used.

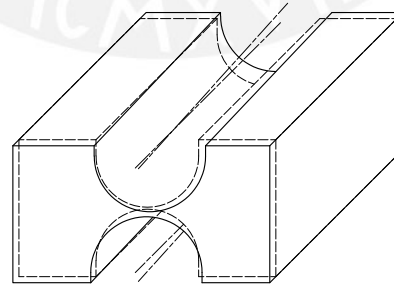
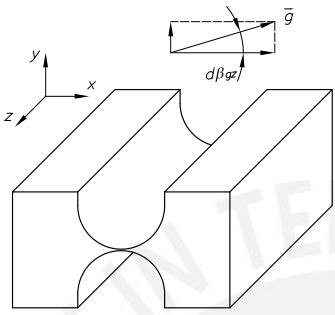
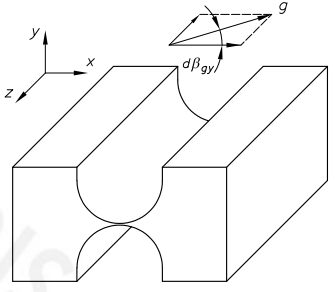


Figure 4.4: Geometry of the flexure hinge. Continuous: non-ideal; dashed: ideal.

External influences such as temperature or corrosion are not considered. Temperature alters the geometry and material properties of the hinge. However, due to the small temperature variations allowable in high precision systems, the deviations already considered produce a higher variation of the same parameters as temperature effects would. Corrosion produces the same geometric deviations but its time dependent. Gravity introduces an additional load to the system, the weight force, which depends on the relative direction of the hinge to the gravity acceleration vector. In fact, a flexure hinge can have any direction in space depending on the designed mechanism. When in a specific position,

the hinge orientation still deviates during application due to the ground tilt. Gravity orientation relative to the flexure hinge is considered as two parameters, rotation around z -axis $d\beta_{gz}$ and around y -axis $d\beta_{gy}$. The initial direction of the gravity vector is the positive x -axis $\beta_{gz} = \beta_{gy} = 0$.

Table 4.2: Gravity deviation parameters

| Symbol | Representation | Symbol | Representation |
|---------------|---|---------------|--|
| $d\beta_{gz}$ |  | $d\beta_{gy}$ |  |

4.3. Model behavior

Before passing onto the sensitivity analysis, it is important to verify how the model behaves when changing the parameters defined. Verification of results is supported by the observation from other contributions. The number of elements is kept constant to allow comparison of results [74]. It is important to verify how the mesh adapts to the new geometries. Varying the geometry will help to identify points where the model does not support deviations anymore so that it can be corrected. In a first attempt, the deviation parameters are set at ranges of values which are comparable, although these may not be realistic in actual applications. Results using too small parameter values may run into numerical errors, such as round-off errors. For values to be comparable, percentual deviations are used but this is only possible for the basic parameters h , R , b , E and ν . Parameters like hole positions are deviated as a percentage of the hinge length l . Hole orientation parameters must necessarily be set at a certain angle value. These values are shown in Table 4.3. Rotational stiffness deviations are calculated using the same bending moment M in all cases. The bending moment M is one that produces a rotation of $\varphi = 1^\circ$ on the ideal flexure hinge. Gravity is only considered for parameters $d\beta_{gz}$ and $d\beta_{gy}$ and is assumed to amount 9.81 m/s^2 .

Table 4.3: Parameter deviations.

| Parameter | Relative value | Absolute value | Parameter | Relative value | Absolute value |
|-----------|----------------|-----------------------|---------------|-----------------|------------------------|
| dh | $\pm 5\% h$ | $\pm 2.5 \mu\text{m}$ | $d\theta_x$ | $\pm 1^\circ$ | $\pm 1^\circ$ |
| dR | $\pm 5\% R$ | $\pm 150 \mu\text{m}$ | $d\theta_y$ | $\pm 1^\circ$ | $\pm 1^\circ$ |
| db | $\pm 5\% b$ | $\pm 500 \mu\text{m}$ | dE | $\pm 5\% E$ | $\pm 3.55 \text{ GPa}$ |
| dx_c | $\pm 5\% l$ | $\pm 300 \mu\text{m}$ | $d\nu$ | $\pm 5\% \nu$ | ± 0.0165 |
| dx | $\pm 5\% l$ | $\pm 300 \mu\text{m}$ | $d\beta_{gz}$ | $\pm 180^\circ$ | $\pm 180^\circ$ |
| dy | $\pm 5\% l$ | $\pm 300 \mu\text{m}$ | $d\beta_{gy}$ | $\pm 180^\circ$ | $\pm 180^\circ$ |

Behavior of the mesh when considering geometric deviations can be observed in Figure E.1. The meshing strategy presented in Chapter 3 ensures that the zone of highest stress gradient is always finely meshed so that results are trustworthy. This zone is always around the minimum value of $h(x)$, which is contained in zone 1. Zone 1 of the model adapts to the new geometry following the settings presented in Section 3.4, trying to avoid high element distortion while capturing the mentioned zone as in Figure 4.5.



Figure 4.5: Bending stress σ_x in MPa: (a) ideal flexure hinge (b) non-ideal flexure hinge.

Results of the deviation of the rotational stiffness e_{k_φ} using the range of values presented in Table 4.3 are presented in Appendix E. It can be observed that deviation of basic parameters h , R , b , E and ν produces an almost linear variation of the rotational stiffness. This behavior was also observed for displacement in the work of SHEN [74] for h , R and b . In fact, these effects are not all linear. The nonlinear relationship between k_φ and basic parameters h and b can be observed in Figure 3.17, where R was set at a constant value. When the width is sufficiently large k_φ is almost linearly proportional to b and proportional to $h^{2.5}$. In that case, k_φ should also be inversely proportional to $R^{0.5}$ for the dimensions to correspond. E is linearly proportional to k_φ due to the assumption made for this work. In plate-like hinges, k_φ is inversely proportional to $1 - \nu^2$. This apparent linearity occurs due to the range of values considered. In Figure 3.17, h was increased by 100 %, so nonlinearity can be observed. Hole orientation parameters $d\theta_x$ and $d\theta_y$ produce parabolic deviations with $d\theta_x$ producing much more deviation, as was also observed in the work of SHEN [74]. Hole center separation parameter dx_c produces also a parabolic deviation. This parabolic behavior is caused due to the geometric symmetry around the axes of the hinge. Hole center position parameters dx and dy produce also linear deviations of k_φ . Effect of dx can be also be interpreted as a variation of the lever arm.

Gravity has a particular effect on the stiffness. Stiffness deviation in the presence of gravity orientation deviations $d\beta_{gz}$ and $d\beta_{gy}$ behaves like a sine and cosine function of these parameters, respectively. This occurs due to existence of additional loading on the flexure hinge, i.e. the weight force. When the hinge weight force points to the same direction as the deformation produced by pure bending (negative y -direction), stiffness reduces due to the increasing loading. When pointing to the opposite direction, stiffness increases. In fact, the stiffening effect when $d\beta_{gz} > 0$ produces more deviation than when k_φ decreases due to $d\beta_{gz} < 0$ (see Figure E.4). This deviation is also dependent on the value of the applied bending moment. The sine-like behavior when rotating the gravity vector relative to the flexure hinge occurs mainly due to the component of the weight force acting in the direction of the deformation. Even when $d\beta_{gz} = 0$, there is still a small stiffening effect ($e_{k_\varphi} > 0$) on the hinge produced by a beam-column behavior. This is observed in the

next chapter. Results considering these ranges of values show an important influence of parameters dh , dx_c and $d\beta_{gz}$. Nevertheless, only dh is considered between realistic values ($\pm 2.5 \mu\text{m}$). This suggests that dh is an influential parameter, as has been concluded in other works [70, 74]. The degree of influence compared to other parameters is measured in the next section.

4.4. Sensitivity analysis

A sensitivity analysis can be understood as the study of how uncertainty in the output of a model can be apportioned to different sources of uncertainty in the model input [71]. The result of this analysis is granted in the form of numerical values known as sensitivity measures, which represent the individual effect of an input parameter on the output. As such, its main purpose is to identify most influential parameters. Its reliability is based on different factors like the number of parameters used for the study, the dependency between one another, the capability of measures to capture the model behavior and the exploration of the input space. False set up of the analysis would lead to errors in the assessment of the influence of each parameter. These are classified in three types [71]:

- Type I: Erroneously defining a non-influential error as important.
- Type II: Non-identification of an influential parameter.
- Type III: Framing errors, e.g. due to parameter values off the mark.

For a trustworthy estimation of the influences of each aforementioned parameter, a decision on the sensitivity measures and sampling methods must be made. To that matter, some comparisons are made.

Sensitivity measures

Sensitivity measures are compared in Table 4.4 based on the following criteria:

- Model nonlinearity.
- Input space exploration.
- Parameter interaction.

It was observed in Appendix E that some of the parameters produce a nonlinear response of the model. In fact, the behavior of the model can be separated in a linear and a nonlinear fraction and sensitivity measures S_i should be able to capture both effects so that:

$$\sum_{i=1}^n S_i = 1$$

The use of linear sensitivity measures would overestimate the influence of a parameter as the linear fraction of a model is always less than one. Also important in the selection of a measure is that it can properly capture the global effect of a parameter rather than at particular points of the input space. In local methods, the effect of changing one parameter at a time is tested. In global methods, all parameters are changed simultaneously and a much larger range of parameter combinations is tested. They take interactions between parameters into account, explore the effect of each parameter across a wide range of values, and can deal with nonlinear relationships between the parameters and the model output [71]. Interaction between parameters, or higher-order effects, are important to capture

as one parameter may have no first-order influences but can produce significant variation when combined with other parameters. Although this is important for understanding the overall model behavior, it is preferred to have parameters as independent as possible. Another comparison criteria is usually the analysis efficiency. However, as the calculation time for needed combinations is usually high, especially for FE analysis, it is regarded as irrelevant. Further explanation on the measures compared can be found in Appendix F.

Table 4.4: Comparison of sensitivity measures.

| Measure | Model nonlinearity | Input space | Parameter interaction | Overall |
|--------------------------------------|--------------------|-------------|-----------------------|---------|
| Derivatives | - | - | - | - |
| Sigma-normalized derivatives | - | +/- | - | - |
| Standardized regression coefficients | +/- | + | - | +/- |
| First-order indices | + | + | - | +/- |
| Total effect | + | + | + | + |

According to the comparison made in Table 4.4, the total effect sensitivity index would be more suitable for this analysis since there are non-linear responses of the model, the great number of parameters (12) would require a proper exploration of the input space and unknown parameter correlations, especially geometric, may exist. It is also possible for linear sensitivity indices to be suitable, due to the apparent linearity of most parameters and the small individual effects of the nonlinear ones. Nevertheless, to be on the safe side, total effect indices will be used.

Experimental design

The degree of how precise global sensitivity analysis are lies on how well the space of input parameters is explored. This means that, ideally, points in all regions of the multidimensional space must be considered for the analysis. These points are combinations of input values, or samples, generated following certain rules, a process known as experimental design. There exist a vast amount of experiments or sampling methods in the literature which are suitable to different types of analysis and models. To find one suitable to the study in this work, a comparison is done in terms of [22]:

- Number of samples required.
- Space filling.
- Orthogonality.

To properly capture main effects and interactions between parameters, a certain number of values of each parameter may be needed depending on the response of the model. For a high number of parameters, the number of samples can highly increase to have significant results. This fact is very important when working with numerical simulations that are already computationally expensive so the number of samples must be the least possible without losing a proper space filling. Another important consideration is how combination of parameters are selected and in which order. Ideally, selection of independent parameters is necessary to reduce the complexity of the model. This means that parameters are not correlated, i.e. orthogonality. However, interactions between parameters may still appear as undesired statistical correlation between parameters can be introduced depending on

the combination ordering, leading to false results. This was evidenced by FLORIAN [24] and is caused by generating random input combinations. To that matter, a comparison between sampling methods is presented in Table 4.5. These methods are included inside OptiSlang so that combination of parameters can be generated and then computed by ANSYS. Further explanation of the sampling methods can be found in Appendix G.

Table 4.5: Comparison of sampling methods.

| Method | Number of samples | Space filling | Orthogonality | Ref. |
|---------------------|-------------------|---------------|---------------|------|
| Koshal linear | $k + 1$ | - | + | [41] |
| Koshal quadratic | $(k+1)(k+2)/2$ | - | + | [41] |
| D-optimal linear | N | +/- | - | [89] |
| D-optimal quadratic | N | +/- | - | [89] |
| Full factorial | a^k | - | + | [22] |
| Plain Monte Carlo | N | +/- | +/- | [86] |
| LHS | N | + | +/- | [55] |
| A-LHS | N | + | + | [35] |

k - number of parameters; a - number of levels per parameter; N - number of combinations.

According to Table 4.5, the A-LHS method is most suitable for a correct exploration of the multidimensional space while keeping the number of samples as low as possible. In fact, the number of combinations N required for a sensitivity analysis using this method is obtained by the convergence of the sensitivity measures, unlike fixed values as for factorial or one-at-a-time experiments [71].

Study cases

Using the parameters defined in Section 4.2, two sets of values are used for the analysis. First, the ranges of values considered are those that can be obtained with high accuracy within common methods, e.g. WEDM tolerances (see Table 4.6). Second, values for conventional accuracy are used, e.g. drilling or milling tolerances (see Table 4.7). The purpose of two analysis lies in showing how sensitivity measures vary for different ranges of values due to the order of the errors produced by each parameter. The range of deviations of dh is kept the same for both cases since deviations of 25 μm would result in $h = 0$ mm and higher deviations than 2.5 μm are already imprecise for this geometry (5%). It is also to remark that gravity deviations are considered as those produced by ground tilt. Although a flexure hinge can be designed in any position in space [30], the use of such range of values in this analysis leads to a type III error. It is necessary to set a certain position of the hinge. This decision is based on the stiffness deviations produced by the parameters in their range of values.

In Appendix H, stiffness deviations are calculated for each parameter in their according range of values for high and conventional accuracy. Deviation produced by ground tilt in both directions are calculated for three hinge positions $\beta_{gz} = 0^\circ$, $\beta_{gz} = 90^\circ$ and $\beta_{gz} = 270^\circ$. It can be appreciated that ground tilt around the z -axis $d\beta_{gz}$ produces a greater deviation for $\beta_{gz} = 0^\circ$ than for other positions and ground tilt around the y -axis $d\beta_{gy}$ does not produce a deviation at all in this range of values. In fact, deviations in such small range of input values may coincide with numerical errors of the FE model. This is also the case of parameter $d\theta_y$. Since their effects cannot be measured with the FE model, these parameters are not used in the analysis. The position of the hinge is considered as $\beta_{gz} = 0^\circ$.

Table 4.6: Parameter values for high accuracy.

| Parameter | Value | Ref. | Parameter | Value | Ref. |
|-------------|-----------------------|------|-----------|------------------------|------|
| dh | $\pm 2.5 \mu\text{m}$ | [61] | dx | $\pm 2.5 \mu\text{m}$ | [61] |
| dR | $\pm 2.5 \mu\text{m}$ | [61] | dy | $\pm 2.5 \mu\text{m}$ | [61] |
| db | $\pm 2.5 \mu\text{m}$ | [61] | dE | $\pm 0.71 \text{ GPa}$ | [77] |
| $d\theta_x$ | $\pm 0.005^\circ$ | [61] | $d\nu$ | ± 0.001 | [25] |
| $d\theta_y$ | $\pm 0.005^\circ$ | [61] | dg_z | $\pm 0.1^\circ$ | [18] |
| dx_c | $\pm 2.5 \mu\text{m}$ | [61] | dg_x | $\pm 0.1^\circ$ | [18] |

Table 4.7: Parameter values for conventional accuracy.

| Parameter | Value | Ref. | Parameter | Value | Ref. |
|-------------|-----------------------|------|---------------|------------------------|------|
| dh | $\pm 2.5 \mu\text{m}$ | [61] | dx | $\pm 25 \mu\text{m}$ | [23] |
| dR | $\pm 25 \mu\text{m}$ | [23] | dy | $\pm 25 \mu\text{m}$ | [23] |
| db | $\pm 25 \mu\text{m}$ | [23] | dE | $\pm 1.42 \text{ GPa}$ | [13] |
| $d\theta_x$ | $\pm 0.017^\circ$ | [63] | $d\nu$ | ± 0.003 | [25] |
| $d\theta_y$ | $\pm 0.017^\circ$ | [63] | $d\beta_{gz}$ | $\pm 0.1^\circ$ | [18] |
| dx_c | $\pm 25 \mu\text{m}$ | [23] | $d\beta_{gy}$ | $\pm 0.1^\circ$ | [18] |

Considerations for the analysis

Prior to the calculation, some considerations of the analysis need to be clarified:

- Loading in all calculations is done by applying a bending moment $M = 0.315 \text{ Nmm}$ ($\varphi \approx 1^\circ$).
- Gravity is considered in all calculations.
- Parameters are uniformly distributed.
- Parameters are assumed independent from one another.
- Number of samples for each study amounts to 100. Convergence of measure was met for a less number of samples due to high influence of some parameters.
- Geometric nonlinearities are considered.

The quality of the model is measured by means of the Coefficient of Optimal Prognosis (CoP) [58], which is included in OptiSlang. This coefficient is defined as:

$$CoP = 1 - \frac{SS_E^{Prediction}}{SS_T}$$

where $SS_E^{Prediction}$ is the sum of squared prediction errors, which are estimated by cross validation, and SS_T is the total variation. The model used as approximation is the one that maximizes this coefficient based on the number of variables, model complexity and support points used [59]. This approach is called Metamodel of Optimal Prognosis (MoP).

Total effect sensitivity indices are calculated for the approximation model and the variance contribution of each input parameter is determined in terms of individual CoP coefficients:

$$CoP(X_i) = CoP S_T^{MoP}(X_i)$$

Results

Table 4.8 shows the results of the sensitivity analysis using all parameters in their according range of values. Results show that parameter dh is by far the most influential for the thin flexure hinge. All other parameters show almost no influence at all. A linear regression model was used for these analysis since almost all deviation is produced by an apparently linear parameter such as dh . The elastic modulus deviation dE stands as the second most important parameter in both cases. Due the approximation nature of the model and dominance of dh , the indices results for less influential parameters may not be trustworthy. For that matter, dh is removed from the analysis and calculations are repeated to see the relative influence of other parameters.

Table 4.8: Sensitivity indices for $\beta_{gz} = 0^\circ$.

| Parameter | CoP _{high} (%) | S _{high} | CoP _{conv} (%) | S _{conv} |
|---------------|-------------------------|-------------------|-------------------------|-------------------|
| Model | 99.96 | 1.000 | 99.93 | 1.000 |
| dh | 98.52 | 0.986 | 98.98 | 0.990 |
| dR | 0.01 | 0.000 | 0.11 | 0.001 |
| db | 0.00 | 0.000 | 0.03 | 0.000 |
| dx_c | 0.01 | 0.000 | 0.00 | 0.000 |
| dx | 0.00 | 0.000 | 0.03 | 0.000 |
| dy | 0.00 | 0.000 | 0.00 | 0.000 |
| $d\theta_x$ | 0.00 | 0.00 | 0.000 | 0.000 |
| $d\theta_y$ | — | — | 0.00 | 0.000 |
| dE | 0.48 | 0.005 | 2.35 | 0.024 |
| $d\nu$ | 0.00 | 0.000 | 0.04 | 0.000 |
| $d\beta_{gz}$ | 0.00 | 0.000 | 0.02 | 0.000 |

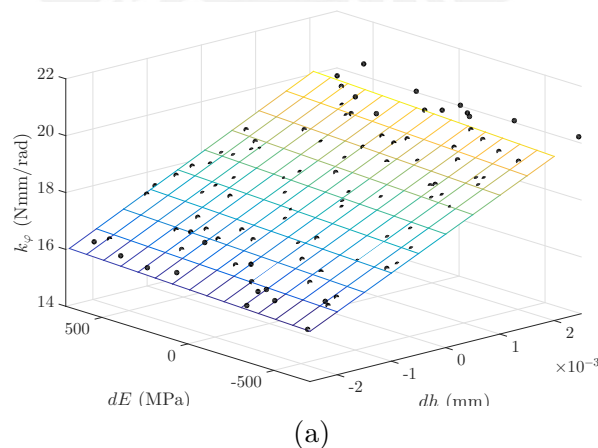


Figure 4.6: Linear regression model. (a) high accuracy; (b) conventional accuracy.

Table 4.9 shows a total influence of one parameter, dE . Since the effect produced by dE is perfectly linear and other nonlinear effects show almost no influence, a linear regression suits perfectly as model. Other parameters, such as $d\nu$, that did not show any influence in the previous analysis, gain certain influence for high accuracy values. However, due to

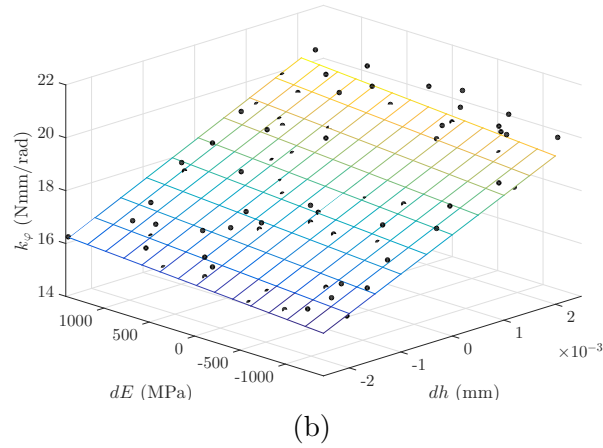


Figure 4.6 (Cont.): Linear regression model. (a) high accuracy; (b) conventional accuracy.

the dominance of dE , an additional analysis is done to better depict the influence of the other parameters. In this case, dE is removed from the analysis.

Table 4.9: Sensitivity indices for $\beta_{gz} = 0^\circ$ without dt .

| Parameter | CoP _{high} (%) | S _{high} | CoP _{conv} (%) | S _{conv} |
|---------------|-------------------------|-------------------|-------------------------|-------------------|
| Model | 100.00 | 1.000 | 99.53 | 1.000 |
| dR | 0.07 | 0.001 | 3.83 | 0.039 |
| db | 0.08 | 0.001 | 1.62 | 0.016 |
| dx_c | 0.00 | 0.000 | 0.01 | 0.000 |
| dx | 0.12 | 0.001 | 2.47 | 0.025 |
| dy | 0.02 | 0.000 | 0.37 | 0.004 |
| $d\theta_x$ | 0.00 | 0.000 | 0.00 | 0.000 |
| $d\theta_y$ | — | — | 0.00 | 0.000 |
| dE | 100.00 | 1.000 | 89.33 | 0.898 |
| $d\nu$ | 0.44 | 0.004 | 1.17 | 0.012 |
| $d\beta_{gz}$ | 0.16 | 0.000 | 0.00 | 0.000 |

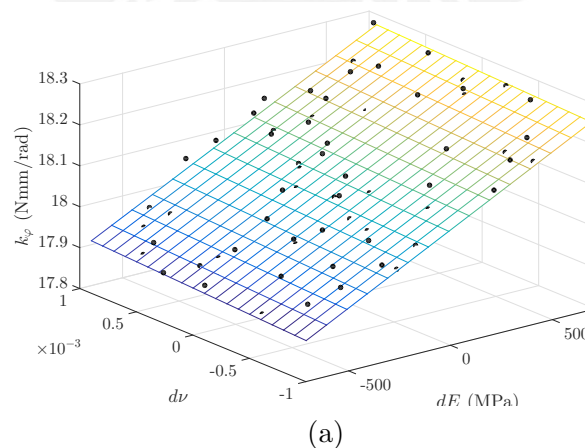
Figure 4.7: Linear regression model without dh . (a) high accuracy; (b) conventional accuracy.

Table 4.10 shows two different behaviors for the high and conventional accuracy cases. In the first case, parameter $d\nu$ contributes with about half of the influence on the stiffness above geometric parameters. In the second case, geometric parameters dR , db and dx are

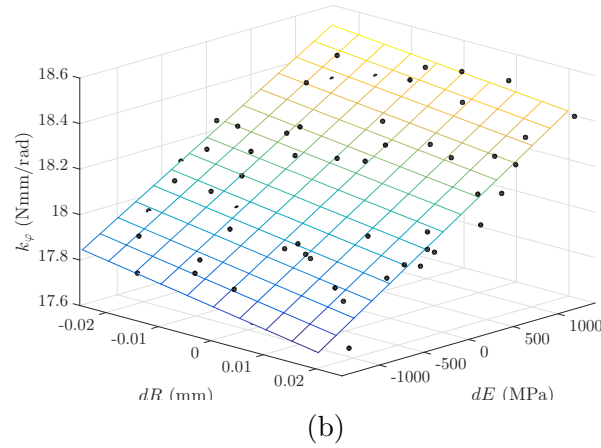


Figure 4.7 (Cont.): Linear regression model without dh . (a) high accuracy; (b) conventional accuracy.

responsible for most of the deviation. The gravity orientation deviation $d\beta_{gz}$ also gains certain influence for when geometric deviations are small, though its effect is small due to the almost neglectable mass of the flexure hinge and its range of value. However, the quality of the model and the fiability of measures decrease if the whole range of possible values is taken into account (see Appendix I).

Table 4.10: Sensitivity indices for $\beta_{gz} = 0^\circ$ without dt and dE .

| Parameter | CoP _{high} (%) | S _{high} | CoP _{conv} (%) | S _{conv} |
|---------------|-------------------------|-------------------|-------------------------|-------------------|
| Model | 99.98 | 1.000 | 99.99 | 1.000 |
| dR | 17.36 | 0.174 | 44.20 | 0.442 |
| db | 6.51 | 0.065 | 17.58 | 0.176 |
| dx_c | 0.04 | 0.000 | 2.26 | 0.023 |
| dx | 9.94 | 0.099 | 24.98 | 0.250 |
| dy | 0.89 | 0.009 | 1.81 | 0.018 |
| $d\theta_x$ | 0.00 | 0.000 | 0.00 | 0.000 |
| $d\theta_y$ | — | — | 0.00 | 0.000 |
| $d\nu$ | 50.85 | 0.509 | 9.58 | 0.096 |
| $d\beta_{gz}$ | 14.80 | 0.148 | 0.20 | 0.002 |

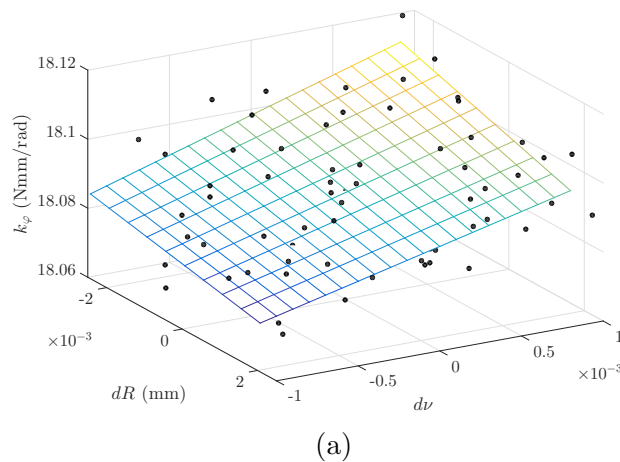


Figure 4.8: Linear regression model without dh and dE . (a) high accuracy; (b) conventional accuracy.

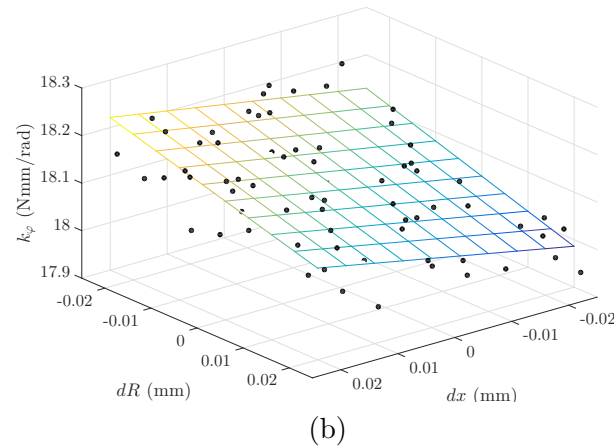


Figure 4.8 (Cont.): Linear regression model without dh and dE . (a) high accuracy; (b) conventional accuracy.

4.5. Summary

In the actual application, the defining characteristics of a flexure hinge are not ideal. Geometric deviations due to manufacturing, errors in measuring material properties and external influences like the existence of additional loads, e.g. the weight force, alter the real performance of the hinge. As such, the rotational stiffness differs to the value obtained through analytical and numerical models. To analyze the behavior of a thin flexure hinge under non-ideal conditions and to find influential parameters, a sensitivity analysis was conducted. For that matter, possible sources of deviation were identified and described by parameters supported by the finite element model. The sensitivity analysis was conducted using values of deviation attainable with high and conventional accuracy using available technologies. Overall results of the analysis show an almost absolute dependence on the minimum height of the flexure hinge, being followed by a small dependence on the elastic modulus. After them, parameters show almost no influence and their effects depend mostly on the range of values in which they can deviate. These results show that actual performance of a thin flexure hinge with $h = 50 \mu\text{m}$ may deviate significantly from the ideal value, about 13.7 % for highly accurate values. Tolerances achievable through WEDM and common processes like milling are not sufficiently accurate for manufacturing the thinnest flexure hinges. Attention should also be placed on material properties, since they gain influence as geometric deviations are reduced. Deviations due to non-ideal conditions are sometimes expected to compensate the modeling approach errors. In fact, deviations due to analytical modeling and actual operation may lie around the same order (≈ 10 to 12%), so current analytical models are still considered by some authors suitable for flexure hinges [19].

5. Application of thin flexures in weighing cells

Application of flexures in force-measuring devices has been reported since the end of the 19th century [20]. They are used to replace the knife-edge pivots in sensitive balances since they present practically no wear, so their resistance to motion can be regarded as constant. This resistance is of utmost interest in such systems. Stiffness of a flexure limits the sensitivity of a balance. In fact, the sensitivity depends mostly on the stiffness of its central flexure [69, 79]. In this chapter, this flexure is the object of study.

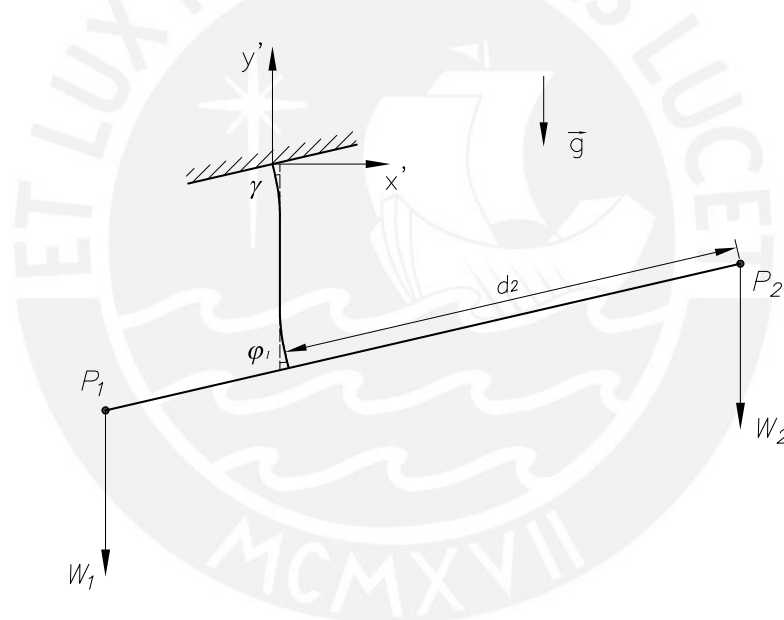


Figure 5.1: Transmission lever in a weighing cell. Adapted from [79].

Weighing cells work using the principle shown in Figure 5.1. The weight force W_1 is measured by applying a counter force W_2 while measuring the position of point P_2 of the transmission lever. The value of W_2 is controlled by the measurement of the position of point P_2 , increasing W_2 until a position detector marks zero. This means that the measured value of W_1 occurs when the beam is parallel to the base. W_2 should be equal to W_1 if both lever arms to the pivot are equal, as in some mass comparators [69], but this is not necessarily the case [18, 54]. If moment equilibrium of the lever is evaluated, W_2 cannot be directly used to determine W_1 due to the existence of the restoring moment M produced by the flexure (see Figure 5.2). Then, the determination of W_1 depends on the knowledge of the restoring moment M , which depends on the rotational stiffness k_φ of the flexure, as in Equation 2.1.

It was stated in Section 2.2 that k_φ depends on the loading conditions. Figure 5.2 shows the free-body diagram of the transmission lever of a weighing cell. Point P_f is the location of the flexure hinge. The weight of the beam is located along the longitudinal axis of the

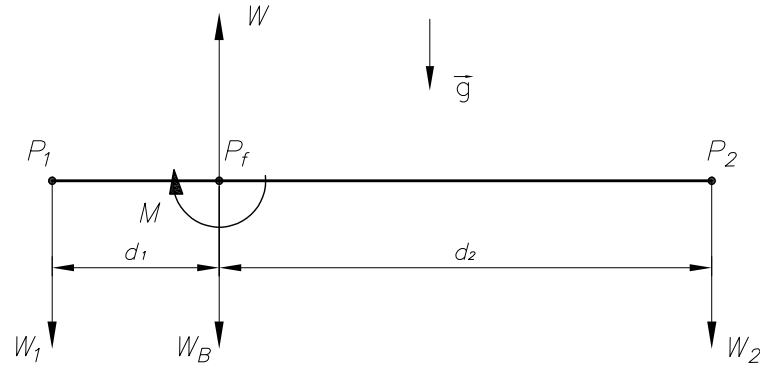


Figure 5.2: Free-body diagram of the transmission lever.

flexure to avoid additional moments. Equilibrium shows that the flexure is subjected not only to a bending moment M but to an axial force W as well which equals the sum of all supported weights, i.e. beam-column behavior. The existence of an axial force on a flexure hinge generates an additional bending moment which increases with deformation (see Figure 5.3). If the force is tensile, the stiffness increases and if it is compressive, the stiffness decreases. The effect of this axial force on the stiffness of a flexure strip was modeled by EASTMAN [20] and the following equation was derived:

$$k_\varphi = \frac{EI_z}{j \tanh \frac{s}{j}} \quad (5.1)$$

where $j = \sqrt{EI_z/W}$, s is the length of the strip and EI_z its flexural rigidity. However, such an expression has not been derived for notch hinges, where I_z is not constant. Only a numerical solution of great complexity has been proposed in the work of AWTAR [5] for beams of variable cross-section.

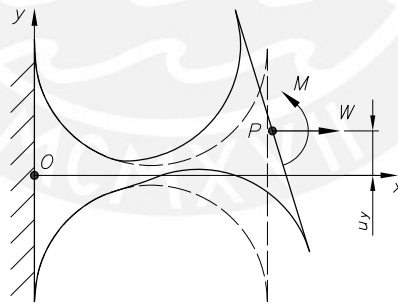


Figure 5.3: Notch flexure hinge subjected to bending and axial loading.

In weighing cells, foundation of the device may not be perfectly perpendicular to the gravity acceleration vector \vec{g} due to either misalignment or ground tilt caused by vibrations. This is expressed by the angle γ in Figure 5.1. The analysis done in Chapter 4 showed a small influence of the gravity orientation deviation $d\beta_{gz} \equiv \gamma$ on the rotational stiffness when \vec{g} had ideally a positive x -direction ($\beta_{gz} = 0^\circ$). $d\beta_{gz}$ produces an undesired additional rotation of the flexure hinge, which was measured as a deviation of k_φ (see Appendix H). Important is to remark that the small value of the stiffness deviation was due to the mass of the flexure hinge. Masses measured in weighing cells are many times greater than that of the hinge, so this effect will have greater influence. Then, W_2 needs to compensate for the additional rotation for the beam to be parallel to the base of the device ($\gamma = \varphi_1$), producing a false measure of W_1 .

In this chapter, the stiffening effect due to the tensile force and the deviations produced due to ground tilt will be further studied in circular-contour flexure hinges. For that matter, the model defined in Chapter 3 is utilized and modified for the required studies.

5.1. Axially-loaded flexure hinges

The flexure hinge model from Chapter 3 is subjected to a tensile weight force W and deviation of the rotational stiffness e_{k_φ} is calculated. Compressive forces are not taken into account as solution may not converge. Calculations are conducted assuming geometric nonlinearities, since in the linear case this effect cannot be captured, i.e. constant stiffness. Axial load W is better described by the supported mass parameter m as $W = mg$. In fact, the mass is the value of interest to be measured. The force is applied through a point mass m located at coordinate $(L/2 + R, 0, 0)$, at the end of the contour. The point mass is modeled using the element MASS21 defined in a node. This node is connected to the free end face of the model through multipoint constraints. Results are presented in Figure 5.4, where e_{k_φ} is calculated for supported masses up to 2 kg:

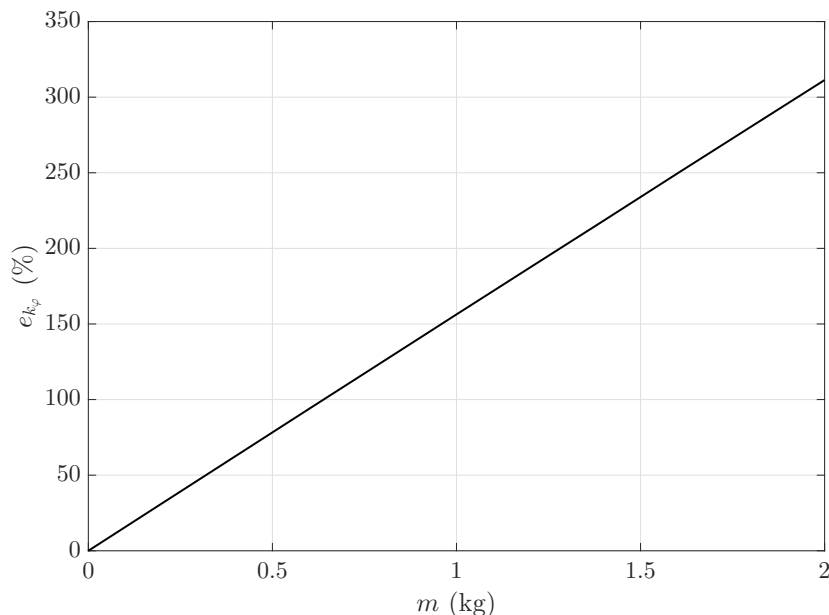


Figure 5.4: Deviation of k_φ due to axial loading according to FE results.

When supporting masses up to 2 kg, the rotational stiffness of the flexure hinge can increase up to 311%. This means that, in force measuring systems, knowledge of the beam-column behavior of flexure hinges becomes mandatory. Even when the application does not require that the hinge supports axial force, existence of additional constraints can generate these loading conditions, e.g. parallel mechanisms [4].

Minimizing stiffness

The sensitivity of the system in Figure 5.1 can be increased by reducing the stiffness of the central flexure strip by either decreasing the moment of inertia I_z or increasing its length. Decreasing I_z by reducing b is not effective and might increase the sensitivity to parasitic motions while h cannot be reduced much further than 50 μm . The term $\tanh(s/j)$ of Equation 5.1 suggests that there is a value of s for which the reduction of the stiffness k_φ is almost neglectable for given E , I_z and W values. For flexure strips,

this value is approximately $s = 3j = 3\sqrt{EI_z/W}$, since $\tanh(3) \approx 1$. This means that increasing the value of s further would not produce a significant variation of k_φ . In the case of circular contour flexure hinges, a geometry for minimum stiffness cannot be analytically determined. Increasing the radius too much would result in loss of rotational precision. In their design of a mass comparator, QUINN ET AL. proposed to add a strip-like zone, with length denoted as s , on the thinnest region ($h(x) = h$) of a semi-circular flexure hinge, resulting similar to a corner-filletted flexure hinge with large fillet radius [69] (see Figure 5.5). This way the rotational stiffness can be reduced while sacrificing little rotational precision.

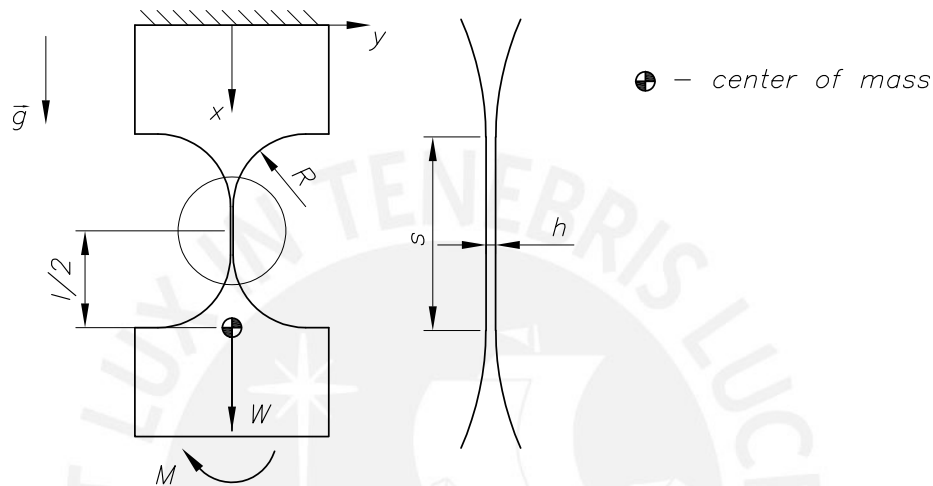


Figure 5.5: Flexure hinge by QUINN ET AL. [69].

The behavior of this hinge was modeled using the equation from EASTMAN (see Equation 5.1), expecting it to be a good approximation [69]. However, ignoring the compliance of the circular section is a simplification. The use of modeling based on the plane stress assumption also constitutes an oversimplification for this approach. The accuracy of Equation 5.1 is validated by modifying the model of Chapter 3 by adding the additional length s and applying the axial load W at end of the contour.

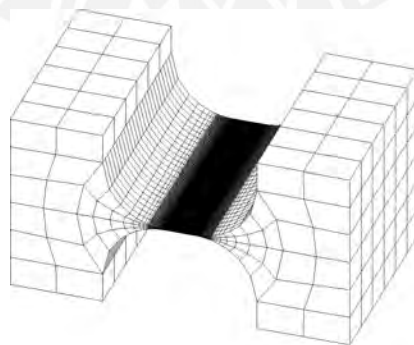


Figure 5.6: New FE model for $s = 1.5$ mm.

Modeling

The model is presented in Figure 5.6. The strip of variable length s with a constant cross section was added to the center of zone 1. The weight force W is applied through a point mass m located at coordinate $(L/2 + s/2 + R, 0, 0)$ at the end of the contour. The point mass is modeled in same way as before. According to the strategy of Chapter 3,

the number of elements in zone 1 would need to be increased to preserve the in-plane aspect ratio of 1. However, this highly increases the number of elements and, thus, the computational time. For example, a simulation for $s = 1.5$ mm, $M = 0.1$ Nmm and $m = 2$ kg using the parameters from Table 3.1 requires approximately 240 minutes for geometrical nonlinear calculations with the same settings as in Chapter 3. Using the same number of elements as the previous model or using a fixed number would produce high distortion and bad element transition when s is too large or small. With this approach, numerical errors such as non-continuity of results started to appear for $m > 1$ kg when $s = 1.5$ mm using 20 additional elements along the straight section. This occurs because some highly distorted elements get more distorted during deformation, especially for large masses. To reduce both problems, element size along the length of zone 1 is set to the same as size as along the height in $h(x) = h'$ (see Section 3.4). Parameter h' was determined only from the circular contour dimensions, so it is not affected when s was added. In the first approach, transition of element size stops when reaching the straight section. In the new proposed one, it stops when reaching zone 1. Number of elements using the first approach for $s = 1.5$ mm amounts to 61927 while in the new approach it amounts to 21607.

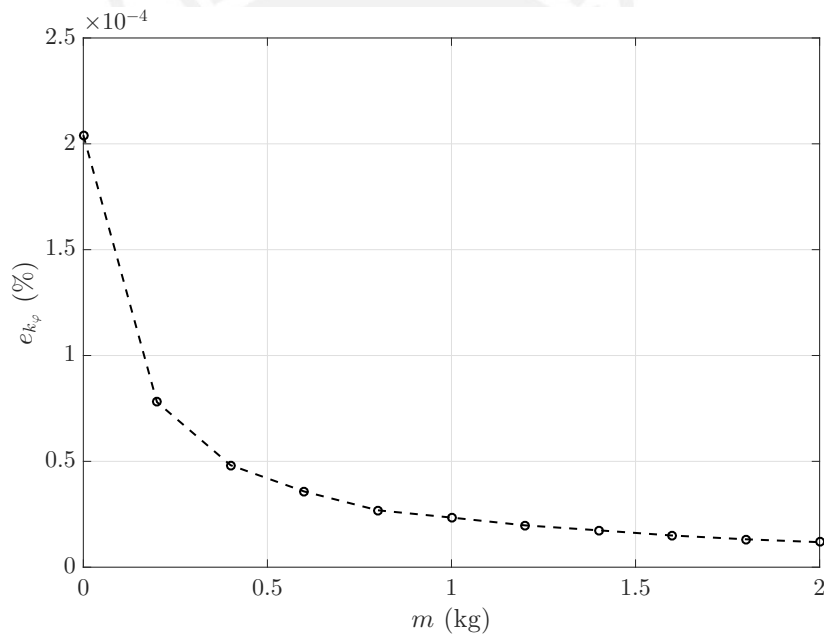


Figure 5.7: Deviation of k for reduced element number to full model.

Results between both mesh approaches are compared for a flexure hinge with $s = 1.5$ mm for different values of m . The applied bending moment M equals 0.1 Nmm. Figure 5.7 shows that maximum deviation is around 0.0002 %, which is acceptable. Later calculations are conducted using the reduced model. Simulation time was highly reduced from 240 to approximately 20 minutes.

Comparison

Using the model defined before, the rotational stiffness k_φ is calculated for masses from 0 to 2 kg for hinges with increasing lengths s until its variation is sufficiently small. The case for which $s = 0$ mm is calculated using the model from Chapter 3. The applied bending moment M is the same for every flexure hinge and amounts to 0.1 Nmm. The authors in [69] considered the circular section to be rigid for their calculations. It means that Equation 5.1 cannot be used for this calculation since it would consider the axial

load applied at the end of straight region ($x = L/2 + s/2$). To consider a displaced load application point, the following expression can be derived from Equation 5.1 [69]:

$$k_\varphi = W \left(x_{CM} + \frac{j}{\tanh \frac{j}{s}} \right) \tag{5.2}$$

x_{CM} is the position of the center of mass of the supported mass, i.e. axial load application point, relative to the end of the contour (see Figure 5.8). Setting the value $x_{CM} = R$ would match with the assumption made by QUINN ET AL. FE results are presented in Figure 5.9(a) while results using Equation 5.2 in Figure 5.9(b). The elastic modulus used for these calculations is the modified value $E' = E/(1 - \nu^2)$ to compensate for the plane stress assumption.

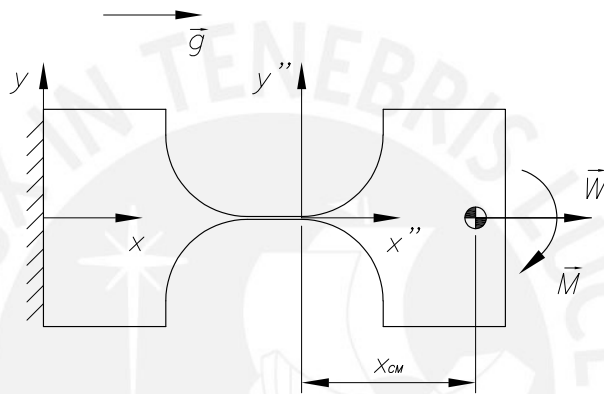


Figure 5.8: Loading conditions for the flexure hinge model.

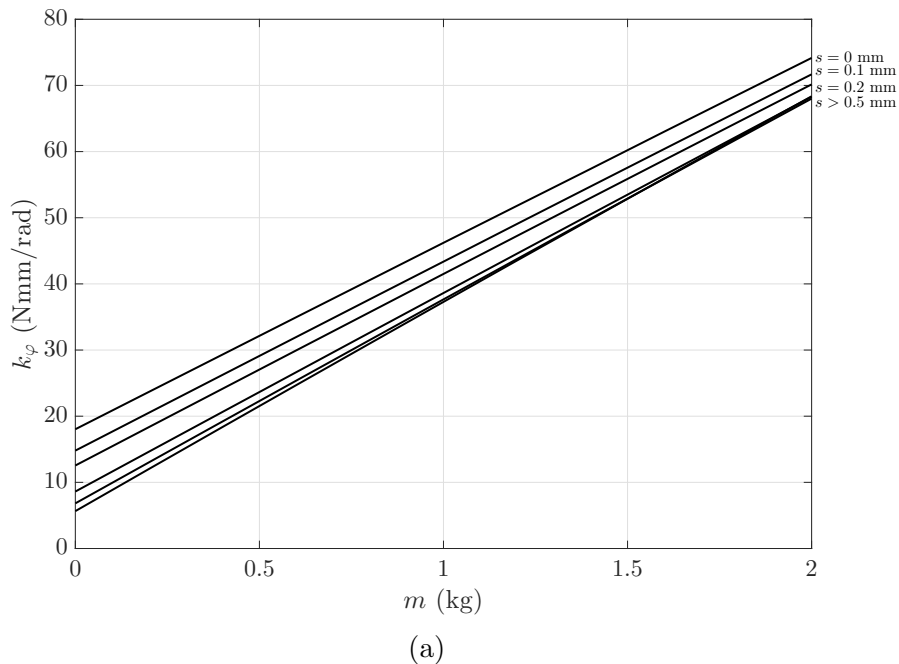


Figure 5.9: Behavior of the flexure hinge according to (a) FE model; (b) Equation 5.2.

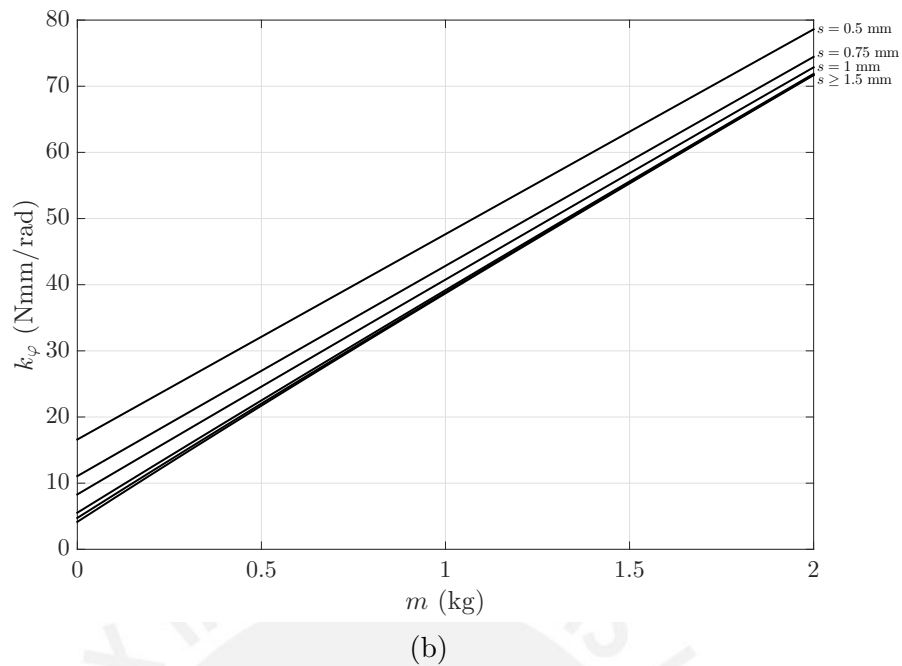


Figure 5.9 (Cont.): Behavior of the flexure hinge according to (a) FE model; (b) Equation 5.2.

Results show that the behavior according to Equation 5.2 is stiffer than to the FE model for the same value of s . This was to be expected, since the FE model still has the compliance of the circular section and its stress state is not completely plane strain. While analytical results do not have an upper limit value since $k_\varphi \rightarrow \infty$ for $s \rightarrow 0$ mm, FE results have the stiffness of the circular contour flexure hinge as an upper limit value. Figure 5.9(a) shows that k_φ can be minimized for $m > 1$ kg when $s \approx 1$ mm while Figure 5.9(b) shows that the minimum occurs when $s \approx 1.5$ mm. This means that Equation 5.2 cannot be used to accurately describe the behavior of the flexure hinge as proposed by QUINN ET AL. [69].

Stiffening effect

According to Equation 5.2, s can be increased infinitely while k_φ converges to a minimum value. The value of s for an acceptable converged k_φ depends on the supported mass m . This can be better depicted in a graph of k_φ against s for different values of m rather than as was done in Figure 5.9. The values of s for both cases are considered from 0 to 2 mm. Results are shown in Figure 5.10, where an unexpected behavior can be observed. FE results show that rather than converging with the increasing length, k_φ reaches a minimum value and, then, increases again. This behavior appears only for high values of m in Figure 5.10 but can be expected for low masses if s is sufficiently large.

The explanation for this behavior can be done with help of Equation 5.2. The rotational stiffness can be separated in two parts:

$$k_\varphi = \frac{Wj}{\tanh \frac{s}{j}} + Wx_{CM} \quad (5.3)$$

The first term of the right side is equivalent to Equation 5.1, which models the beam-column behavior when loading is applied at the end of the flexure strip. The second term is the additional stiffness due to the displaced load application point. Assuming geometric nonlinearities, the length s increases during deformation, which is

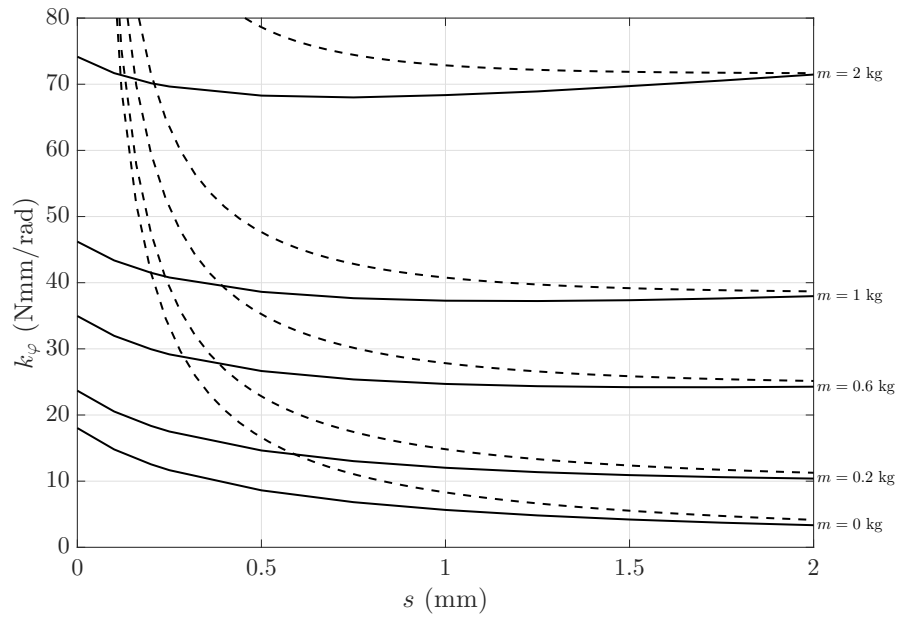


Figure 5.10: Comparison between FE results (continuous) and Equation 5.2 (dashed).

not considered by Equation 5.2. When s is large enough that the first term cannot be significantly decreased anymore, the elongation has practically no effect. On the other hand, the center of mass is displaced due to the elongation of the strip, i.e. x_{CM} increases. The second term of Equation 5.3 affects the stiffness to a much higher degree than the first term. This means that when the elongation is sufficiently large due to s and W , the effect of the second term will overcome the other one and the rotational stiffness increases. This can be observed in Figure 5.10 for the high load values.

Equation 5.1 suggested that k_φ could be minimized for supported masses above a certain value if the flexure was sufficiently large. Increasing the length any further would have no significant effect. However, the effect caused by the elongation implies that k_φ can only be minimized by a specific length for a certain supported mass. This would mean that when supporting other values of m , the stiffness of the flexure represents a non-minimum value.

5.2. Ground tilt effect

In the previous section, the center of mass of the supported system was considered at the end of the contour ($x = L/2 + s/2 + R$). The position of the center of mass can be adjusted to vary the stiffness of the flexure. This can be seen in Equation 5.2. If $x_{CM} < 0$, k_φ can be reduced. This is further developed in the work of QUINN ET AL. [69], where the angle of rotation φ_1 of a flexure strip in the global coordinate system $x'-y'$ (see Figure 5.1) can be determined for given ground tilt angle γ and position of the center of mass x_{CM} relative to the free end (coordinate system $x''-y''$), as in:

$$\varphi_1 = \frac{\gamma}{\frac{x_{CM}}{j} \sinh \frac{s}{j} + \cosh \frac{s}{j}} \quad (5.4)$$

According to Equation 5.4, the condition where the base of the hinge and the supported beam are parallel occurs when the denominator equals 1. A value of x_{CM} can be determined in terms of s , E , I_z and W , so that ground tilt has no effect, i.e. zero tilt

sensitivity. This is called the autostatic state [16]. It is to remark that this is only valid for very small values of γ . An expression of this type is yet to be proposed for other types of flexures. In this work, circular contour flexure hinges will be studied.

Study approach

The circular contour flexure hinges modeled in Section 3.4 ($s = 0$ mm) and Section 5.1 will be used to find the location of the center of mass for the autostatic state, labeled as \bar{x}_{CM} . The position of the center of mass x_{CM} according to Equation 5.4 is measured from the free end of the strip. In this section, it will be measured from the midpoint of the flexure hinge ($x = L/2$), as in Figure 5.11. Since \bar{x}_{CM} cannot be directly determined using ANSYS, it will be approximated for given γ and m values and geometric configuration. In the local coordinate system x - y , the gravity acceleration vector is deviated by $d\beta_{gz} = \gamma$ and the position x_{CM} for $\varphi = 0^\circ$ is to be found (see Figure 5.11). Rotations are considered positive around the positive z -axis.

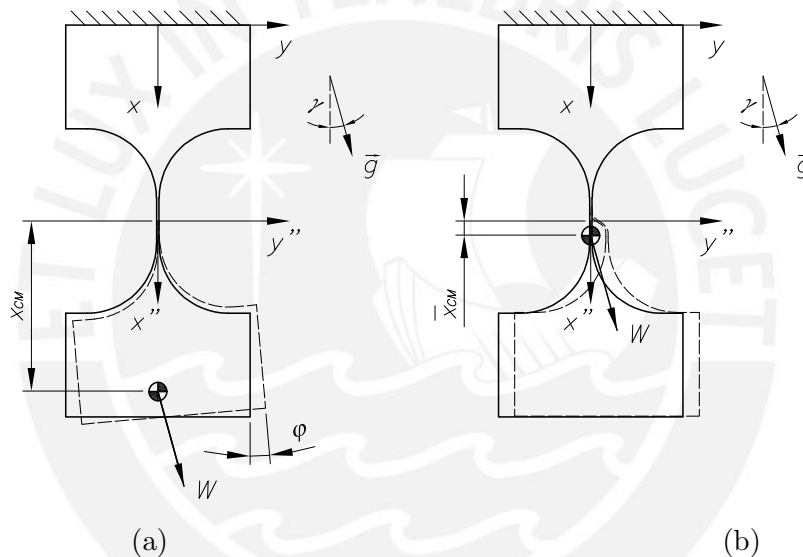


Figure 5.11: Rotation angle φ produced by ground tilt angle γ : (a) generic state; (b) autostatic state ($\varphi = 0^\circ$).

The approach for finding \bar{x}_{CM} consists on changing the value of x_{CM} while measuring the rotation angle φ . \bar{x}_{CM} can be determined from either the linear interpolation of two points, one positive and one negative, for which φ is closest to zero or by fitting a function $\varphi(x_{CM})$ using the results as support points and evaluating it at $\varphi = 0^\circ$. This function can be visualized using Equation 5.4 edited for the coordinate system at the middle of the strip as an example. In Figure 5.12, φ was calculated while changing x_{CM} for different values of γ considering $E = 71$ GPa, $\nu = 0.33$, $h = 0.05$ mm, $b = 10$ mm, $s = 1.5$ mm and $m = 1$ kg. As in the previous section, calculations will be done using the modified elastic modulus E' and the circular section is assumed rigid.

\bar{x}_{CM} amounts to approximately 0.131 mm, as appreciated in Figure 5.12. It can also be observed that the solution tends to infinite, i.e. system instability, for a certain value of x_{CM} , which will be labeled x'_{CM} and equals -0.194 mm in this case. There are two things to remark from Figure 5.12, which will serve later for correct modeling. First, \bar{x}_{CM} for each value of γ is always the same due to the simplification of the sine function for small angles used in the derivation of Equation 5.4. As such, the approximated \bar{x}_{CM} in the simulations will be found dependent on γ . Second, \bar{x}_{CM} locates below the middle

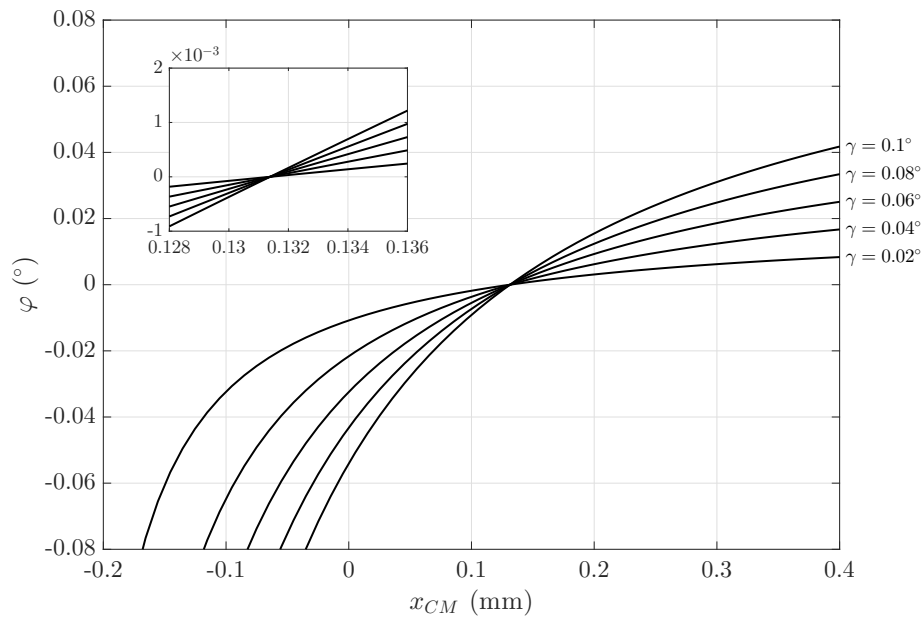


Figure 5.12: Determination approach for \bar{x}_{CM} using analytical results.

the flexure ($x_{CM} > 0$) while x'_{CM} locates above ($x_{CM} < 0$). This is better depicted in Figure 5.13, where normalized values of \bar{x}_{CM} and x'_{CM} , calculated as $\hat{x}_{CM} = x_{CM}/s$, are calculated for different values of s . It can be appreciated that \bar{x}_{CM} is always located below the middle of the flexure and gets closer to the free end as the strip gets longer. x'_{CM} locates mostly above the middle of the flexure but, as the strip gets larger, it can overcome the middle of the flexure and both points get closer. From the FE modeling point of view, knowledge of the behavior of these points becomes important for limiting the range of values of x_{CM} for which the curves in Figure 5.12 will be approximated. If results are sought near x'_{CM} , the solution may never converge.

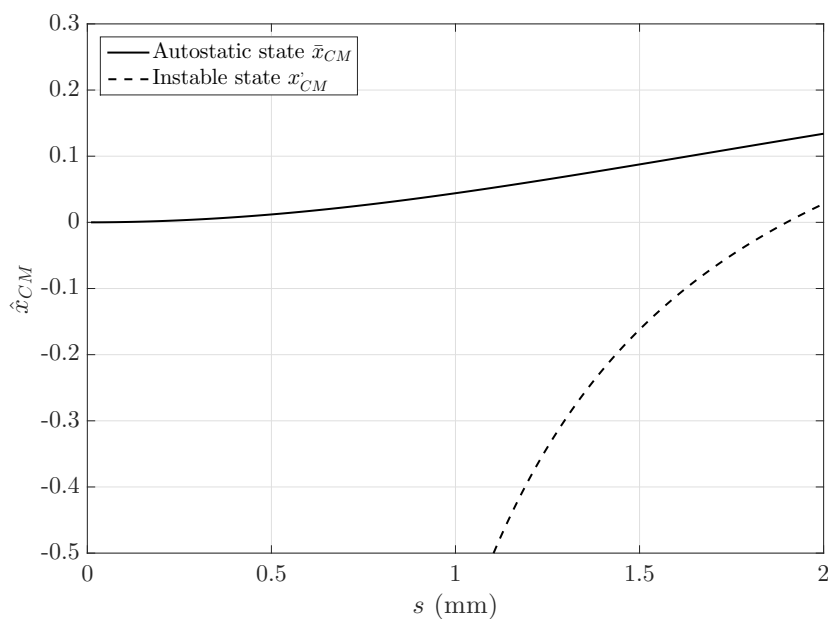


Figure 5.13: \hat{x}_{CM} for autostatic and instable state for different values of s .

Convergence criteria

In a first step, convergence criteria is evaluated using the models from Chapter 3 ($s = 0$ mm) and Section 5.1 with $s = 1.5$ mm for the new loading conditions. The value of the tolerance $\varepsilon_{\mathbf{R}}$ is reduced from $5 \times 10^{-4} \%$, which was defined in Chapter 3, to $5 \times 10^{-8} \%$ and the deviation of the value of φ compared to its value for $\varepsilon_{\mathbf{R}} = 5 \times 10^{-8} \%$ is evaluated using masses of 1 and 2 kg (see Figure 5.14). The point mass is located at $x = L/2$. Results are presented in Figure 5.14. A tolerance of $5 \times 10^{-4} \%$ produces results for $s = 0$ mm $s = 1.5$ which deviate $e_{\varphi} \approx 0.15 \%$ to those using the reference value. Acceptable deviations ($e_{\varphi} \approx 0.02 \%$) for both cases can be obtained with $\varepsilon_{\mathbf{R}} = 5 \times 10^{-5} \%$. The use of more precise tolerances produces a high increment in the simulation time, especially for $s = 1.5$ mm. To that matter, $\varepsilon_{\mathbf{R}} = 5 \times 10^{-5} \%$ will be set for this work.

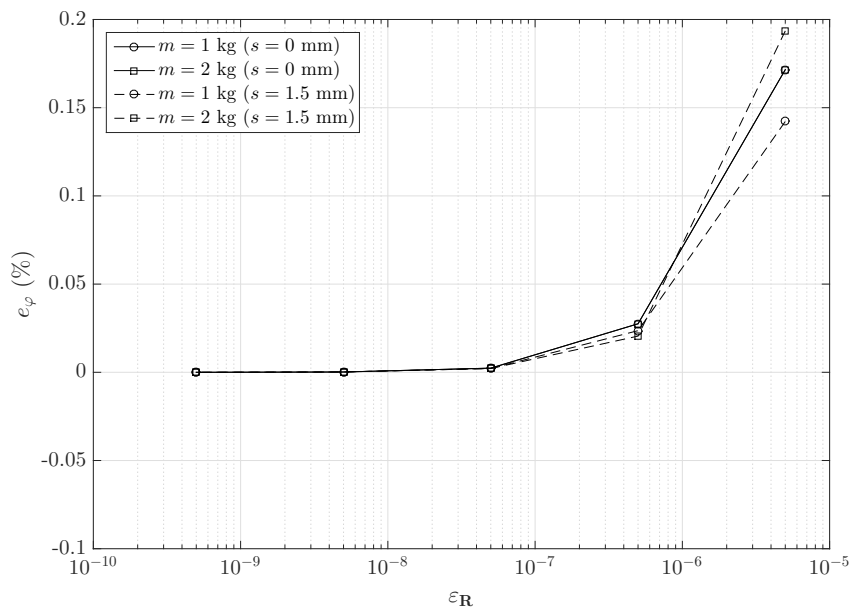


Figure 5.14: Convergence criteria for ground tilt effect.

Autostatic compensation

The value of \bar{x}_{CM} for $s = 0$ mm will be obtained through the process previously defined (see Figure 5.11). Using the circular contour flexure hinge model, φ was calculated for tilt angles γ from 0.01 to 0.1° for a supported mass of $m = 1$ kg. Results are presented in Figure 5.15. Calculations for some values of γ were omitted for better visualization. In a first attempt, x_{CM} was set at values from -0.3 to 0.3 mm, knowing that \bar{x}_{CM} should be close to the center of the hinge ($x_{CM} = 0$ mm) and $x_{CM} \rightarrow -\infty$ for very short hinges. Stepping was set at $\Delta x_{CM} = 0.03$ mm.

Results show that \bar{x}_{CM} locates near the center of the hinge, as expected. In contrast to Figure 5.12, the curves presented do not intersect at a fixed point. This means \bar{x}_{CM} also depends on the value of γ . Being that the case, \bar{x}_{CM} is approximated for all considered values of γ . Two approaches were previously proposed: linear interpolation of two points and function fitting. \bar{x}_{CM} was calculated using both approaches and results are presented in Figure 5.16. The fitted function used is a fourth-order polynomial.

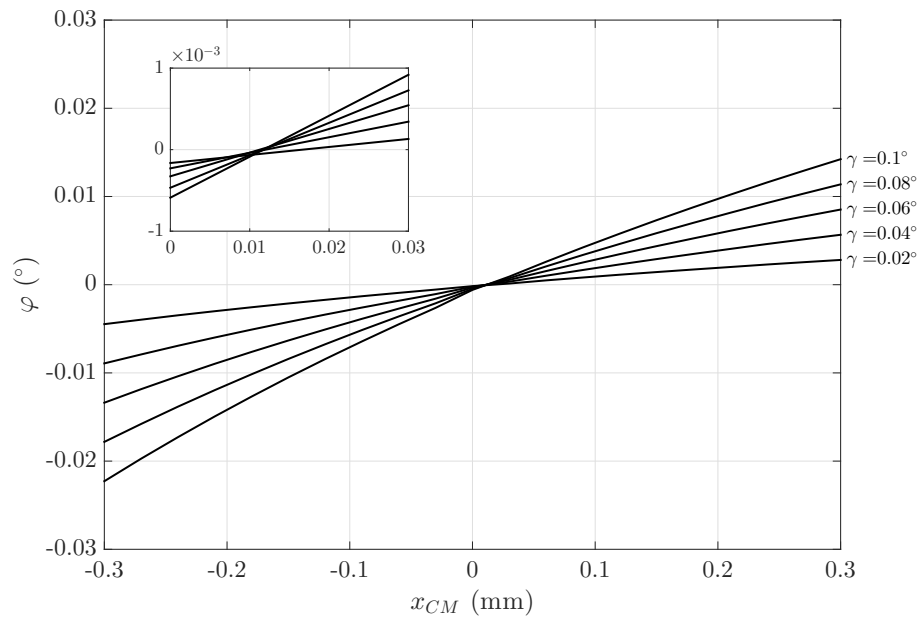


Figure 5.15: Determination approach for \bar{x}_{CM} using FE results for $s = 0$.

Results from both approaches are similar when the ground tilt angle is small ($\gamma < 0.02^\circ$). For larger angles results deviate in approximately $2 \mu\text{m}$. The cause of this deviation is mostly due to the numerical errors occurring near \bar{x}_{CM} . For very small angles φ , as those encountered near the sought autostatic state, errors start to appear in the solution. The fact that \bar{x}_{CM} is larger for the smallest values of γ may lie in the component of the weight force in the x -direction being larger. However, numerical errors have also been observed around these values. In the actual application, ground tilt angles can be even smaller but the FE model cannot capture these effects.

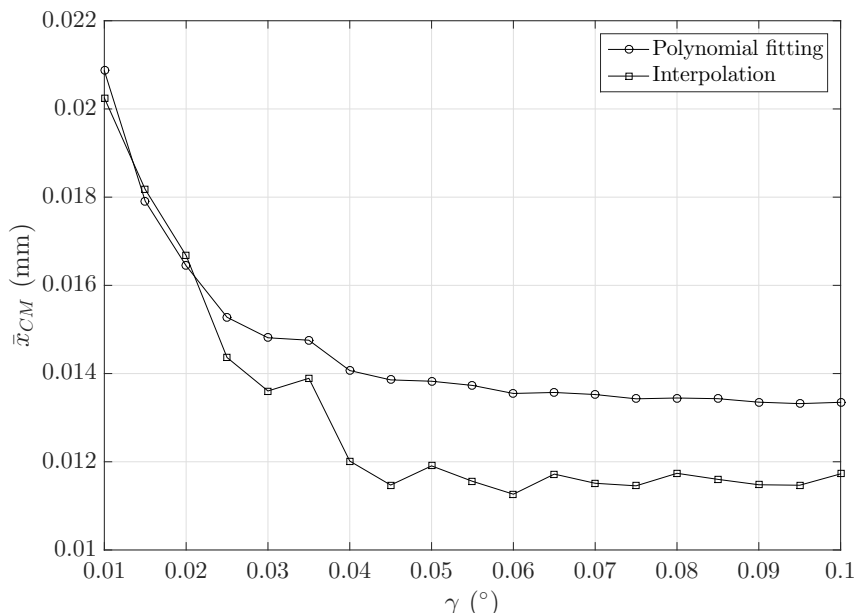


Figure 5.16: \bar{x}_{CM} for different tilt angles.

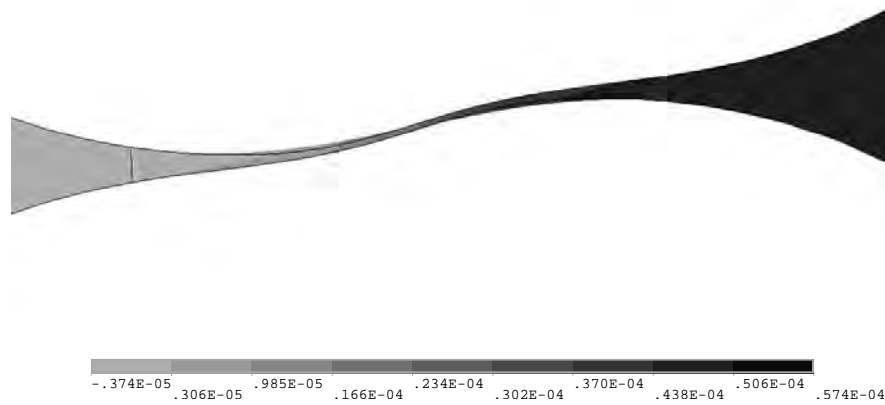


Figure 5.17: Displacements in y -direction in mm. Deformation scaled by a factor of 2500.

In the autostatic state, at $\varphi = 0^\circ$, the deformed flexure hinge presents an s-shape, as reported in [18]. The deformed state of the flexure hinge for $\gamma = 0.1^\circ$ when $x_{CM} = 0.014$ mm is depicted in Figure 5.17. From the deformation point of view, the s-shape is generated by deformation due to bending produced by the y -component of the weight force being compensated by the nonlinear bending from the x -component and an additional bending moment from the displaced load application point. The loading in the point of zero slope is similar as in flexure hinges of parallel mechanisms [4]. From an idealistic point of view, the autostatic state can be understood as the center of mass being located at the pivot of a physical pendulum (see Figure 5.18). When loading is applied below the pivot, rotations are positive and when applied above, rotations are negative.

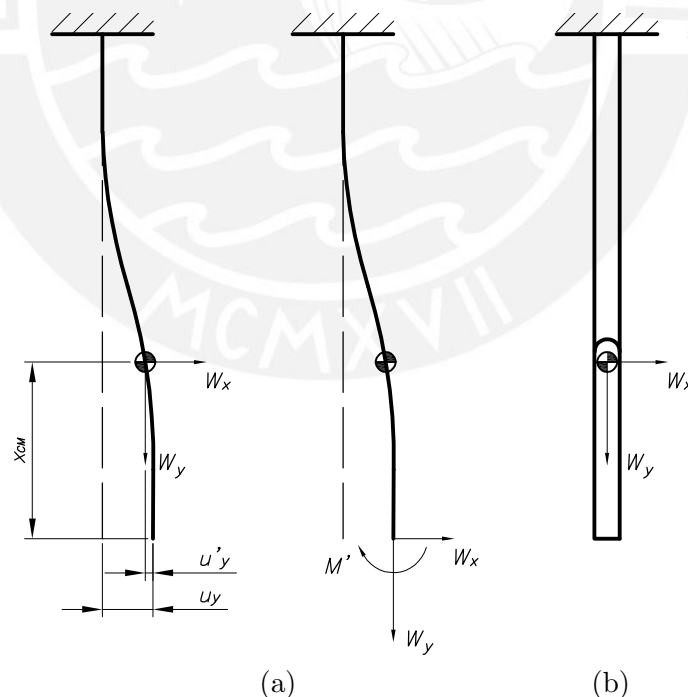


Figure 5.18: Autostatic state interpretation: (a) Deformation; (b) Idealization.

Limitations

False results due to numerical errors can be observed in Figure 5.19, where results are recalculated using a step of $\Delta x_{CM} = 0.0015$ mm. For that matter, \bar{x}_{CM} cannot be reliably determined using linear interpolation. If a solution point is too close to the error

zone, results will not be trustworthy. Smaller steps cannot be used either due to the same reason, even when fitting a function.

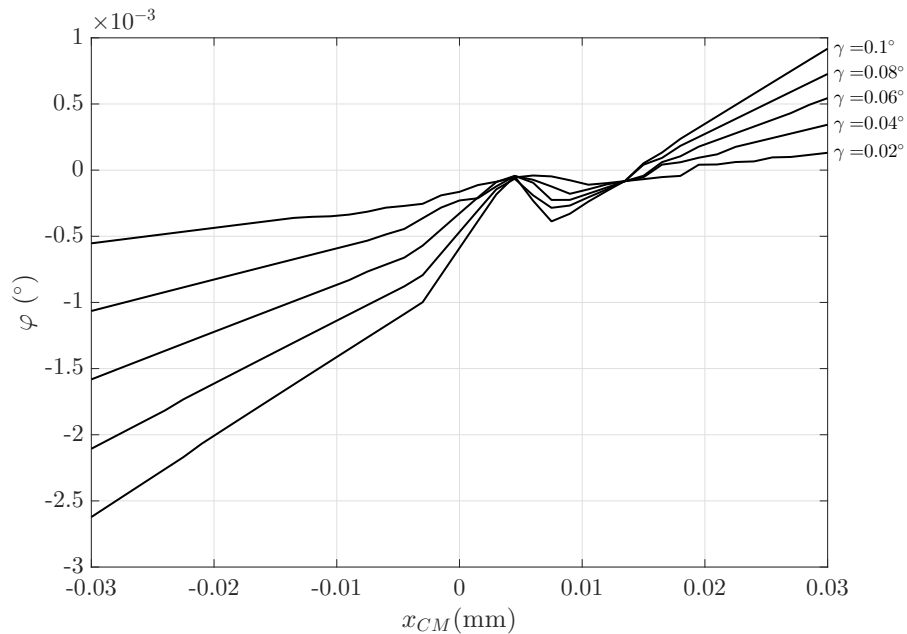


Figure 5.19: Determination approach for \bar{x}_{CM} using FE results for $s = 0$.

Fitting can still compensate for small numerical errors if sufficient number of large steps are used. Taking for example the results from Figure 5.15, the fourth-order polynomial function is presented in Figure 5.20 in the range of -0.06 to 0.06 mm. Solutions at $x_{CM} = 0$ mm are false results produced by numerical errors (see Figure 5.19). Nevertheless, the fitted function still follows the overall behavior of the results, which is almost linear near \bar{x}_{CM} . As such, polynomial fitting represents a more robust approach for determining \bar{x}_{CM} and is used.

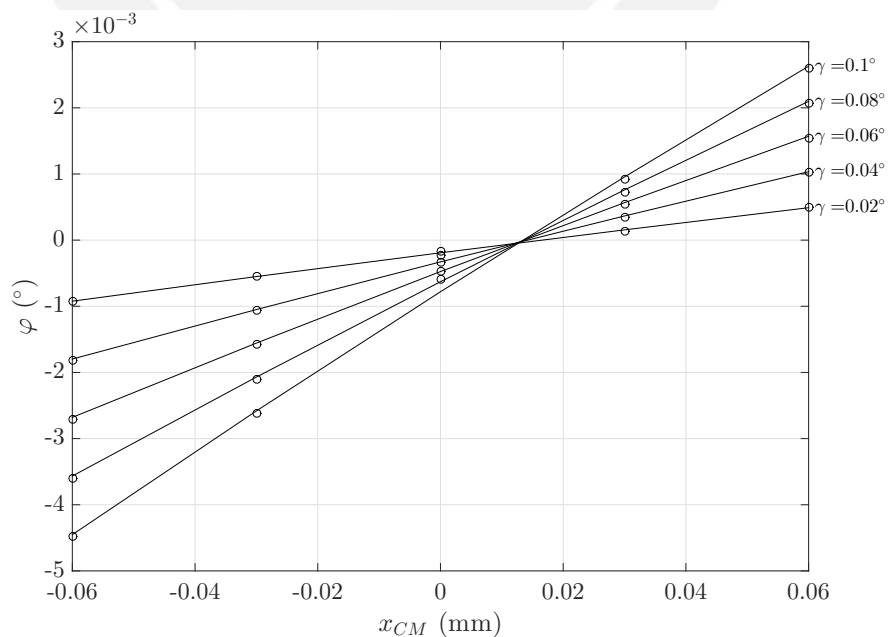


Figure 5.20: Determination approach for \bar{x}_{CM} using FE results for $s = 0$.

Since the position of \bar{x}_{CM} for any value of s is unknown and also due to its proximity to x'_{CM} for large strips, it is required to search for \bar{x}_{CM} from the free end towards the

center of the flexure. That way, it is less likely to find non-convergent points even with large steps. Calculating many points past the region where \bar{x}_{CM} might locate, as in Figure 5.15, would still be risky for longer strips. The least computationally expensive approach would require to look for \bar{x}_{CM} until a negative value of φ is found. Since φ is positive when the mass point is closer to the free end, this approach minimizes the risk of finding non-convergent points and reduces simulation time of additional points. ANSYS Mechanical APDL provides the possibility to use the mentioned approach to look for the value of \bar{x}_{CM} due to its programming capabilities. x_{CM} can be relocated in a single program while calculating φ in an iterative process until a negative value is found. Then, results of φ are fitted with a polynomial function and \bar{x}_{CM} can be approximated.

Mapping numerous x_{CM} close to the free end would be unnecessary and would affect the approximation of the fitted function, especially for large values of s . Since φ seems to converge for values of x_{CM} closer to the free end (see Figure 5.12), polynomial functions cannot correctly fit the results, even when using higher orders. This can be better observed in Figure 5.21, where the searching approach is applied for $s = 1.5$ mm, $m = 1$ kg and $\gamma = 0.02^\circ$. Step size was set as 1/40 of hinge length l and polynomial functions of order n are used for the interpolation.

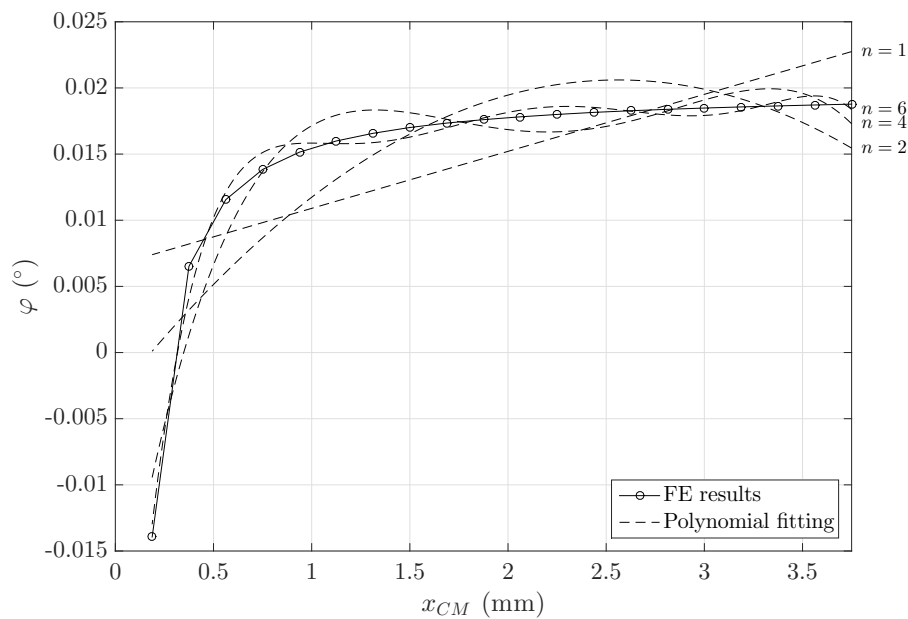


Figure 5.21: Determination approach for \bar{x}_{CM} using FE results for $s = 1.5$ mm, $m = 1$ kg and $\gamma = 0.02^\circ$.

Calculating only one negative value of φ would be risky if such point were too close to $\varphi = 0^\circ$. In that case, the fitted function would produce false results, especially for higher-order polynomials. Higher-order polynomials fit better the individual FE results rather than the overall behavior. If a support point is near the error zone, the function will have a wave-like form as in Figure 5.21. To compensate for these errors, some additional points must be calculated and the order of the polynomial must be kept as low as possible.

Settings

To avoid false fitting, the search for \bar{x}_{CM} should start closer to it, where the behavior is almost linear, with sufficient support points. It is known that \bar{x}_{CM} will be close to the center of the flexure hinge when $s = 0$ mm but it is unknown where it is approximately

located for higher values of s . According to Figure 5.13, as s increases, \bar{x}_{CM} moves closer to the free end. The value of s for the minimum rotational stiffness lies around 0.5 to 1 mm for supported masses between 0.6 to 2 kg using the FE model (see Figure 5.10). When conducting a parametric study, required s for minimum k_φ could either increase or decrease depending on the other parameters. To set a start point to search for \bar{x}_{CM} , its approximate distance from the center for $s = 1.5$ mm is used. Since strips longer than 1 mm would be of no interest, using a distance of 0.45 mm from the center as start point would compensate for parameter variation effects on the location \bar{x}_{CM} . Stepping will be set at $\Delta x_{CM} = 0.05$ mm. Calculations stop when three negative values are found. A polynomial function of second order is used to fit the results. With these settings, an automatic approach has been defined for finding the value of \bar{x}_{CM} in flexure hinges with constant strips. Using this approach, the value of \bar{x}_{CM} for $s = 1.5$ mm amounts to 0.286 mm when $m = 1$ kg and $\gamma = 0.02^\circ$. In comparison to the result obtained from Equation 5.4, the position of the center of mass is closer to the free end when the compliance of the circular region is taken into account.

Parameter effects

Using the mentioned approach, the position of the center of mass for the autostatic state is measured while varying the constructive parameters of the hinge. The considered parameters are as follows:

- supported mass m
- strip length s
- minimum hinge height h
- radius R
- width b
- elastic modulus E

Parameter values will be varied from an initial case when $s = 0$ mm and the value of \bar{x}_{CM} calculated for $\gamma = 0.1^\circ$ and $m = 1$ kg. Results are presented in Appendix J. Variations due to γ were already presented in Figure 5.16. For each parameter, a function of \bar{x}_{CM} is fitted to the FE results. Results show that \bar{x}_{CM} varies almost linearly with parameters m , R , b and E . In fact, the value of \bar{x}_{CM} increases with the compliance, which is proportional to R and inversely proportional to E and b . The FE model does not seem to capture the effect of h due to its small effect and, thus, was not fitted. Approximation errors are most likely the cause. Deviations from the fitted function can be appreciated in each parameter due to the nature of the approximation. Parameter s produces a nonlinear variation of \bar{x}_{CM} that greatly deviates from the analytical results. The behavior of these results difficulties the approximation of an empirical expression, since most expressions of this type are either polynomial or power functions. Correlation between parameters, e.g. h and s , and the fact that giving them zero values results in neither $\bar{x}_{CM} = 0$ or $\bar{x}_{CM} = \infty$ constitute the main limitations for finding a proper function shape.

5.3. Summary

The effect of loading conditions, which were not considered in the previous chapter, were analyzed in the context of the central flexure hinge in monolithic weighing cells. The

existence of a tensile force due to the weights supported by the flexure hinge increases its rotational stiffness. To model this effect, a point mass was added at the end of the circular contour and connected to the FE model through multipoint constraints. Results show an increase of approximately 311 % in the rotational stiffness when supporting a mass of 2 kg. The theory developed by EASTMAN [20] suggests that the rotational stiffness of a flexure strip can be reduced by increasing its length. A certain value of the length can be calculated, for which increasing it further does not produce any significant reduction in stiffness. This minimization of the rotational stiffness was studied by modifying the FE model to include a rectangular strip and by adding the point mass at the end of the contour. The analytical approach, which considers the circular region as rigid, was also used in the calculation. Results showed a stiffer behavior of the analytical approach due to the compliance of the circular region in the FE model. A minimum value of the rotational stiffness can only be obtained in the FE model at a certain strip length for higher supported masses. In the case of the FE model, this length is around 0.5 to 1 mm for masses between 1 and 2 kg. Further increasing the length results in an increase of the stiffness for high masses, in contrast to what analytical results show. This stiffening may occur due to the elongation of the strip, which is not considered in the analytical expression. The elongation generates a displacement of the point mass which produces an increase of the stiffness according to Equation 5.3.

The investigation continues with the consideration of the effect of the ground tilt. The ground tilt produces an additional rotation which can be compensated by adjusting the position of the center of mass of the transmission lever. The autostatic state produces a s-shape of the flexure hinge due to complex loading conditions which was also appreciated in the FE simulations. The study was conducted using the flexure hinges with additional rectangular strips. According to the analytical results, two positions of the center of mass were found of interest: one for the autostatic state and one for instability, for which the FE calculation do not converge. The proximity of both positions with increasing length strip poses as a major problem for FE modeling of this effect. To find the autostatic state for flexure hinges in the range of interest, a searching approach was presented. Robust solutions can only be approximated through function fitting due to numerical errors in the proximity of the autostatic state. Number of support points and step size must also be taken into account. Comparison of FE and analytical results show that the position for the autostatic state of the FE model locates closer to the free end of the hinge. This occurs due to the compliance of the circular region, which is not considered by the analytical expression. The location for the autostatic state was approximated using different parameter values. Results show that the sought position is closer to the free end of the flexure hinge when parameter values favor the increase of compliance.

6. Conclusions

In this work, the mechanical behavior of a thin flexure hinge with circular contour was studied in terms of its rotational stiffness. Flexure hinges constitute a fundamental part of highest precision systems and proper definition of their stiffness is of utmost importance, especially in force metrology. The work was developed throughout five chapters, which deal with different aspects of the mechanical behavior of thin flexure hinges.

In the first chapter, the motivation for this investigation, the studies proposed and structure were presented. The investigation covers three main aspects: proper modeling of an ideal thin flexure hinge, behavior under non-ideal conditions and practical application in weighing cells.

The second chapter focuses on reviewing the investigations to date on the modeling and deformation errors of flexure hinges. Various expressions for the rotational stiffness were found in the literature. Most of them are based on the assumptions of the EULER-BERNOULLI beam theory. Other methods include approximating functions using numerical results from theories like continuum mechanics and nonlinear theory of slender curved rods as well as FEA results. The approaches are based on assumptions that are no longer valid for the geometry of the thinnest flexure hinges. Works by other authors show certain disagreement between common design equations, FEA and experimental results. Additionally, these expressions are limited to the basic constructive parameters. As such, they are not suitable for parametric studies of flexure hinges under non-ideal conditions. Investigations on deformation errors of compliant mechanisms produced by manufacturing deviations have been widely studied. Other effects such as those caused by gravity, material properties and loading conditions on single flexure hinges have not been studied. Inconsistency on independent parameter selection and lack of studies on thin flexure hinges are also limitations that were encountered throughout the literature research.

In the third chapter, a thin semi-circular flexure hinge with a minimum notch height of 50 μm was modeled by means of the finite element method. Dimensions of the flexure hinge were based on values which lie at the limit of presently available manufacturing technology. Material behavior was considered as linear elastic. Requirements for the model were proposed and settings were evaluated to ensure the reliability of the results while keeping computational time to a minimum. A meshing strategy based on partitions connected through multipoint constraints was proposed to reduce element number and distortion due to high aspect ratios. 20-node brick element SOLID186 was used and the total element number including contact elements amounts to 18912. Using the generated model, the rotational stiffness assuming geometric linearity and nonlinearity was calculated. Geometric nonlinearity produces a stiffening effect on the flexure hinge with increasing rotation angle. The FE model shows a behavior around 10% stiffer than design equations based on plane stress assumption. This deviation was evaluated for flexure hinges with minimum heights between 50 to 100 μm . Simulations show that

the 3D-FE model rather complies with the plane strain assumption than with the plane stress assumption while most analytical equations are based on the latter. This occurs due to the width to minimum height ratio b/h . A nonlinear relationship between the rotational stiffness and the width was found, which depends on the distribution of the out-of-plane normal stress. An almost uniform distribution of the out-of-plane stress like in the plane strain state appears as the width gets larger, while limited to the central part of the cross section for small widths. Even for small b/h ratios, such as 10, deviations are still around 3%. The deviation between analytical equations and FE results was found to be dependent only on the b/h and h/R ratios. Other parameters, such as the total height, presented an almost neglectable effect when the full contour is considered, but rapidly increases when it is not. These observations lead to the conclusion that thin flexure hinges, which usually present large aspect ratios, should be modeled considering the width dependency. Models which assume plane stress are no longer valid for large width-minimum height ratios and using the plane strain assumption would be more suitable.

The fourth chapter presents an approach to study flexure hinges under non-ideal conditions. Possible sources of deviation of the stiffness were identified and classified in four groups: geometric deviations, material behavior, loading conditions and other influences. Loading conditions depend on the application case and are studied in the fifth chapter. The model developed in the third chapter was updated to support geometric deviations and calculations were conducted to verify a proper behavior. Geometric parameters deviation show linear and parabolic effects on the rotational stiffness in the specified range of values while gravity produces a sinus-like effect. Using the defined parameters, a sensitivity analysis was conducted. The range of values of the parameters was considered as those attainable with high and conventional accuracy. Gravity effects were considered as those produced by ground tilt, since full space exploration produces false results in the sensitivity measures. Combinations were determined using the Advanced Latin Hypercube Sampling method to approximate a meta-model using linear regression. A linear model was most suitable due to the linear effect produced by most parameters in the range of values. Total effect sensitivity indices show dominance of the minimum height parameter. The elastic modulus appears as the second most influential parameter while effects of other parameters are neglectable and depend on their range of value. Even for high accuracy values, rotational stiffness of the thin flexure hinge can deviate around 13%, in which the minimum hinge height manufacturing errors ($\pm 2.5 \mu\text{m}$) contribute the most. This suggests that manufacturing processes, such as WEDM, which are considered highly accurate, show critical deviations for the precise definition of the stiffness of thin flexure hinges.

Loading conditions are studied in fifth chapter in the context of the application in weighing cells. The flexure hinge which supports the transmission lever in balances is subjected to an additional axial load due to all supported weights. In the usual configuration, the lever is suspended by a flexure hinge and the axial load can almost linearly increase the rotational stiffness up to approximately 311% when 2 kg are supported. To reduce rotational stiffness, a strip is monolithically added to the thinnest region. For that matter, the model previously developed was updated. A strip length around 0.7 to 1 mm was found to be sufficient for reducing the stiffness to a minimum value for supported masses above 1 kg. However, a fixed value that minimizes it above a certain supported mass value, as the analytical approach suggests, could not be found. A stiffening effect could be observed for high masses and long strips due to the elongation of the flexure. This means that a specific load values correspond to a specific required length for a minimized

stiffness of the design. The effect of weight force orientation deviation due to ground tilt was studied as well. According to the theory developed by QUINN ET AL., the center of mass of the supported weight can be adjusted to reduce the tilt sensitivity of a balance. Aside from the position for zero tilt sensitivity, a point of instability also exists, which is in closer proximity to the sought tilt insensitive point for longer strips. An approach was defined for locating the position of the center of mass for the autostatic state for the hinges in the range of interest. Based on this approach, the effect of the parameters on the location of this point were studied.

In summary, the following studies have been conducted in this work:

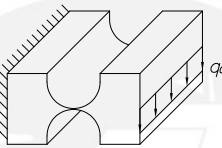
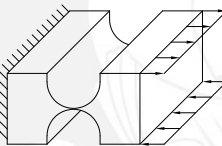
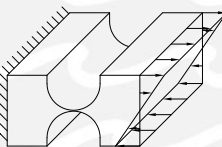
- A finite element model was developed to validate the assumptions of analytical models. The analytical models based on the plane stress assumptions revealed to be inappropriate for an accurate description of the behavior of thin flexure hinges due to a width dependency. The plane strain assumption is proven to be suitable for high width to minimal notch height ratios.
- The same model was updated for analyzing geometric deviations of the hinges due to manufacturing deviations. Rotational stiffness deviates up to 13 % for the presumed parameter ranges. Deviations can be attributed mostly to the manufacturing errors of the minimum hinge height. Common processes such as WEDM have been found inaccurate for really thin geometries.
- Axial loads, like supported weights in balances, produce a significant effect on the rotational stiffness. Values can increase up to 311 % in common weighing applications. The rotational stiffness can be reduced through adding strip-like regions but stiffening effects can also be encountered above certain lengths. Ground tilt produces undesired rotation which can be compensated by adjusting the center of mass of the supported system. The position for the autostatic state displaces towards the free end of the flexure when compliance is increased.

This work is concentrated on flexure hinges of circular contour. Proof of analytical expressions is yet to be done for flexure hinges of other contours and results are still to be compared to experimental results. Expressions that consider the width dependency can be approximated using 3D finite element models for different geometries. Nonlinear material behavior is also of importance in the actual performance of very thin hinges. The precondition for a meaningful study of these effects is the deep knowledge of material anelastic properties. Effects produced by material imperfections, i.e. at the level of microstructure, can only be considered by complex modeling, which would require a study on their own and must be supported by experimentation. For simpler design of weighing cells, empirical equations that can quantify the rotational stiffness under beam-column conditions are required to be derived for other geometries. In the same way, expressions for locating the position of the center of mass still are to be developed. Other various phenomena that affect the actual performance of flexure hinges in weighing cells, e.g. lateral vibrations, have not been thoroughly studied. All these topics could prove necessary for optimizing the performance of weighing cells and simplifying the design of such systems.

Appendix

A. Loading application

Table A.1: Loading conditions

| Load type | Representation | Parameter | Value |
|------------------|---|-----------|-------------------|
| Shear force |  | q_0 | $\frac{2M}{bL}$ |
| Couple of forces |  | n_0 | $\frac{M}{bH}$ |
| Surface force |  | p_0 | $\frac{6M}{bH^2}$ |

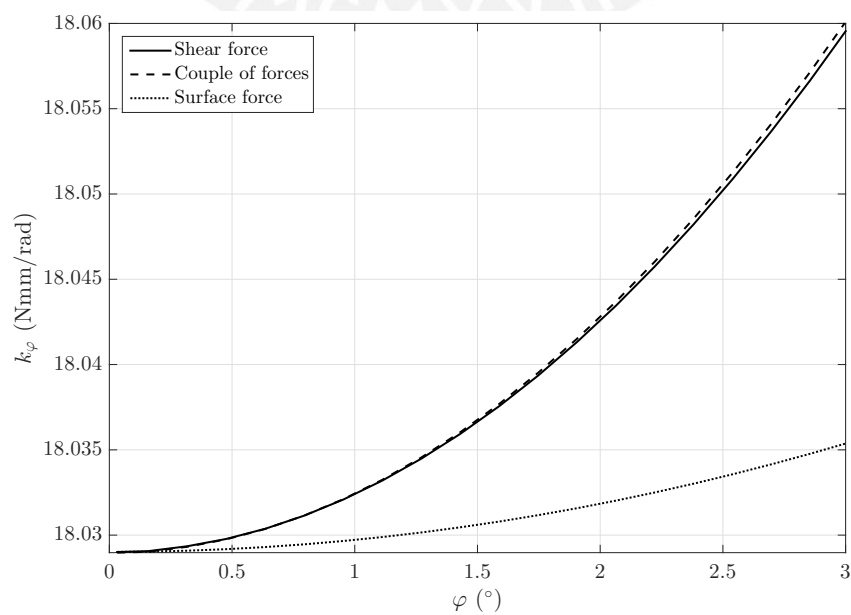


Figure A.1: Rotational stiffness k_φ for different load cases.

B. Mesh sensitivity analysis

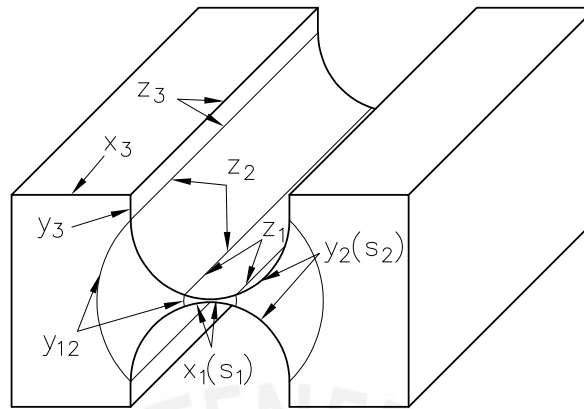


Figure B.1: Local refinements

Table B.1: Mesh parameters.

| Parameter | Description | Value |
|-----------|---|--------------------|
| x_1 | Elements along the length of zone 1 | 10 – 100 |
| x_2 | Elements along the length of zone 2 | 3 – 30 |
| x_3 | Elements along the length of zone 3 | 1 – 10 |
| y_{12} | Elements along the height of zones 1 and 2 | 2 – 10 |
| y_3 | Additional elements along the height of zone 3 | 1 – 5 |
| s_1 | Transition of elements along the length of zone 1 towards the center of the hinge | 0 – 1 |
| s_2 | Transition of elements along the length of zone 2 towards the center of the hinge | 0 – 1 |
| AR | Limiting aspect ratio | 5 – 10 |
| z_1 | Elements along the width of zone 1 | by_{12}/hAR |
| z_2 | Elements along the width of zone 2 | $by_{12}/h'AR$ |
| z_3 | Elements along the width of zone 3 | $by_{12}/(h + 2R)$ |

Considerations for the analysis:

- Sampling method: Advanced Latin Hypercube Sampling.
- Sensitivity analysis method: Metamodel of Optimal Prognosis.
- Applied bending moment $M = 1$ Nmm.
- Geometric linearity assumed.

Table B.2: Sensitivity indices.

| Parameter | $\text{COP}_{\sigma_{x,max}}$ (%) | $\mathbf{S}_{\sigma_{x,max}}$ | COP_{nodes} (%) | \mathbf{S}_{nodes} |
|-----------|--------------------------------------|-------------------------------|-----------------------------|----------------------|
| Model | 88.67 | 1.000 | 98.84 | 1.000 |
| x_1 | 75.06 | 0.847 | 32.15 | 0.325 |
| x_2 | 6.63 | 0.075 | 7.99 | 0.081 |
| x_3 | 0.00 | 0.000 | 0.39 | 0.004 |
| y_{12} | 4.24 | 0.048 | 66.16 | 0.669 |
| y_3 | 0.00 | 0.000 | 0.26 | 0.003 |
| s_1 | 22.07 | 0.249 | 0.32 | 0.003 |
| s_2 | 0.00 | 0.000 | 0.23 | 0.002 |
| AR | 5.63 | 0.064 | 11.34 | 0.115 |

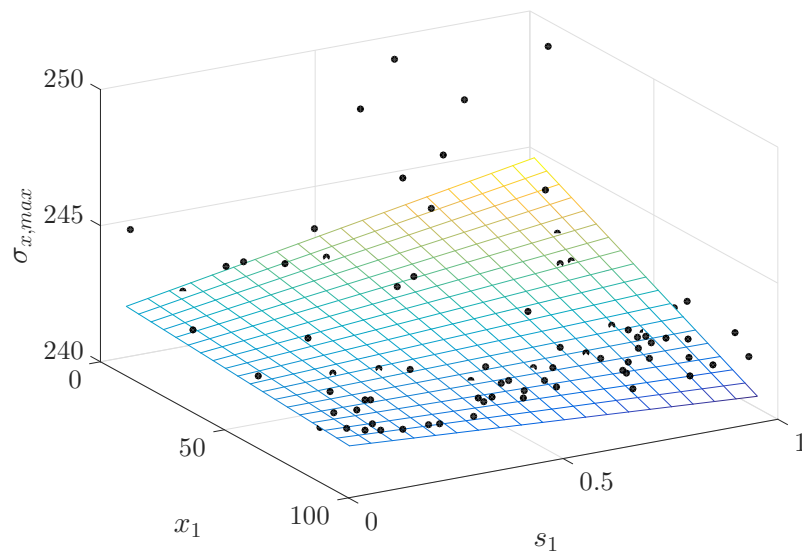
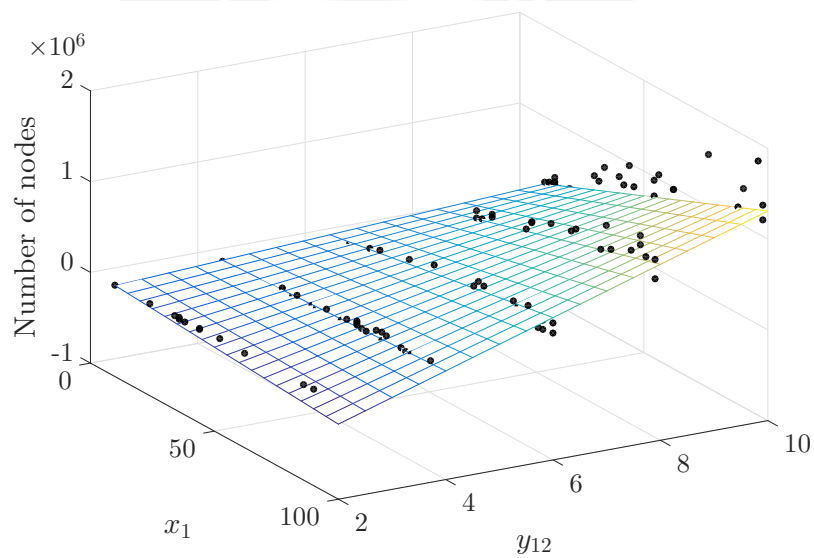
Figure B.2: Linear regression model for $\sigma_{x,max}$.

Figure B.3: Linear regression model for number of nodes.

C. Circular contour flexure hinge design equations

PAROS AND WEISBORD (1965), full equation [62]:

$$k_\varphi = \frac{2EbR^2}{3}(2\xi + \xi^2) \left\{ \left[\frac{1 + \xi}{\zeta^2} + \frac{3 + 2\xi + \xi^2}{\zeta(2\xi + \xi^2)} \right] \sqrt{1 - (1 + \xi - \zeta)^2} + \left[\frac{6(1 + \xi)}{(2\xi + \xi^2)^{3/2}} \right] \tan^{-1} \left(\sqrt{\frac{2 + \xi}{\xi} \frac{(\zeta - \xi)}{\sqrt{1 - (1 + \xi - \zeta)^2}}} \right) \right\}^{-1} \quad (\text{C.1})$$

with $\xi = h/2R$ and $\zeta = 1 + \xi$.

PAROS AND WEISBORD (1965), simplified equation [62]:

$$k_\varphi = \frac{2Ebh^{2.5}}{9\pi\sqrt{R}} \quad (\text{C.2})$$

WU AND ZHOU (2002) [91]:

$$k_\varphi = \frac{EbR^2}{12} \left[\frac{2\lambda^3(6\lambda^2 + 4\lambda + 1)}{(2\lambda + 1)(4\lambda + 1)^2} + \frac{12\lambda^4(2\lambda + 1)}{(4\lambda + 1)^{5/2}} \tan^{-1}(\sqrt{4\lambda + 1}) \right]^{-1} \quad (\text{C.3})$$

with $\lambda = R/h$.

TSEYTLIN (2002) [88]:

For thin hinges, $h/R \leq 0.07$:

$$k_\varphi = \frac{Ebh^2}{16} \left\{ 1 + \left[1 + 0.1986 \left(\frac{2R}{h} \right) \right]^{1/2} \right\}^{-1} \quad (\text{C.4})$$

LOBONTIU (2003) [50]:

$$k_\varphi = \frac{Ebh^3(2R + h)(4R + h)^3}{24R} \left[h(4R + h)(6R^2 + 4Rh + h^2) + 6R(2R + h)^2 \sqrt{h(4R + h)} \tan^{-1} \left(\sqrt{1 + \frac{4R}{h}} \right) \right]^{-1} \quad (\text{C.5})$$

LINß ET AL. (2017) [47]:

$$k_\varphi = k_{M1} E \beta_b \beta_l^{(-k_{M2})} \beta_h^{(2+k_{M2})} H^3 \quad (\text{C.6})$$

with $\beta_b = b/H$, $\beta_l = l/H$, $\beta_h = h/H$.

For circular contours, $k_{M1} = 107.9 \times 10^{-3}$ and $k_{M2} = 0.52$.

D. Bending in plane strain

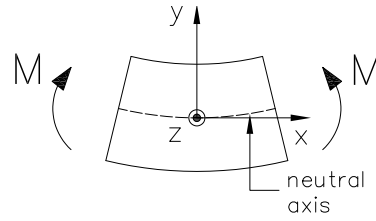


Figure D.1: Pure bending of differential element.

If the dimension in y -direction is small and no pressure loads are applied, the stress $\sigma_y = 0$ can be assumed. Then, according to Hooke's law [85], the strains result:

$$\begin{aligned}\varepsilon_x &= \frac{1}{E}(\sigma_x - \nu\sigma_z) \\ \varepsilon_z &= \frac{1}{E}(\sigma_z - \nu\sigma_x)\end{aligned}$$

When a plane strain state is assumed, $\varepsilon_z = 0$. Then:

$$\begin{aligned}\sigma_z &= \nu\sigma_x \\ \varepsilon_x &= \frac{1}{E}(\sigma_x - \nu^2\sigma_x)\end{aligned}$$

Substituting σ_x by the equation of bending stress:

$$\begin{aligned}\sigma_x &= \frac{My}{I_z} \\ \varepsilon_x &= \frac{1}{E}(1 - \nu^2)\frac{My}{I_z}\end{aligned}\tag{D.1}$$

where I_z is the moment of inertia relative to z . By the definition of a bending beam:

$$\varepsilon_x = \kappa y\tag{D.2}$$

where κ is the curvature of the beam. Finally, equating Equation D.1 and Equation D.2:

$$\kappa = \frac{M}{EI_z}(1 - \nu^2)$$

Results in the bending differential equation in plane strain.

$$\frac{d^2w(x)}{dx^2}_{p.strain} = \frac{M}{EI_z}(1 - \nu^2)\tag{D.3}$$

where $D_{p.strain}$ is the flexural rigidity for plane strain:

$$D_{p.strain} = \frac{1}{1 - \nu^2}EI_z = \frac{1}{1 - \nu^2}D_{p.stress}$$

E. Model behavior

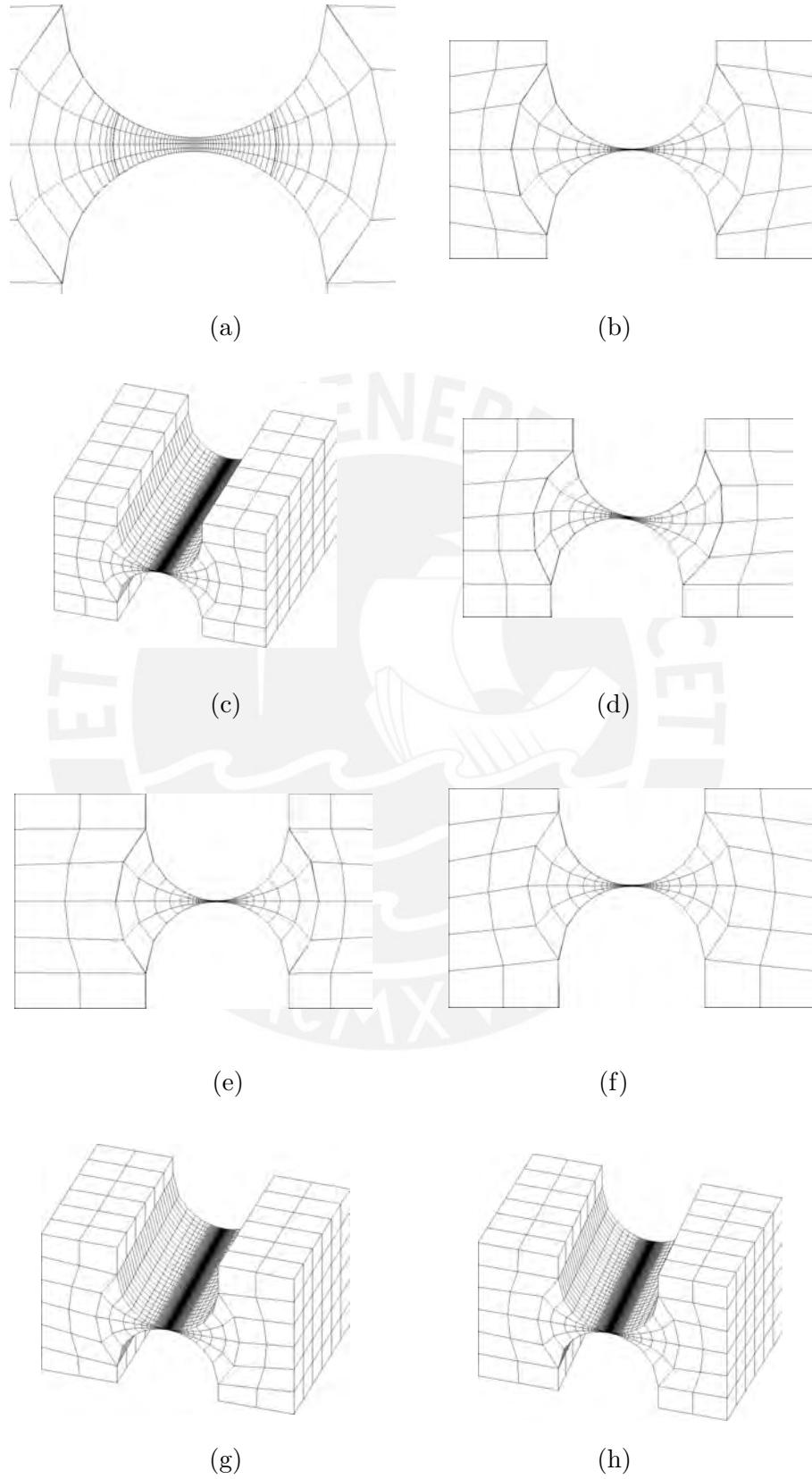
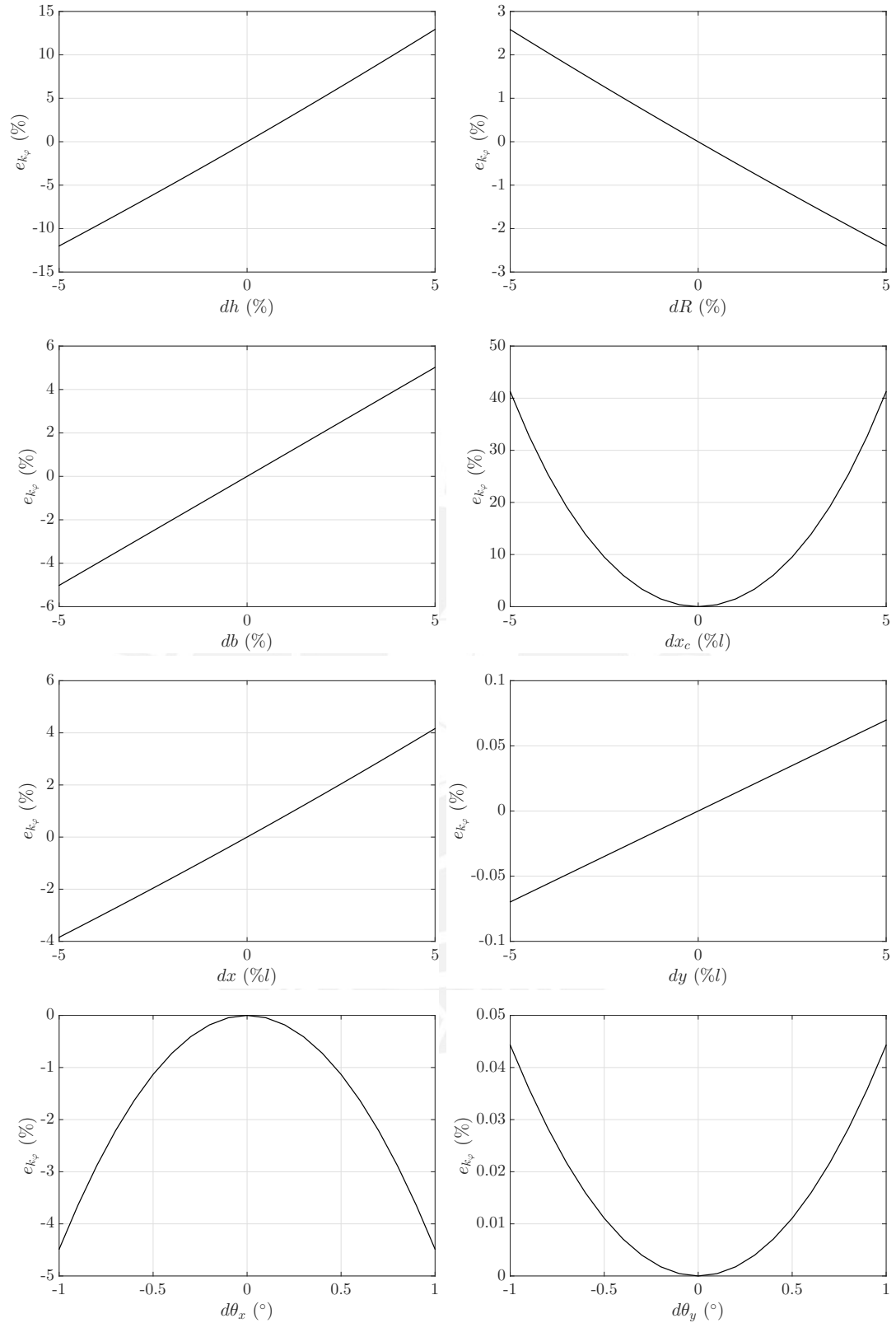


Figure E.1: Mesh adapting to non-ideal geometries. (a) dh ; (b) dR ; (c) db ; (d) dx_c ; (e) dx ; (f) dy ; (g) $d\theta_x$; (h) $d\theta_y$. Representations are exaggerated for better visualization.

Figure E.2: Deviation of k_φ due to geometric deviations.

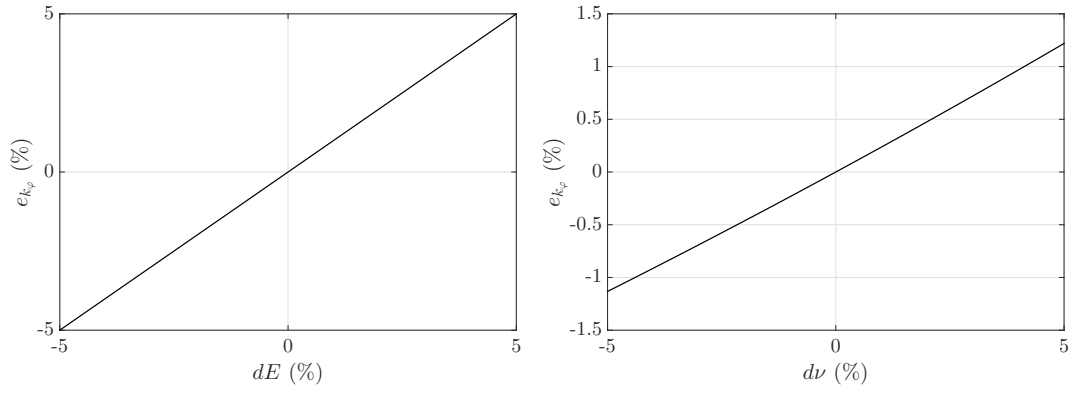


Figure E.3: Deviation of k_φ due to material properties deviations.

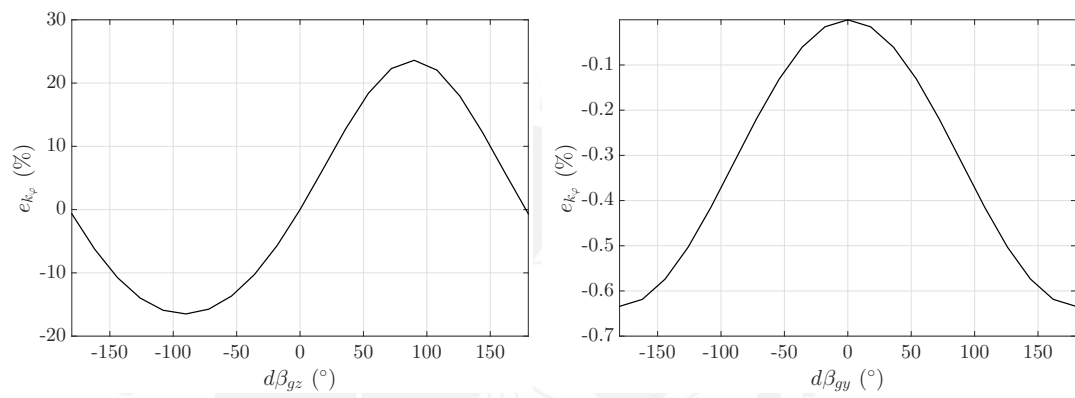


Figure E.4: Deviation of k_φ due to gravity orientation deviations.

F. Sensitivity measures

Derivatives

The most straightforward approach for calculating measures is partial derivative-based. Indeed the partial derivative of an output Y with respect to an input X_i can be thought as a mathematical definition of the sensitivity of Y versus X_i [71]. However, some problems may be encountered with this approach. Since this study is based on numerical calculations using FEM, the output Y , which corresponds to the rotational stiffness k_φ , is not described as a function. Then, partial derivatives need to be calculated in a certain point of the input space, which is not trustworthy. Model nonlinearity and parameter interactions cannot be captured by this measure either.

$$S_i = \frac{\partial Y}{\partial X_i} \quad (\text{F.1})$$

Sigma-normalized derivatives

A more trustworthy approach is to normalize the derivatives using the input and output standard deviations σ_{X_i} and σ_Y . This way, the statistical distribution of each input is included into the measure calculation so the space exploration problem is reduced. Nevertheless, interactions and nonlinearity effects cannot be captured.

$$S_i = \frac{\sigma_{X_i} \partial Y}{\sigma_Y \partial X_i} \quad (\text{F.2})$$

Standardized regression coefficients

A solution for studies based on numerical calculations is metamodeling, in which the simulation model is approximated by a simpler statistically fit function that predicts the output based on the parameter values [71]. A common metamodeling approach is, for example, linear regression using simulation results as support points. In this case, sensitivity measures would be based on the regression coefficients \hat{b}_{X_i} , which are determined by least-square computation. Regression coefficients are often normalized to $\hat{\beta}_{X_i}$, as was done Equation F.2, and sensitivity measures equal $\hat{\beta}_{X_i}^2$ so that their sum would equal 1. This approach can still be used for models of low nonlinearity since $\hat{\beta}_{X_i}$ are multidimensionally averaged measures.

$$S_i = \hat{\beta}_{X_i}^2 = \left(\frac{\sigma_{X_i} \hat{b}_{X_i}}{\sigma_Y} \right)^2 \quad (\text{F.3})$$

First-order sensitivity indices

An approach for models of any degree of linearity are the variance-based methods. Variance methods work by decomposing the variance of the output Y into fractions attributed to the inputs X_i . This is done by using conditional variances $V_{X_{\sim i}}(Y|X_i)$, which are the variances of Y calculated while fixing a parameter X_i to a certain value. It can be inferred that the smaller $V_{X_{\sim i}}(Y|X_i)$, the greater the influence from X_i . To avoid dependencies on a selected fixed value, the average is used $E_{X_i}(V_{X_{\sim i}}(Y|X_i))$ for different fixed values. Since $E_{X_i}(V_{X_{\sim i}}(Y|X_i))$ is the effect caused by all parameters but X_i , the sensitivity index can be defined as:

$$S_i = 1 - \frac{E_{X_i}(V_{X_{\sim i}}(Y|X_i))}{V(Y)} = \frac{V_{X_i}(E_{X_{\sim i}}(Y|X_i))}{V(Y)} \quad (\text{F.4})$$

This measure cannot capture interactions between parameters. In fact, when used in highly linear models it equals $\hat{\beta}_{X_i}^2$. To capture interactions, the same approach could be used by fixing multiple parameters at the same time, but this is not practical.

Total effect sensitivity indices

It can be demonstrated that the variance of Y produced by fixing a parameter X_i to a certain value includes all terms of any order that do not include that fixed parameter X_i [71]. As such, it can capture interactions between parameter of any order. Then, since all sensitivity measures should sum 1, the total effect can be defined as:

$$S_i = 1 - \frac{V(E(Y|X_{\sim i}))}{V(Y)} = \frac{E(V(Y|X_{\sim i}))}{V(Y)} \quad (\text{F.5})$$



G. Sampling methods

Koshal design

In One-at-a-time (OAT) sampling methods, the number of samples is greatly decreased by changing the value of only one parameter between consecutive simulations. In its most basic form, also known as Koshal design for first-order models [60], every variable take two values, 0 or 1 (normalized), so that in the $n + 1$ -th run, variable X_n has value 1 and the others 0, meaning that the number of simulations is $k + 1$. In the first run, all variables have value 0. Another methods consider that in the $n + 1$ -th run, variables X_1 to X_n have value 1 and the others 0, or, in an expanded form, include additional k simulations where variables are returned to value 0 in the same way [71]. These methods demonstrate that if any change occurs in consecutive runs, that means any variation between Y_i and Y_{i+1} , it is only caused by the change in parameter X_i . The Koshal design was originally used for a second-order model, where parameters have three levels (values 0, 1 and 2) and interactions between them are also considered [41].

D-Optimal design

Optimal designs are methods based on optimization. A certain optimality criteria and a model to be fit, either linear or quadratic, are used through an algorithm for generating the experiment. A D-Optimal design is one that is based on the D-optimality criteria, which maximizes the determinant of the information matrix $\mathbf{X}'\mathbf{X}$, minimizing the variance of the regression coefficients of the model [3]. This approach is used when classical designs, like factorial designs, require a great number of samples. The algorithm chooses an optimal candidate set of possible treatment runs based on the mentioned criteria before calculations. However, matrices are not truly orthogonal [3].

Factorial design

Stratified sampling methods divide the sample space in various subspaces or strata. Then, equal number of sample points are selected in each strata. Those points can be selected either randomly or to lie at particular locations in the subspace. This ensures the existence of sample points in all divisions of the hypercube [71]. Full factorial designs are a type of stratified sampling method which divide assign each input parameters a number of levels n , usually 2 or 3, and all possible combinations between all levels of all parameters are sampled. Due to that matter, this approach is computationally demanding but information matrices are orthogonal [3].

Plain Monte Carlo

In this approach, input values of the variable X_i come from a pseudo-random number generator [86]. This way data points are scattered all over the sample space, which could be ideal at first view. However, uncontrolled scattering produces non-uniform density of points. Two problems arise due to this matter: clusters and gaps [71]. Clusters are concentrations of points in certain regions of the space while gaps are regions without points at all. To reduce such problems, large number of samples are required.

Latin Hypercube Sampling

This method ensures that all regions of the space are sampled but also seeks that each input variable X_i has a value in all portions of its distribution. In a first approach, the range of known values of an input variable X_i is divided in n intervals of equal marginal probability $1/n$ and one value per interval is assigned [55]. Then, values of each variable are ordered randomly. This way, the output Y is dominated by few components of \mathbf{X} , but undesired correlation between some variables can be observed. An update of Latin Hypercube Sampling (LHS) to reduce the randomly introduced correlation is proposed by FLORIAN [24]. In his work, the rank numbers, which are values of i used to generate the samples, are arranged in the same way as in a pseudo-ordering matrix whose correlation matrix is very close to the identity matrix, thus, reducing it. In the mentioned methods, values were chosen from the cumulative distribution function of each variable. This approach produces samples with a mean close to the desired one but different variances. Such problems can be corrected with increased number of samples. A more accurate approach was proposed by HUNTINGTON [35]. He proposes the use of the random mean of each interval as sample value. This way, errors in the mean are eliminated and errors in the variance are greatly decreased. Another contribution in this work includes an iterative optimized ordering scheme. The procedure computes the change in the error in correlation coefficients between the n -th column and each of the previous ones of an initial unordered sample matrix if a pair of samples of that n -th variable is switched. The pair of samples with the greatest reduction are then switched, and the process is repeated in an iterative way as no further improvement is possible or the coefficients are within the expected accuracy. Then the procedure is repeated for each variable. This approach is known as the Advanced Latin Hypercube Sampling (A-LHS) method.

H. Stiffness deviations

Case 1: High accuracy.

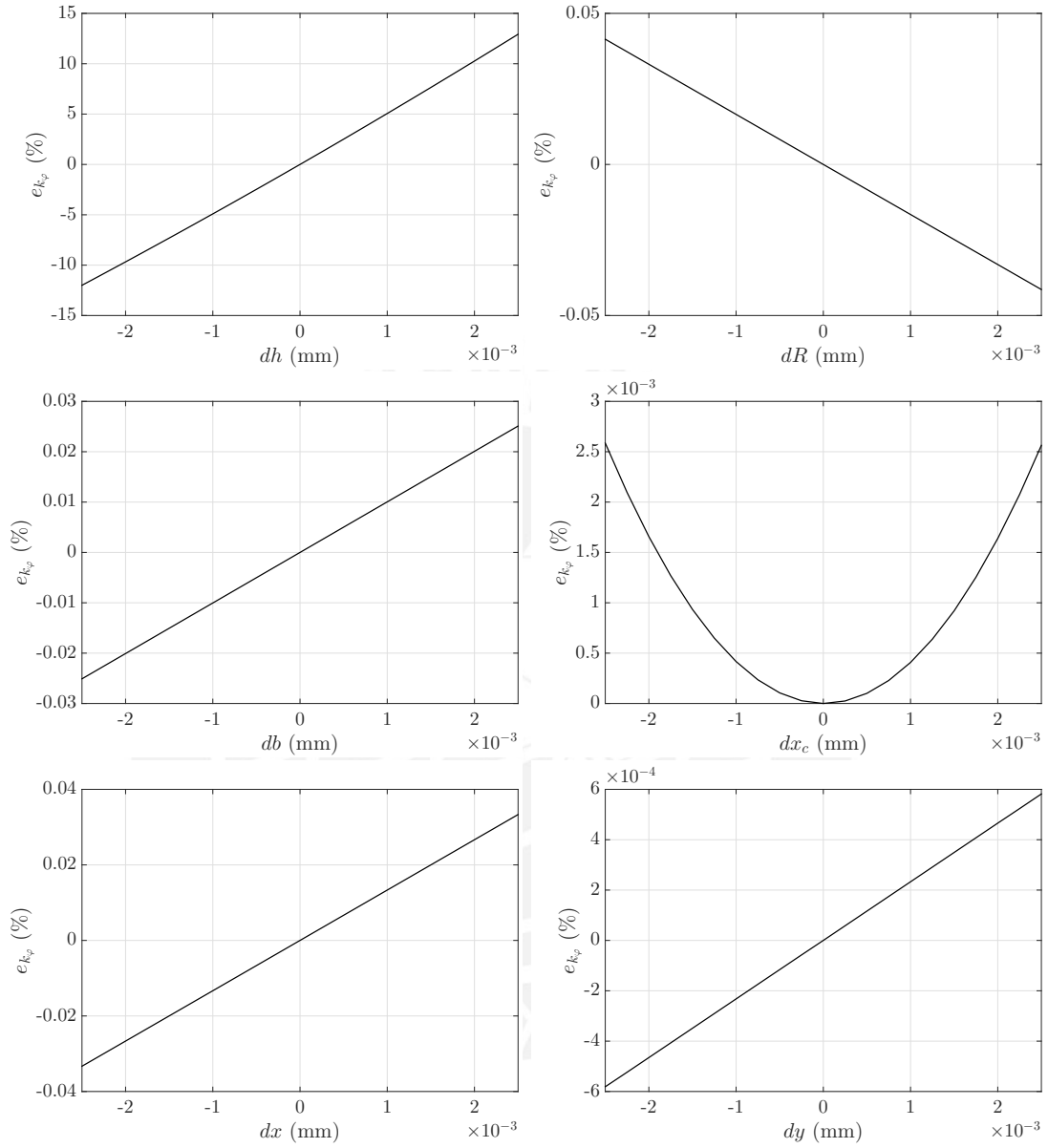
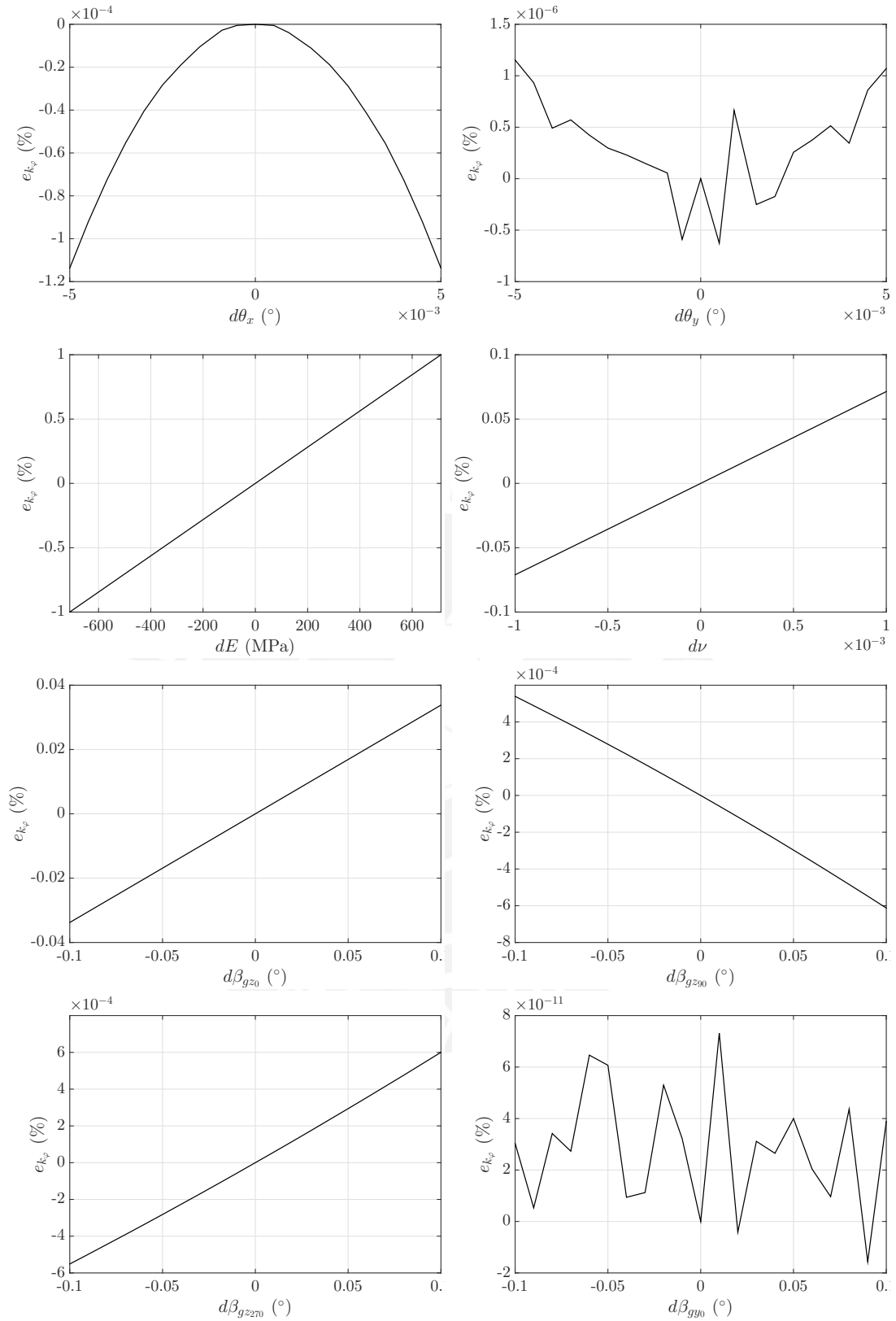
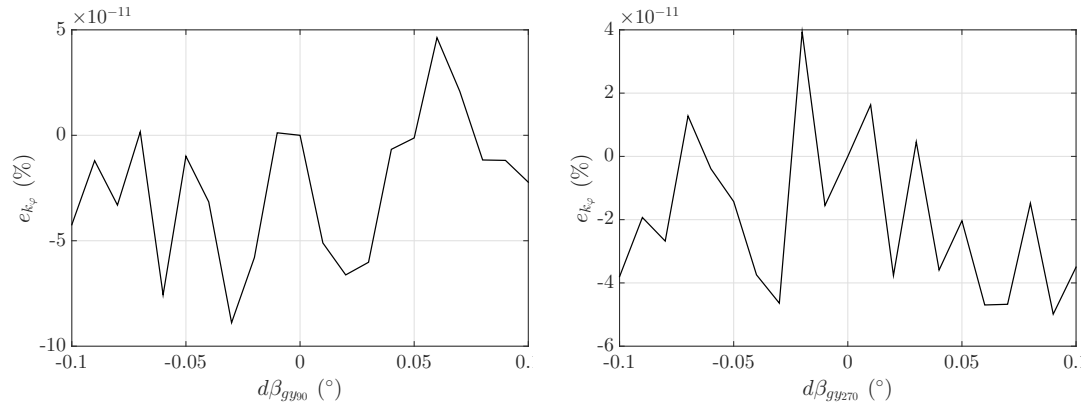
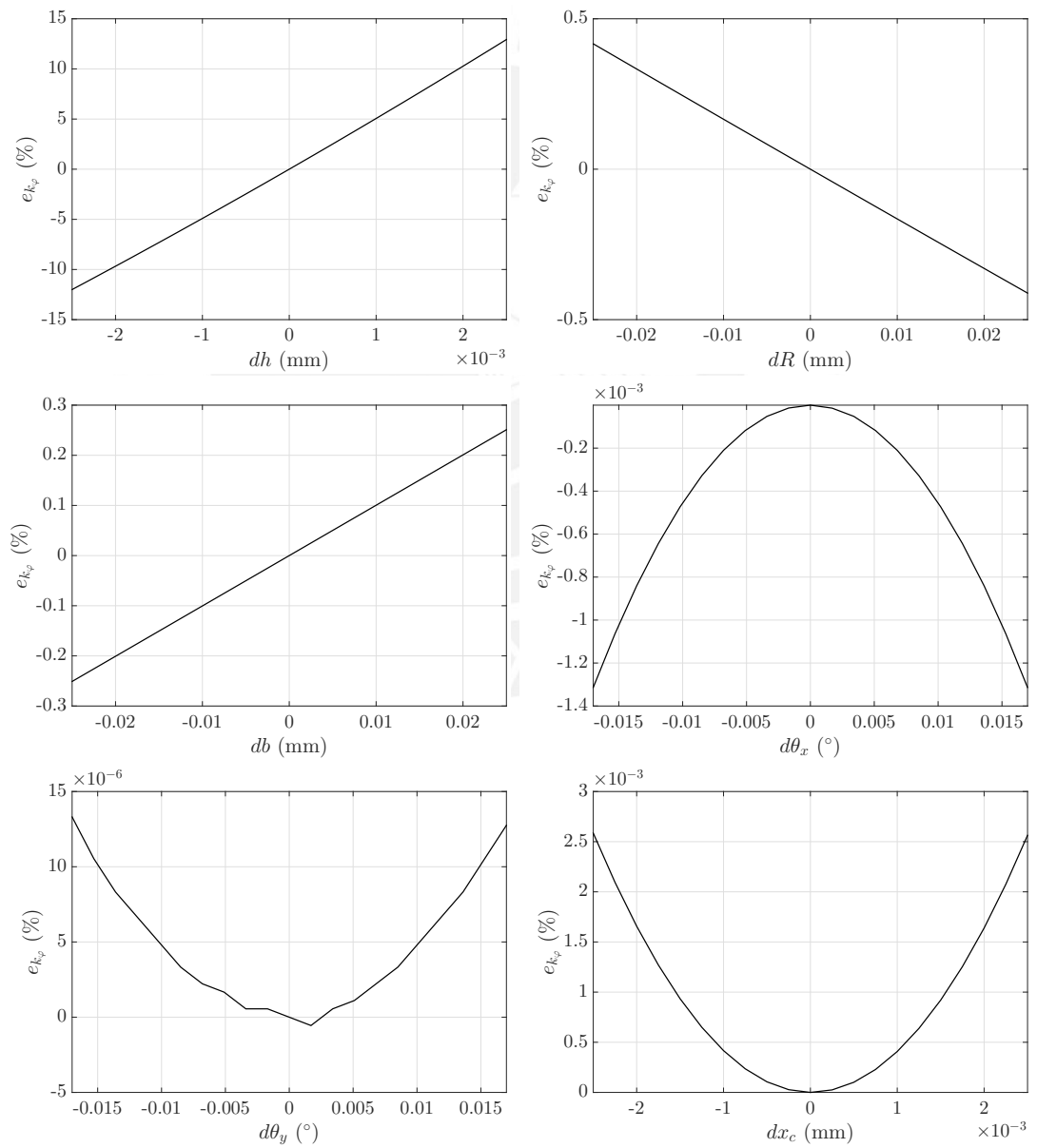
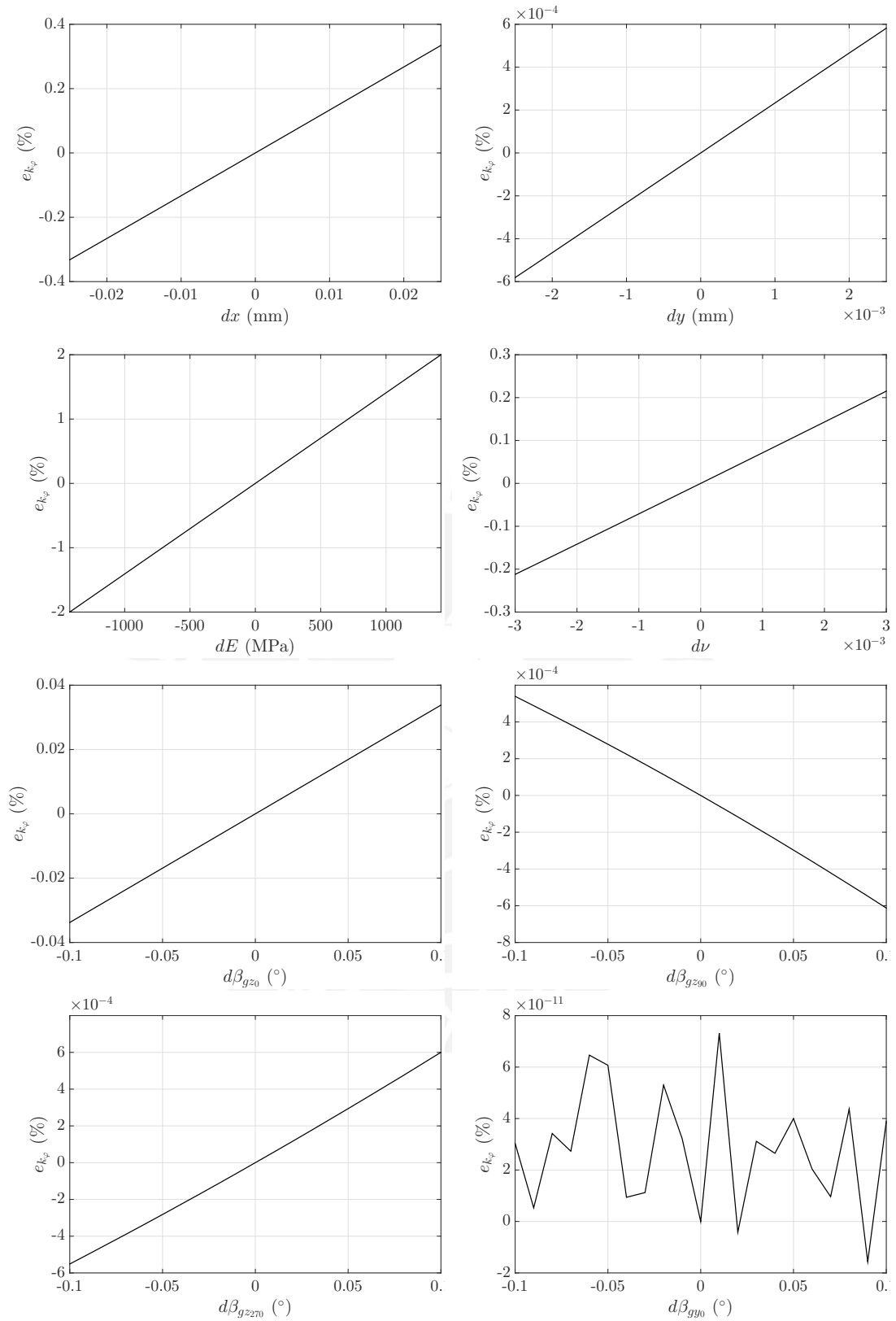


Figure H.1: Deviation of k_φ for different parameter deviations.

Figure H.1 (Cont.): Deviation of k_φ for different parameter deviations.

Figure H.1 (Cont.): Deviation of k_φ for different parameter deviations.**Case 2: Conventional accuracy.**Figure H.2: Deviation of k_φ for different parameter deviations.

Figure H.2 (Cont.): Deviation of k_φ for different parameter deviations.

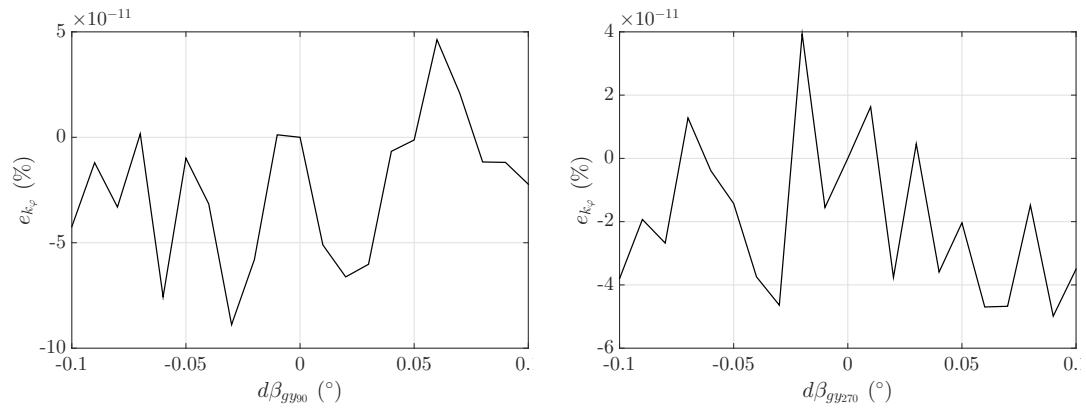


Figure H.2 (Cont.): Deviation of k_φ for different parameter deviations.



I. Gravity effect in sensitivity measures.

Table I.1: Sensitivity indices for $d\beta_{gz} = \pm 180^\circ$.

| Parameter | CoP _{high} (%) | S _{high} | CoP _{conv} (%) | S _{conv} |
|---------------|-------------------------|-------------------|-------------------------|-------------------|
| Model | 41.87 | 1.000 | 24.20 | 1.000 |
| dh | 17.70 | 0.423 | 18.86 | 0.779 |
| dR | 5.25 | 0.130 | 1.10 | 0.045 |
| db | 7.92 | 0.172 | 1.05 | 0.043 |
| dx_c | 5.73 | 0.137 | 0.44 | 0.018 |
| dx | 7.38 | 0.176 | 0.56 | 0.023 |
| dy | 7.09 | 0.169 | 0.76 | 0.031 |
| $d\theta_x$ | 8.59 | 0.205 | 1.00 | 0.041 |
| $d\theta_y$ | – | – | 0.43 | 0.018 |
| dE | 8.72 | 0.208 | 0.61 | 0.025 |
| $d\nu$ | 7.80 | 0.186 | 1.37 | 0.057 |
| $d\beta_{gz}$ | 8.70 | 0.208 | 0.84 | 0.035 |
| $d\beta_{gy}$ | 7.51 | 0.179 | 0.12 | 0.005 |

J. Center of mass position for autostatic state.

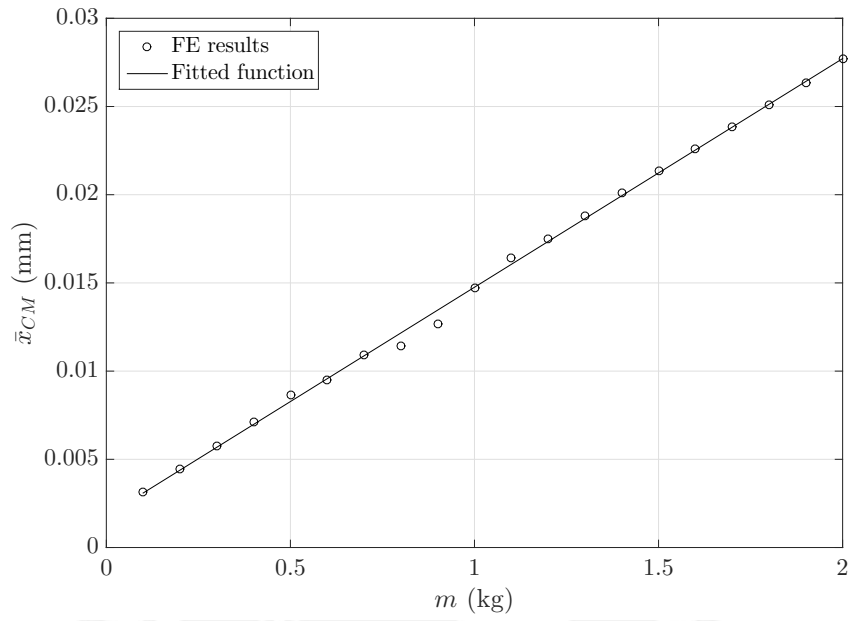


Figure J.1: Variation of \bar{x}_{CM} due to supported mass m .

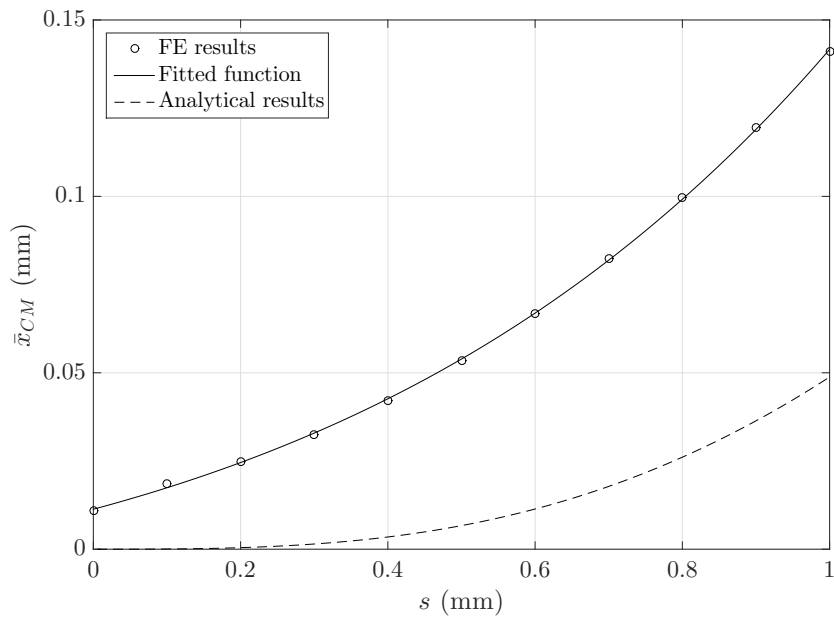


Figure J.2: Variation of \bar{x}_{CM} due to strip length s .

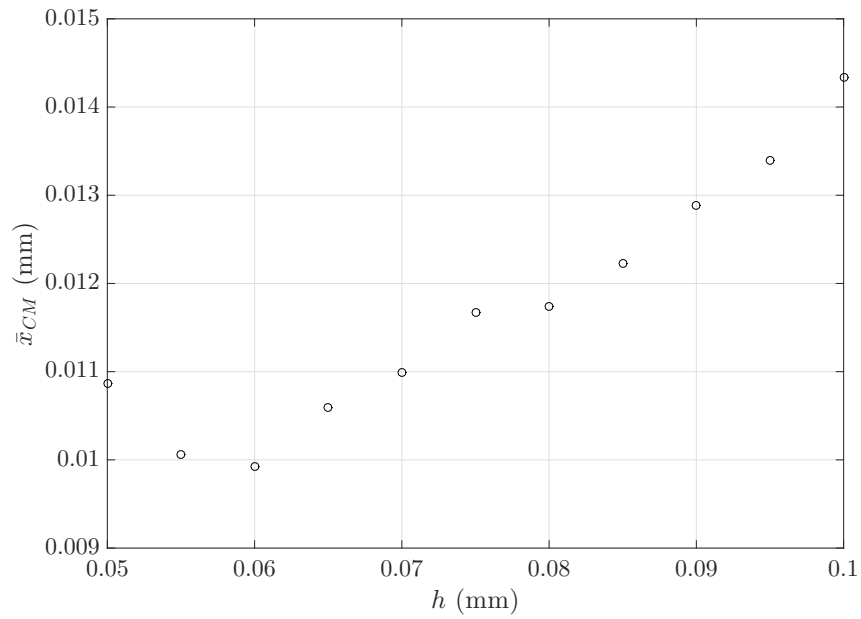


Figure J.3: Variation of \bar{x}_{CM} due to minimum height hinge h .

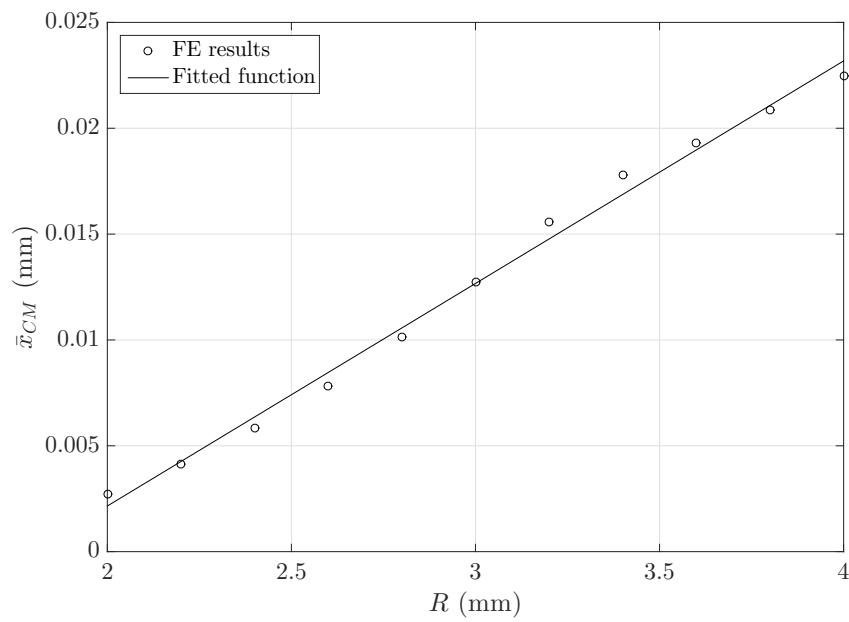


Figure J.4: Variation of \bar{x}_{CM} due to radius R .

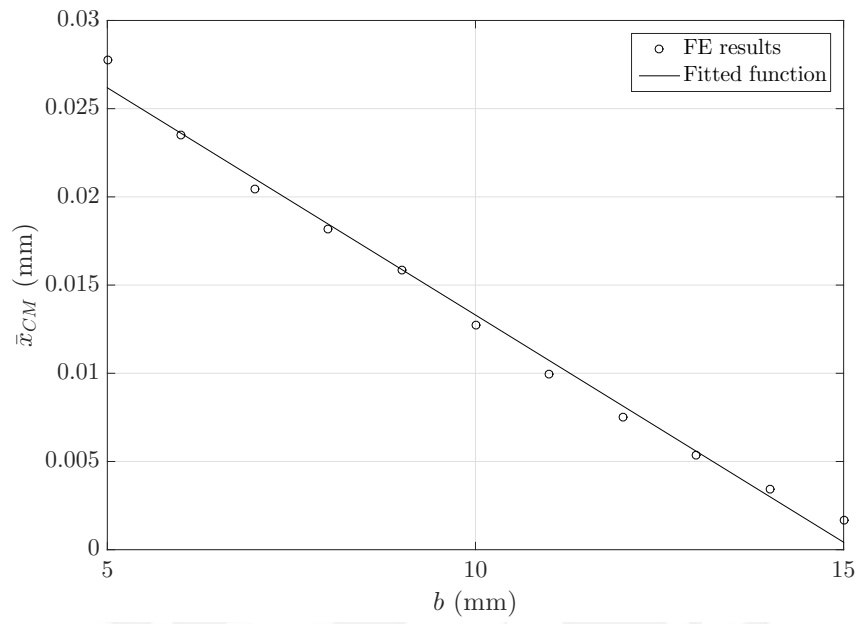


Figure J.5: Variation of \bar{x}_{CM} due to width b .

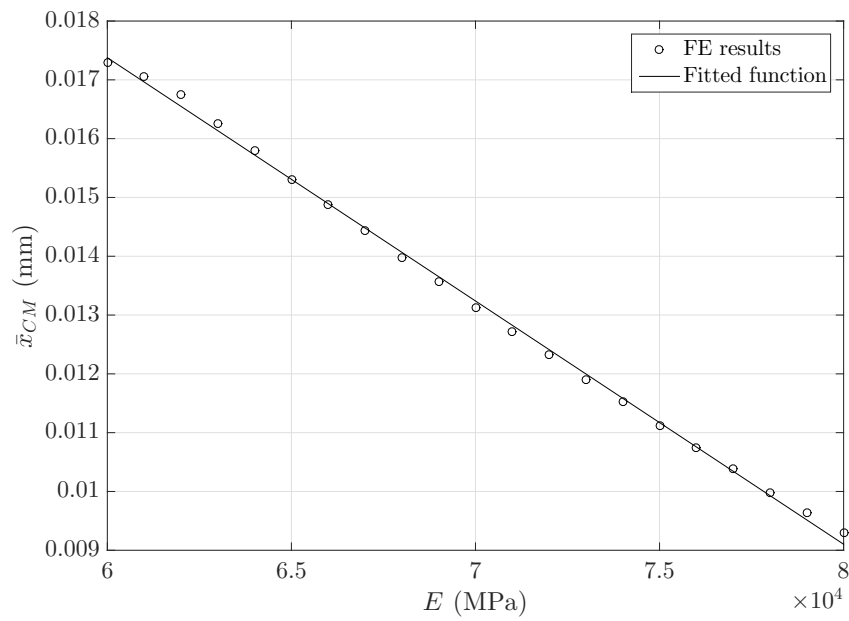


Figure J.6: Variation of \bar{x}_{CM} due to elastic modulus E .

Bibliography

- [1] ANSYS, INC. *ANSYS Mechanical APDL Basic Analysis Guide*. Pennsylvania, 2013.
- [2] ANSYS, INC. *ANSYS Mechanical APDL Contact Technology Guide*. Pennsylvania, 2013.
- [3] ATKINSON, A. C., DONEV, A. N., AND TOBIAS, R. D. *Optimum experimental designs, with SAS*, vol. 34 of *Oxford statistical science series*. Oxford University Press, Oxford, 2007.
- [4] AWTAR, S. *Synthesis and Analysis of Parallel Kinematic XY Flexure Mechanisms*. PhD thesis, Massachusetts Institute of Technology, 2004.
- [5] AWTAR, S., AND SEN, S. A Generalized Constraint Model for Two-Dimensional Beam Flexures: Nonlinear Load-Displacement Formulation. *Journal of Mechanical Design* 132, 8 (2010), 081008–1–11.
- [6] BACHER, J.-P., JOSEPH, C., AND CLAVEL, R. Flexures for high precision robotics. *Industrial Robot: An International Journal* 29, 4 (2002), 349–353.
- [7] BARBUTO, D. Strain Gage vs Electromagnetic Force Compensation, 2015. Retrieved from <https://sartoriusintec-blog.com/2015/01/30/strain-gage-vs-electromagnetic-force-compensation/>.
- [8] BATHE, K.-J. *Finite element procedures*, 2nd ed. Prentice Hall, Pearson Education, Inc., Massachusetts, 2014.
- [9] CALLISTER, W. D. *Materials science and engineering: An introduction*, 7th ed. John Wiley & Sons, New York, 2007.
- [10] CAO, L., DOLOVICH, A. T., SCHWAB, A. L., HERDER, J. L., AND ZHANG, W. Toward a Unified Design Approach for Both Compliant Mechanisms and Rigid-Body Mechanisms: Module Optimization. *Journal of Mechanical Design* 137, 12 (2015), 122301–1–10.
- [11] CHEN, G., LIU, X., GAO, H., AND JIA, J. A generalized model for conic flexure hinges. *The Review of scientific instruments* 80, 5 (2009), 055106–1–10.
- [12] CHEN, S. H., AND FENG, B. Size effect in micro-scale cantilever beam bending. *Acta Mechanica* 219, 3-4 (2011), 291–307.
- [13] CHEN, Z., GANDHI, U., LEE, J., AND WAGONER, R. H. Variation and consistency of young’s modulus in steel. *Journal of Materials Processing Technology* 227 (2016), 227–243.
- [14] CHETWYND, D. G. Selection of structural materials for precision devices. *Precision Engineering* 9, 1 (1987), 3–6.

- [15] CONDE, A., SANCHEZ, J. A., PLAZA, S., AND RAMOS, J. M. On the Influence of Wire-lag on the WEDM of Low-radius Free-form Geometries. *Procedia CIRP* 42 (2016), 274–279.
- [16] CONRADY, A. A Study of the Balance. *Proceedings of the Royal Society of London. Series A, Containing Papers of a Mathematical and Physical Character* 101, 710 (1922), 211–224.
- [17] CONWAY, H. D., AND NICKOLA, W. E. Anticlastic action of flat sheets in bending. *Experimental Mechanics* 5, 4 (1965), 115–119.
- [18] DARNIEDER, M., THESKA, R., FRÖHLICH, T., PABST, M., WENIG, R., AND HILBRUNNER, F. Design of high-precision weighing cells based on static analysis. In *59th Ilmenau Scientific Colloquium* (2017).
- [19] DIRKSEN, F., AND LAMMERING, R. On mechanical properties of planar flexure hinges of compliant mechanisms. *Mechanical Sciences* 2, 1 (2011), 109–117.
- [20] EASTMAN, F. S. *Flexure pivots to replace knife edges and ball bearings: An adaptation of Beam-Column Analysis*, vol. 86 of *Engineering Experiment Station*. University of Washington, Seattle, 1935.
- [21] FARHADI MACHEKPOSHTI, D., TOLOU, N., AND HERDER, J. L. A Review on Compliant Joints and Rigid-Body Constant Velocity Universal Joints Toward the Design of Compliant Homokinetic Couplings. *Journal of Mechanical Design* 137, 3 (2015), 032301–1–10.
- [22] FISHER, R. *The Design of Experiments*, 1st ed. Oliver and Boyd, Edinburgh, 1935.
- [23] FLEMING, A. J., AND LEANG, K. K. *Design, Modeling and Control of Nanopositioning Systems*. Advances in Industrial Control. Springer International Publishing, Cham, 2014.
- [24] FLORIAN, A. An efficient sampling scheme: Updated Latin Hypercube Sampling. *Probabilistic Engineering Mechanics* 7, 2 (1992), 123–130.
- [25] FOSTER, C. R. Accurate measurement of Poisson’s ratio in small samples. *Experimental Mechanics* 16, 8 (1976), 311–315.
- [26] FRIEDRICH, R., LAMMERING, R., AND HEURICH, T. Nonlinear modeling of compliant mechanisms incorporating circular flexure hinges with finite beam elements. *Precision Engineering* 42 (2015), 73–79.
- [27] GABAUER, W. *Manual of Codes of Practice for the Determination of Uncertainties in Mechanical Tests on Metallic Materials*, 2000.
- [28] GAN, S. W. *Development of Hybrid Fine Tool Servo System for Nano-machining*. PhD thesis, National University of Singapore, 2009.
- [29] GOYAL, A. Investigation of material removal rate and surface roughness during wire electrical discharge machining (WEDM) of Inconel 625 super alloy by cryogenic treated tool electrode. *Journal of King Saud University - Science* 29, 4 (2017), 528–535.
- [30] GRÄSER, P., LINß, S., ZENTNER, L., AND THESKA, R. On the influence of the flexure hinge orientation in planar compliant mechanisms for ultra-precision applications. In *59th Ilmenau Scientific Colloquium* (2017).

- [31] HENEIN, S., AYMOUN, C., BOTTINELLI, S., AND CLAVEL, R. Fatigue failure of thin wire-electrodischarge-machined flexure hinges. In *Microrobotics and Microassembly* (1999), vol. 3834, pp. 112–121.
- [32] HENGGEN, L. *Auswirkung der Drahtfunkenerosion auf die mechanischen Eigenschaften von Festkörpergelenken*. PhD thesis, RWTH Aachen, 2017.
- [33] HOWELL, L. L., AND MIDHA, A. A Method for the Design of Compliant Mechanisms With Small-Length Flexural Pivots. *Journal of Mechanical Design* 116, 1 (1994), 280.
- [34] HUH, J. S., KIM, K. H., KANG, D. W., GWEON, D. G., AND KWAK, B. M. Performance evaluation of precision nanopositioning devices caused by uncertainties due to tolerances using function approximation moment method. *Review of Scientific Instruments* 77, 1 (2006), 015103–1–9.
- [35] HUNTINGTON, D. E., AND LYRINTZIS, C. S. Improvements to and limitations of Latin Hypercube Sampling. *Probabilistic Engineering Mechanics* 13, 4 (1998), 245–253.
- [36] HWANG, D., BYUN, J., JEONG, J., AND LEE, M. G. Robust Design and Performance Verification of an In-Plane XY θ Micropositioning Stage. *IEEE Transactions on Nanotechnology* 10, 6 (2011), 1412–1423.
- [37] INTERNATIONAL FEDERATION FOR THE PROMOTION OF MECHANISM AND MACHINE SCIENCE. IFToMM Dictionaries, May 2014. Retrieved from http://www.iftomm-terminology.antonkb.nl/2057_1031/frames.html.
- [38] ISLAM, M. N., RAFAI, N. H., AND SUBRAMANIAN, S. S. Dimensional Accuracy Achievable in Wire-Cut Electrical Discharge Machining. In *Electrical Engineering and Applied Computing*, vol. 90 of *Lecture Notes in Electrical Engineering*. Springer Netherlands, Dordrecht, 2011, pp. 543–553.
- [39] JENSEN, B. D., AND HOWELL, L. L. The modeling of cross-axis flexural pivots. *Mechanism and Machine Theory* 37, 5 (2002), 461–476.
- [40] KOSEKI, Y., TANIKAWA, T., KOYACHI, N., AND ARAI, T. Kinematic Analysis of Translational 3-DoF Micro Parallel Mechanism Using Matrix Method. *Advanced Robotics* 16, 3 (2002), 251–264.
- [41] KOSHAL, R. S. Application of the Method of Maximum Likelihood to the Improvement of Curves Fitted by the Method of Moments. *Journal of the Royal Statistical Society* 96, 2 (1933), 303–313.
- [42] KOSTER, M., ROSIELLE, P., AND REKER, E. Constructies voor het nauwkeurig bewegen en positioneren (6). *Mikroniek* 32, 3 (1992), 68–72.
- [43] KOTA, S., JOO, J., LI, Z., RODGERS, S. M., AND SNIEGOWSKI, J. Design of Compliant Mechanisms: Applications to MEMS. *Analog Integrated Circuits and Signal Processing* 29, 1 (2001), 7–15.
- [44] KUMAR, A., KUMAR, V., AND KUMAR, J. Effect of machining parameters on dimensional deviation in wire electric discharge machining process using pure titanium. *Journal of Engineering and Technology* 3, 2 (2013), 105.

- [45] LI, Q., PAN, C., AND XU, X. Closed-form compliance equations for power-function-shaped flexure hinge based on unit-load method. *Precision Engineering* 37, 1 (2013), 135–145.
- [46] LINß, S., AND MILOJEVIC, A. Model-based design of flexure hinges for rectilinear guiding with compliant mechanisms in precision systems, 29. - 31. August 2012.
- [47] LINß, S., SCHORR, P., AND ZENTNER, L. General design equations for the rotational stiffness, maximal angular deflection and rotational precision of various notch flexure hinges. *Mechanical Sciences* 8, 1 (2017), 29–49.
- [48] LINß, S., ZENTNER, L., KOLEV, E., AND PAVLOVIĆ, N. D. *Ein Beitrag zur geometrischen Gestaltung und Optimierung prismatischer Festkörpergelenke in nachgiebigen Koppelmechanismen*. PhD thesis, Technische Universität Ilmenau, 2015.
- [49] LIU, M., ZHANG, X., AND FATIKOW, S. Design and analysis of a high-accuracy flexure hinge. *Review of Scientific Instruments* 87, 5 (2016), 055106.
- [50] LOBONTIU, N. *Compliant Mechanisms: Design of Flexure Hinges*. CRC Press, Boca Raton, 2003.
- [51] LOBONTIU, N., PAINE, J. S., GARCIA, E., AND GOLDFARB, M. Design of symmetric conic-section flexure hinges based on closed-form compliance equations. *Mechanism and Machine Theory* 37, 5 (2002), 477–498.
- [52] LOBONTIU, N., PAINE, J. S. N., GARCIA, E., AND GOLDFARB, M. Corner-Filletted Flexure Hinges. *Journal of Mechanical Design* 123, 3 (2001), 346.
- [53] LU, Y. Rigidity analysis of elliptic flexible hinges. In *2013 2nd International Symposium on Instrumentation and Measurement, Sensor Network and Automation (IMSNA)* (2013), IEEE, pp. 1064–1066.
- [54] MARANGONI, R. R., RAHNEBERG, I., HILBRUNNER, F., THESKA, R., AND FRÖHLICH, T. Analysis of weighing cells based on the principle of electromagnetic force compensation. *Measurement Science and Technology* 28, 7 (2017), 075101–1–9.
- [55] MCKAY, M. D., BECKMAN, R. J., AND CONOVER, W. J. A Comparison of Three Methods for Selecting Values of Input Variables in the Analysis of Output from a Computer Code. *Technometrics* 42, 1 (2000), 55–61.
- [56] MENG, Q., BERSELLI, G., VERTECHY, R., AND CASTELLI, V. P. An improved method for designing flexure-based nonlinear springs. In *Volume 4: 36th Mechanisms and Robotics Conference, Parts A and B* (2012), ASME, p. 211.
- [57] MERKEN, P., SMAL, O., DEBONGNIE, J.-F., AND RAUCENT, B. Mechanical based circular notch hinge design. *Université de Liège - Méthodes de Fabrication LMF/D47* (2007), 8.
- [58] MOST, T., AND WILL, J. Meta-model of optimal prognosis - an automatic approach for variable reduction and optimal meta-model selection. In *Weimar Optimization and Stochastic Days 2008* (2008).
- [59] MOST, T., AND WILL, J. Sensitivity analysis using the metamodel of optimal prognosis. In *Weimar Optimization and Stochastic Days 2011* (2011).

- [60] MYERS, R. H., MONTGOMERY, D. C., AND ANDERSON-COOK, C. M. *Response surface methodology: Process and product optimization using designed experiments*, 3rd ed. Wiley Series in Probability and Statistics. Wiley, Hoboken N.J., 2009.
- [61] NIARITSIRY, T.-F., FAZENDA, N., AND CLAVEL, R. Simulation analysis of the sources of inaccuracy of a parallel manipulator. In *IEEE International Conference on Robotics, Intelligent Systems and Signal Processing* (2003), IEEE, pp. 266–271.
- [62] PAROS, J., AND WEISBORD, L. How to design flexure hinges. *Machine Design* 25 (1965), 151–156.
- [63] PATIL, C. B., SREENIVASAN, S. V., AND LONGORIA, R. G. Analytical Representation of Nano-Scale Parasitic Motion in Flexure-Based Selectively Compliant Mechanisms. In *Volume 3: 19th International Conference on Design Theory and Methodology; 1st International Conference on Micro- and Nanosystems; and 9th International Conference on Advanced Vehicle Tire Technologies, Parts A and B* (2007), ASME, pp. 775–784.
- [64] PATIL, C. B., SREENIVASAN, S. V., AND LONGORIA, R. G. Analytical and experimental characterization of parasitic motion in flexure-based selectively compliant precision mechanisms. In *Volume 2: 32nd Mechanisms and Robotics Conference, Parts A and B* (2008), ASME, pp. 393–404.
- [65] PINOT, P., GENEVÈS, G., FILTZ, J.-R., LARQUIER, B., CLAUDEL, P., AND FAVREAU, J.-O. Characterization of flexure hinges for the french watt balance experiment. *EPJ Web of Conferences* 77 (2014), 00005–1–6.
- [66] PURI, A., AND BHATTACHARYYA, B. An analysis and optimisation of the geometrical inaccuracy due to wire lag phenomenon in WEDM. *International Journal of Machine Tools and Manufacture* 43, 2 (2003), 151–159.
- [67] QUINN, T. J. The beam balance as an instrument for very precise weighing. *Measurement Science and Technology* 3, 2 (1992), 141–159.
- [68] QUINN, T. J., SPEAKE, C. C., AND BROWN, L. M. Materials problems in the construction of long-period pendulums. *Philosophical Magazine A* 65, 2 (1992), 261–276.
- [69] QUINN, T. J., SPEAKE, C. C., AND DAVIS, R. S. A 1 kg Mass Comparator Using Flexure-Strip Suspensions: Preliminary Results. *Metrologia* 23, 2 (1986), 87–100.
- [70] RYU, J. W., AND GWEON, D.-G. Error analysis of a flexure hinge mechanism induced by machining imperfection. *Precision Engineering* 21, 2-3 (1997), 83–89.
- [71] SALTELLI, A. *Global sensitivity analysis: The primer*. John Wiley, New Jersey, 2008.
- [72] SCHÖNEN, D., LERSCH, S., HÜSING, M., CORVES, B., KLOCKE, F., HENSGEN, L., AND KLINK, A. Entwicklung, Konstruktion und Anwendung eines Prüfstands zur Ermittlung der ertragbaren Lastzyklen filigraner hochgenauer stoffschlüssiger Gelenke. In *11. Kolloquium Getriebetechnik* (2015).
- [73] SCHOTBORGH, W. O., KOKKELER, F. G., TRAGTER, H., AND VAN HOUTEN, F. J. Dimensionless design graphs for flexure elements and a comparison between three flexure elements. *Precision Engineering* 29, 1 (2005), 41–47.

- [74] SHEN, J. Y. Analysis on Displacement Performance Affected by Machining Errors of Single-Notch Right Circular Flexure Hinge. *Applied Mechanics and Materials* 302 (2013), 343–346.
- [75] SMITH, S. T. *Flexures: Elements of Elastic Mechanisms*. CRC Press, Boca Raton, 2000.
- [76] SMITH, S. T., BADAMI, V. G., DALE, J. S., AND XU, Y. Elliptical flexure hinges. *Review of Scientific Instruments* 68, 3 (1997), 1474–1483.
- [77] SMITH, S. T., AND CHETWYND, D. G. *Foundations of ultraprecision mechanism design*, vol. 2 of *Developments in nanotechnology*. Gordon and Breach Science Publishers, Yverdon, 1992.
- [78] SMITH, S. T., CHETWYND, D. G., AND BOWEN, D. K. Design and assessment of monolithic high precision translation mechanisms. *Journal of Physics E: Scientific Instruments* 20, 8 (1987), 977–983.
- [79] SPEAKE, C. C. Fundamental Limits to Mass Comparison by Means of a Beam Balance. *Proceedings of the Royal Society A: Mathematical, Physical and Engineering Sciences* 414, 1847 (1987), 333–358.
- [80] SPEAKE, C. C. Anelasticity in flexure strips revisited. *Metrologia* 55, 1 (2018), 114–119.
- [81] SREENIVASA RAO M AND VENKAIAH N. Modeling of circularity error while machining Inconel-690 using WEDM. *International Journal of Applied Engineering Research* 11, 6 (2016), 3999–4006.
- [82] SYDENHAM, P. H. Elastic design of fine mechanism in instruments. *Journal of Physics E: Scientific Instruments* 17, 11 (1984), 922–930.
- [83] SYDENHAM, P. H. *Mechanical design of instruments*. Instrument Society of America and the Institute of Measurement and Control, Research Triangle Park N.C., 1986.
- [84] TIAN, Y., SHIRINZADEH, B., ZHANG, D., AND ZHONG, Y. Three flexure hinges for compliant mechanism designs based on dimensionless graph analysis. *Precision Engineering* 34, 1 (2010), 92–100.
- [85] TIMOSHENKO, S., AND GOODIER, J. *Theory of Elasticity*, 2nd ed. McGraw-Hill Book Company, 1951.
- [86] TÖRN, A. Crude Monte Carlo quadrature in infinite variance case and the Central Limit Theorem. *BIT Numerical Mathematics* 6, 4 (1966), 339–346.
- [87] TSEYTLIN, Y. Tractable model for concave flexure hinges. *The Review of scientific instruments* 82, 1 (2011), 015106–1–4.
- [88] TSEYTLIN, Y. M. Notch flexure hinges: An effective theory. *Review of Scientific Instruments* 73, 9 (2002), 3363–3368.
- [89] WALD, A. On the Efficient Design of Statistical Investigations. *The Annals of Mathematical Statistics* 14, 2 (1943), 134–140.
- [90] WORONKO, A., HUANG, J., AND ALTINTAS, Y. Piezoelectric tool actuator for precision machining on conventional CNC turning centers. *Precision Engineering* 27, 4 (2003), 335–345.

- [91] WU, Y., AND ZHOU, Z. Design calculations for flexure hinges. *Review of Scientific Instruments* 73, 8 (2002), 3101–3106.
- [92] XI, X., CLANCY, T., WU, X., SUN, Y., AND LIU, X. A MEMS XY -stage integrating compliant mechanism for nanopositioning at sub-nanometer resolution. *Journal of Micromechanics and Microengineering* 26, 2 (2016), 025014–1–9.
- [93] YANG, C. Calculation and analysis of parabolic flexure hinge. In *Proceedings of 2012 International Conference on Measurement, Information and Control* (2012), IEEE, pp. 5–8.
- [94] YANG, M., DU, Z., AND DONG, W. Modeling and analysis of a superelastic elliptic flexure hinge using co-rotational beam elements. In *2015 International Conference on Manipulation, Manufacturing and Measurement on the Nanoscale (3M-NANO)* (2015), IEEE, pp. 1–6.
- [95] YONG, Y. K., LU, T.-F., AND HANDLEY, D. C. Review of circular flexure hinge design equations and derivation of empirical formulations. *Precision Engineering* 32, 2 (2008), 63–70.
- [96] ZENTNER, L. *Nachgiebige Mechanismen*. Oldenbourg Wissenschaftsverlag, München, 2014.
- [97] ZENTNER, L., AND BÖHM, V. On the Mechanical Compliance of Technical Systems. In *Mechanical Engineering*, M. Gokcek, Ed. InTech, 2012.
- [98] ZHANG, Y. Y., CHEN, X. Y., AND SHA, L. Strength Behaviour of Polysilicon Thin Film Flexure Hinge. *Advanced Materials Research* 33-37 (2008), 545–552.
- [99] ZHU, Z., TO, S., ZHOU, X., WANG, R., AND ZHANG, X. Characterization of Spatial Parasitic Motions of Compliant Mechanisms Induced by Manufacturing Errors. *Journal of Mechanisms and Robotics* 8, 1 (2016), 011018–1–9.
- [100] ZHU, Z., ZHOU, X., WANG, R., AND LIU, Q. A simple compliance modeling method for flexure hinges. *Science China Technological Sciences* 58, 1 (2015), 56–63.